Palaeontology
The Palaeontological Association
www.palass.org

[Palaeontology, Vol. 64, Part 3, 2021, pp. 429–474]

STRANGER THAN A SCORPION: A REASSESSMENT OF *PARIOSCORPIO VENATOR*, A PROBLEMATIC ARTHROPOD FROM THE LLANDOVERIAN WAUKESHA LAGERSTÄTTE

by EVAN P. ANDERSON[1], JAMES D. SCHIFFBAUER[1,2], SARAH M. JACQUET[1], JAMES C. LAMSDELL[3], JOANNE KLUESSENDORF[4,†] *and* DONALD G. MIKULIC[4]

[1]Department of Geological Sciences, University of Missouri, 101 Geology Building, Columbia, MO 65211, USA; andersonep@missouri.edu
[2]X-ray Microanalysis Core Facility, University of Missouri, 101 Geology Building, Columbia, MO 65211, USA
[3]Department of Geology & Geography, West Virginia University, 98 Beechurst Avenue, Brooks Hall, Morgantown, WV 26505, USA
[4]Weis Earth Science Museum, University of Wisconsin–Oshkosh, Fox Valley Campus, 1478 Midway Road, Menasha, WI 54952, USA

Typescript received 17 December 2019; accepted in revised form 21 December 2020

Abstract: A relatively uncommon arthropod of the Waukesha lagerstätte, *Parioscorpio venator*, is redescribed as an arthropod bearing a combination of characters that defy ready classification. Diagnostic features include sub-chelate 'great appendages', a lack of antennae, multiramous anterior trunk appendages, filamentous fan-like rear trunk appendages, and apparently thin and poorly preserved pleural fields. Phylogenetic analysis resolves this organism as basal to crown-group Mandibulata and Chelicerata, but its exact placement is inconclusive. Thus, we compare its morphology to several stem groups of arthropods in a discussion of its plausible taxonomic affinities. The examined specimens are probably carcasses and preserve a variety of soft-tissue details, including muscle blocks in the head, eyes and eye facets, likely ventral nerve cords, a central gut tract and trunk legs with multiple filamentous elements organized into stiff bundles. The preservation habits of *P. venator* are characterized and compared to previous assessments of Waukesha lagerstätte taxa. Four preservation habits are observed: a phosphatized habit showing flattened to partly three-dimensional mineralization in francolite; a mouldic habit largely left behind by removed francolite that shows no carbon enrichment despite a darkened colour; sheet-like or speckled carbonaceous compressions; and scattered pyrite crystals. This redescription highlights both the palaeobiological value of 'small' lagerstätten typical of the middle Palaeozoic and the caution that must be taken when interpreting their more enigmatic constituents.

Key words: stem-group Arthropoda, taphonomy, phosphatization, nerve cord, appendage morphology, tagma.

ARTHROPODS represent a particularly diverse group of living organisms, and have been integral components of animal ecosystems since the early Cambrian. Understanding how extant arthropods came to occupy their modern niches requires accurate accounts of past taxonomic diversity, morphological disparity, and the succession and evolution from early to modern forms. Soft-bodied faunas from the Cambrian contain a great diversity of arthropods, particularly those from the celebrated Burgess (e.g. Briggs *et al.* 1994; Briggs & Collins 1999; García-Bellido & Collins 2007; Haug *et al.* 2012*a*, *b*) and Maotianshan (Hou & Bergström 1997; Hou 1999; Hou *et al.* 2004) shales, although there are many noteworthy deposits besides these. Unfortunately, the fate of many of these arthropod taxa has proven difficult to track, given the paucity of post-Cambrian marine lagerstätten, particularly in the middle Palaeozoic (Muscente *et al.* 2017).

Discoveries of novel non-biomineralized arthropod taxa from the middle Palaeozoic highlight the diversity of the arthropod bauplan (e.g. Orr *et al.* 2000; Rudkin *et al.* 2013; Siveter *et al.* 2014), help determine age ranges for clades (e.g. Rudkin *et al.* 2008; Kühl *et al.* 2009; Lamsdell *et al.* 2015*a*) and provide crucial links for phylogenetic analyses connecting Cambrian taxa to their relatives or descendants (e.g. Briggs *et al.* 2012; Rak *et al.* 2013; Lamsdell *et al.* 2015*b*). Many such studies have attempted to relate early arthropods over the past several decades, some considering only fossil characters and taxa (Budd

[†]Deceased.

doi: 10.1111/pala.12534

2002; Hendricks & Lieberman 2008; Lamsdell *et al.* 2013; Lerosey-Aubril *et al.* 2017), others also incorporating modern taxa and characters to relate extinct and modern groups (Vaccari *et al.* 2004; Scholtz & Edgecombe 2006; Legg *et al.* 2013). In either case, these phylogenies are constantly evolving and the steady stream of discovery of new or better-preserved taxa has the potential to clarify (e.g. Dunlop 2002; Waloszek & Dunlop 2002; Yang *et al.* 2013; Lerosey-Aubril *et al.* 2017), or occasionally upend (Müller & Walossek 1987; Ma *et al.* 2012; Lamsdell *et al.* 2013), our understanding of arthropod relationships.

Here, we rediagnose and redescribe an unusual arthropod from the Silurian Waukesha lagerstätte of Wisconsin, USA, which bears a character combination that has similarities with various arthropod groups. This taxon, *Parioscorpio venator* Wendruff *et al.*, 2020*a*, was originally figured by Mikulic *et al.* (1985*a*), called a 'branchiopod or remipede crustacean' by Mikulic *et al.* (1985*b*), and recently described as the earliest known scorpion by Wendruff *et al.* (2020*a*). Our observations refute a placement in Scorpiones, and instead initially suggested a placement of the species in the 'short great appendage' Megacheira due to the lack of antennae and the possession of great appendages. However, incorporating *P. venator* into the character matrix of Aria & Caron (2017*a*) produced phylogenies that do not consistently place this species within a well-established arthropod group. The purpose of this report is to redescribe the morphologies of this species in greater detail, based on additional specimens, and consider how its characters compare to other basal arthropods, with particular attention focused on short-great appendage Megacheira, Fuxianhuiida and Mandibulata. Regardless of its ultimate taxonomic placement, the revised diagnosis presented herein highlights intriguing soft-bodied morphological details of this species, and serves to underscore the preservation potential of fossils at this undercharacterized lagerstätte.

GEOLOGICAL SETTING

The Waukesha lagerstätte is a soft-bodied fossil deposit in the Brandon Bridge Formation of south-eastern Wisconsin, laid down during the Telychian Age (late Llandoverian) of the Silurian (Kluessendorf 1990; Mikulic & Kluessendorf 1999). The deposit is of limited area and stratigraphic extent, the main interval being a 12 cm thick exposure at Waukesha Lime and Stone Quarry in Waukesha County, WI. The specimens considered in this study were sourced from this exposure, although finer stratigraphic control is no longer possible as samples were collected quickly from areas of active quarrying (Kluessendorf 1990).

Unlike surrounding sediments, which are composed primarily of wavy and crinkly laminated calcilutites signifying intertidal zone deposition, the Waukesha lagerstätte beds are planar laminated and dark in colour, suggesting a relatively high organic content. The lithology of the laminae varies in varve-like fashion (Kluessendorf 1990) between smooth, shaly and dolomitized calcilutites and coarser, lighter-coloured dolosiltstones, the so-called fäulen and flinzen, respectively, of Wendruff *et al.* (2020*b*). The interlaminations between the two lithologies may be at a sub-millimetric scale, although thicker and slightly coarser dolosiltstone beds are common. Thicker beds of the calcilutite may also be found, and some calcilutite finely interlaminates with very thin organic-rich laminae.

Kluessendorf (1990) interpreted the dark beds forming the lagerstätte to be a hydrodynamic trap, where moults and carcasses carried along on tidal currents were dropped out of suspension when the currents washed onto a locally developed, subaerially exposed palaeoscarp adjacent to the trap. The confined nature and high organic input of the trapped materials caused anoxic conditions to develop, facilitating preservation, probably in conjunction with the permeability-sealing effects of microbial mats, which have been found in association with the exceptionally preserved fossils (Wendruff *et al.* 2020*b*).

Despite the limited extent of the deposit, the Waukesha lagerstätte represents one of the most diverse Silurian soft-bodied fossil deposits of Laurentia (Kluessendorf 1994). Many of the taxa, including an abundant, apparently highly specialized dalmanitid trilobite found nowhere else, remain undescribed. In addition to *Parioscorpio venator*, other fossils that have been formally described include: a synziphosuran chelicerate, *Venustulus waukeshaensis* Moore *et al.*, 2005; a thylacocephalan arthropod, *Thylacares brandonensis* Haug *et al.*, 2014; a dasycladalean alga, *Heterocladus waukeshaensis* LoDuca *et al.*, 2003; and three species of phyllocarid crustacean within the genus *Ceratiocaris* (Jones *et al.* 2015).

MATERIAL AND METHOD

Studied material

The material referred to in this paper was loaned from the University of Wisconsin Geology Museum (UWGM), located in the Department of Geology and Geophysics in Madison, Wisconsin. All types and material are permanently reposited at this location. A total of 15 specimens were analysed, and the reanalysis and redescription efforts were based primarily on the following specimens: UWGM2793 (Fig. 1A), 2785 (Fig. 1B), 2764 (Fig. 1C and

counterpart to the designated paratype UWGM2163), 2857 (Fig. 1D, E), 2854 (Fig. 1F, G), 2798 (Fig. 1H) and 2885 (Fig. 1I, J). These specimens had multiple measurements taken of their morphology (Anderson *et al.* 2021, tables S1, S2). Since the pleural regions of the head and trunk and anterior region of the head shield are usually poorly preserved, if they are preserved at all, lengths and widths only incorporate those regions that can plausibly be inferred to belong to the axial portion of the body. Further, rather than separately measuring features on each individual trunk segment, segments 2, 7 and 11 were measured as representatives of the anterior, medial and posterior trunk, respectively. These specific segments were selected as most were preserved well enough to be confidently measured. Additional figured specimens that aided in the rediagnosis and redescription include UWGM2778 and 2787 (Fig. 2A, B), 2803 (Fig. 2C), 2779 (Fig. 2D, counterpart to UWGM2785, although it was not available during initial study of the species), 4558 (Fig. 2E) and 2796 (Fig. 2F). These specimens were examined to provide details on specific morphologies and preservation habits. Photographs of UWGM 2436, 2437 and 2575 from Wendruff (2016) and Wendruff *et al.* (2018) were consulted for their insights on the pleural regions of the exoskeleton and the terminus of the animal, although they were not available for physical examination.

Imaging methods and analysis

Standard photographs were taken using a Nikon D3300 and processed with open-source software digiCamControl v. 2.1 (István 2018). Photomicrographs were taken using a Nikon D600 camera attached to a Nikon SMZ1500 binocular microscope. Select specimens were imaged for compositional analysis with scanning electron microscopy (SEM) and energy dispersive x-ray spectroscopy (EDS) using a Zeiss Sigma 500 VP field emission SEM with dual coplanar Bruker X Flash 6|30 spectrometers. SEM imaging was conducted with a signal mix between a five-segment high definition backscattered electron detector and a cascade current low vacuum secondary electron detector. Photos and images were edited using Affinity Photo (v. 1.6.4.104) and Affinity Designer (v. 1.6.4.104) on a Wacom Cintiq 27QHD Creative Pen Display tablet. Measurements were taken on photographs and photomicrographs using ImageJ (v. 1.49; Schneider *et al.* 2012).

Phylogenetic analysis

Phylogenetic analysis was based on the dataset of Aria & Caron (2017*a*), where *Parioscorpio venator* Wendruff *et al.*, 2020*a* was added as a new, ninety-second taxon (Anderson *et al.* 2021, appendix S1). This dataset was chosen because: (1) it is a recently published dataset; (2) it was assembled from multiple sources; (3) its characters have been optimized for the inclusion of fossil taxa; and (4) it is comprehensive in the breadth of represented extinct and extant arthropod clades. This final point figured particularly heavily in our selection of Aria & Caron (2017*a*), as we were unsure of where to place *P. venator*, and phylogenetic analyses which cover all the major clades of Panarthropoda in more than cursory detail are unusual. While we were aware of some of the limitations of the finer scale resolutions of the dataset (e.g. Phosphatocopina and Ostracoda resolving as sister groups in the cladograms of Aria & Caron 2017*a*), the inclusion of primarily fossil-based characters that would not leave phalanxes of uncertain and inapplicable character states in the character row for *Parioscorpio* was appealing. Our purpose was to determine, at least generally, where in the arthropod family tree *Parioscorpio* fits in accordance with parsimony.

In our analysis, character gaps were coded as '-', missing or ambiguous states as ?, and inapplicable states were treated as missing data (Aria *et al.* 2015). There were some characters for which multiple interpretations were plausible. For example, character 19 codes for the presence of median eyes, of which convincing evidence was never found in the studied specimens of *P. venator*. This would suggest entering a state of 0 for the absence of this character. Yet, the portion of the exoskeleton in which the median eyes are likely to be found was usually poorly preserved on specimens of *P. venator*, such that it could also reasonably be coded as missing, or ?.

In these circumstances, we ultimately coded the character with what we felt was the most likely state for the primary analysis, but retained note of alternative potential states. We then ran further analyses where: (1) alternative states were coded ? for characters where ? was an optional alternative state; (2) alternative states were coded 1 (or whatever character state represented a higher number for a character, such as podomere number) when this was an optional alternative state; and (3) alternative states were coded as 0 (or whatever character state represented a lower number for a character) when this was an optional alternative state. Additionally, these three sets of analyses were run for two interpretations of the anteriormost (as it is preserved in the fossils) ramus of the trunk limbs: one with it coded as an exopod (the default interpretation, see the Redescription, below), the other with it coded as an epipod (the alternative interpretation, see Features of the Trunk, below). These alternative arrangement analyses were done in order to observe how relatively minor changes in the interpretation of the morphology of *P. venator* could affect its taxonomic placement.

Analysis follows the standard of Aria & Caron (2017*a*) using PAUP* v. 4.0a167 (X86) (Swofford 2002). In

summary, the dataset was processed with parsimony analysis using an heuristic search with tree bisections and reconnection using 1000 replicates and a maximum of 10 trees with a score above 1 for each replicate. The backbone constraints of Aria & Caron (2017*a*) were retained. Strict consensus trees were constructed and compared, and branch support was evaluated using Bremer, bootstrap and jackknife support values.

Bremer support was calculated by re-running the analysis with 10 locally optimal trees retained for each of the 1000 replicates, whether or not their score was optimal for all replicates. This allowed for the retention of

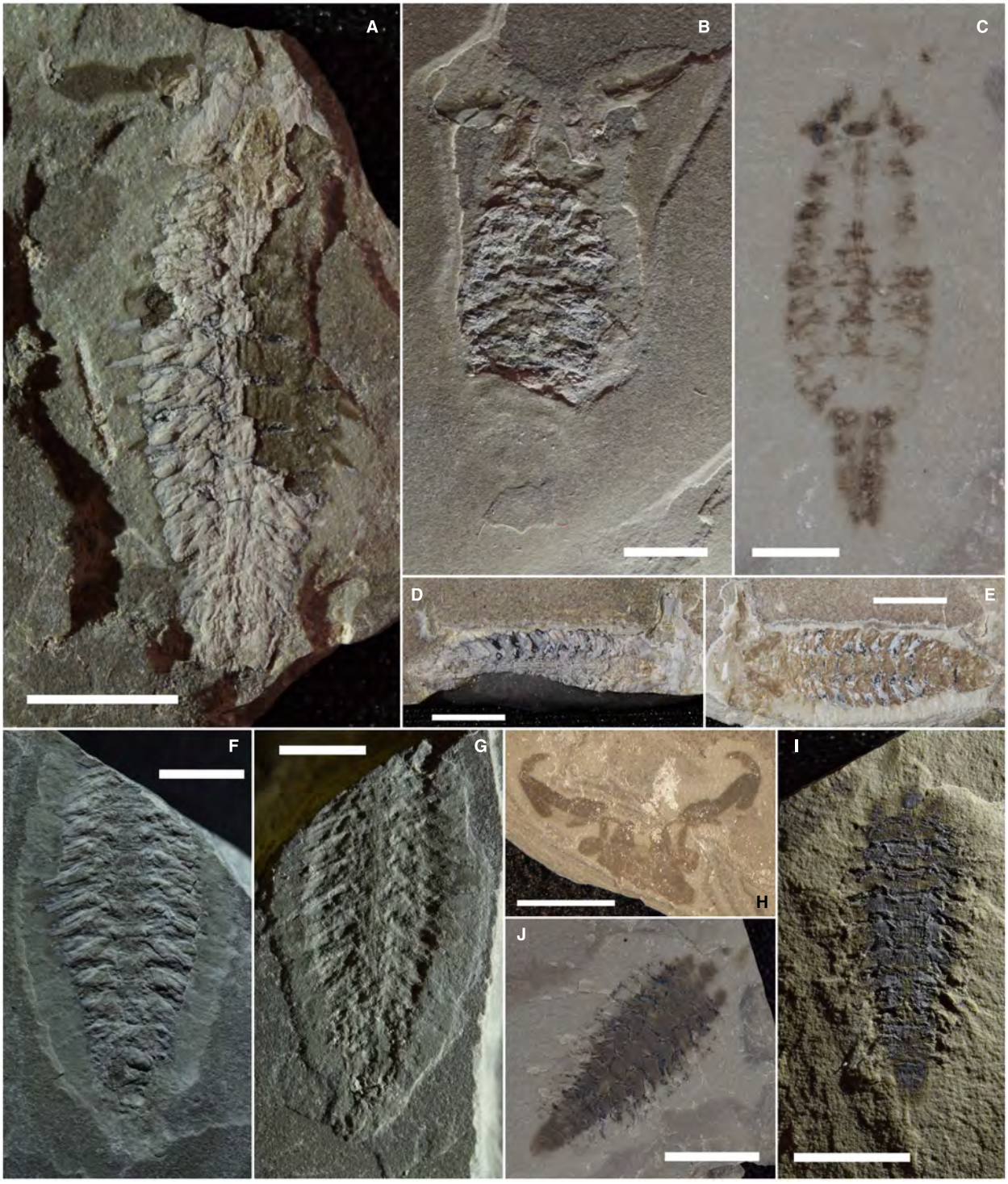

FIG. 1. Specimens upon which the rediagnosis and redescription of *Parioscorpio venator* Wendruff *et al.*, 2020*a* are primarily based. A, UWGM2793, a nearly complete specimen with an entire left great appendage. B, UWGM2785, a specimen with all cephalic appendages intact, including both great appendages, which are nearly complete; note that the posterior portion of the body is still buried beneath the matrix. C, UWGM2764, paratype and counterpart to UWGM2163, preserved as a thin film with the right great appendage barely visible on the upper right; no trunk appendages are preserved, which makes the posterior constriction of the axial trunk easy to see compared to other specimens. D–E, part and counterpart of UWGM2857, a nearly complete specimen with numerous head and trunk details. F–G, part and counterpart of UWGM2854, which preserves many three-dimensional limbs, but whose head is cut off by the border of the matrix. H, UWGM2798, a largely mouldic specimen showing excellent preservation of the cephalic appendages, including two complete great appendages. I–J, part and counterpart of UWGM2885, a nearly complete specimen which shows limited three-dimensional preservation, but preserves many walking legs as dark compressions. All scale bars represent 5 mm.

suboptimal scores, and consensus trees were computed for the most parsimonious trees and trees one step longer, then for the most parsimonious trees and trees one and two steps longer, and so on (Bremer 1988) to suboptimal trees five steps longer than the most parsimonious tree. Bremer scores were assigned to nodes based on how many additional steps were needed to collapse it, with nodes surviving in consensus trees with five additional steps allowed assigned a score of '>5'.

Bootstrap and jackknife support analyses were conducted using their respective commands in PAUP* v. 4.0a167 (Swofford 2002). For both jackknife and bootstrap analyses, 500 replications of a 'fast' stepwise-addition search were run with a random number seed of 1, groups compatible with the 50% majority-rule consensus trees were retained for display, and for the jackknife analysis 10% of characters were randomly deleted. In the primary analysis, the results of Bremer, bootstrap, and jackknife support analyses appeared broadly similar, so only Bremer analyses were run for the alternative interpretations.

After the analysis, we compared the characters of *P. venator* to those of several stem-group taxa featured in the character table of Aria & Caron (2017*a*) to analyse potential synapomorphies. The selected taxa include: (1) *Surusicaris elegans* Aria & Caron, 2015 representing Isoxyidae; (2) Leanchoiliidae Raymond, 1935 and *Yohoia tenuis* Walcott, 1912 representing Megacheira, along with *Oelandocaris oelandica* Müller, 1983, which is more likely to be a member of Crustacea *sensu lato* (e.g. Stein *et al.* 2008; Haug *et al.* 2010) but resolved with Megacheira in Aria & Caron (2017*a*); (3) *Offacolus kingi* Orr *et al.*, 2000 representing stem-group Eucheliceratа; (4) *Sidneyia inexpectans* Walcott, 1911 representing Artiopoda; (5) *Fuxianhuia* Hou, 1987, representing Fuxianhuiida and its relatives; (6) *Tokummia katalepsis* Aria & Caron, 2017*a* representing Hymenocarina and stem-group Mandibulata; (7) *Marrella splendens* Walcott, 1912; and (8) *Agnostus pisiformis* Wahlenberg, 1818. These last two species were chosen not because of a particularly close morphological resemblance to *P. venator*, but because they have also proven to be difficult to place phylogenetically (e.g. Walossek & Müller 1990; Rak *et al.* 2013).

SYSTEMATIC PALAEONTOLOGY

Phylum ARTHROPODA von Siebold, 1848
Subphylum INCERTAE SEDIS

Genus PARIOSCORPIO Wendruff *et al.*, 2020*a*

Type species. *Parioscorpio venator* Wendruff *et al.*, 2020*a*.

Rediagnosis. As for species.

Parioscorpio venator Wendruff *et al.*, 2020*a*
Figures 1–10, 13A

1985*a* ?branchiopod crustacean; Mikulic *et al.*, p. 716, fig. 2d.
1985*b* branchiopod or remipede crustacean; Mikulic *et al.*, p. 79, pl. 2 fig. 16.
2016 *Latromirus tridens* Wendruff, pp 150–153 (pars), figs 5.1. 4–7, 5.1.9–11 (non figs 5.1.1–3, 5.1.8, 5.1.12–13).
2018 *Xus yus* Wendruff *et al.*, pp 7–10 (pars), fig. 1e–l (non fig. 1a–d).
2020*a* *Parioscorpio venator* Wendruff *et al.*, figs 1a, c, 2a.
2020*b* scorpion; Wendruff *et al.* p. 1, 7, fig. 5a.
2020*b* cheloniellid arthropod; Wendruff *et al.* fig. 7b (non fig. 7c).

Holotype. UWGM2162 from the Waukesha Lime and Stone Quarry, Waukesha, Wisconsin, USA.

Paratypes. UWGM2163 and UWGM2764 (Figs 1C, 3E, 6A–D, 10D), part and counterpart; from the same locality as the holotype.

Additional material. UWGM2436; UWGM2437; UWGM2575; UWGM2778 (Figs 2A, 5E) and UWGM2787 (Figs 2B, 5F), part and counterpart; UWGM2779 (Fig. 2D) and UWGM2785 (Figs 1B, 4D–F, H), part and counterpart; UWGM2793 (Figs 1A, 3A, B, 5A, H, 7A, F, G, 8A, C, 13A); UWGM2796 (Figs 2F, 9F); UWGM 2798

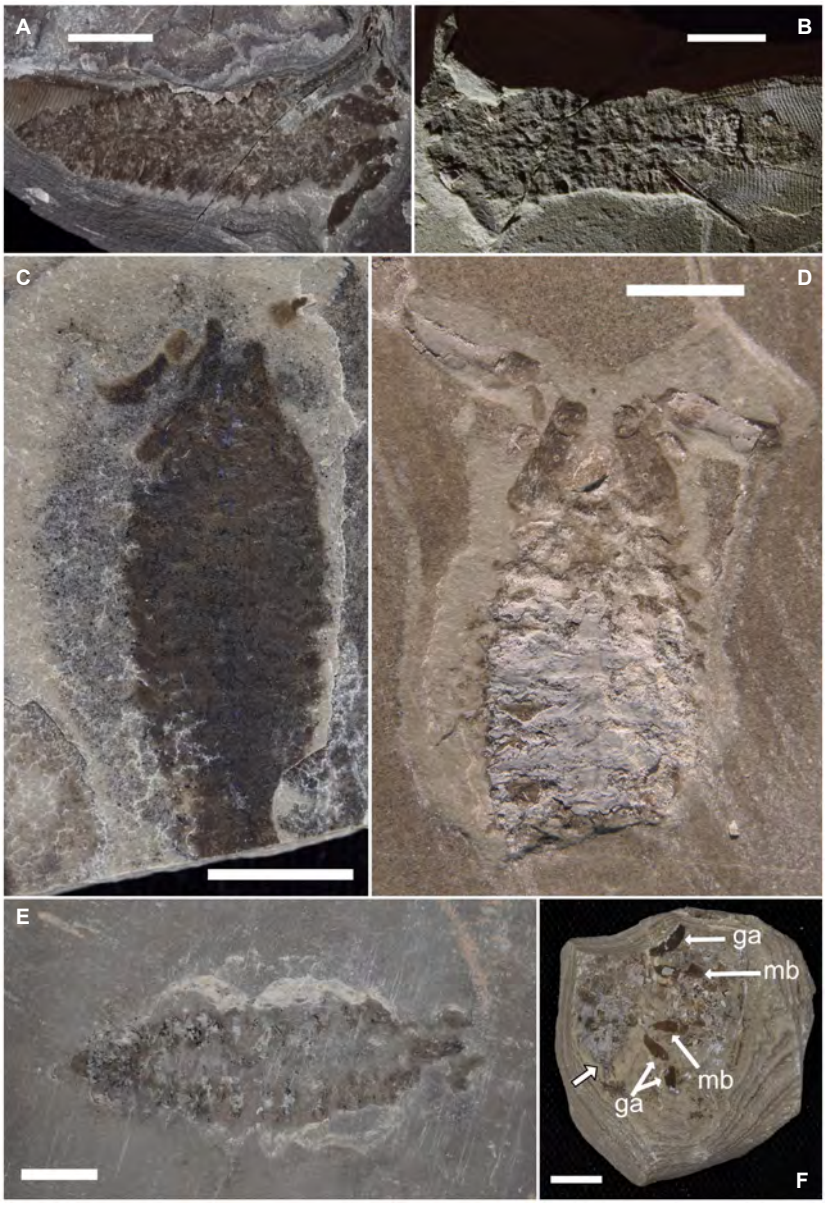

FIG. 2. Additional available specimens of *Parioscorpio venator* that aided in the rediagnosis and redescription. A–B, UWGM2778 and UWGM2787, part and counterpart of a nearly complete but largely effaced specimen associated with a conulariid. C, UWGM2803, a nearly completely flattened specimen that preserves the axial body in stark contrast with the matrix; the pleural field may be partly preserved as a halo of darker speckled material on the specimen's left side. D, UWGM2779, the counterpart to UWGM2785, which was not initially available for study; its great appendages are preserved by three-dimensional phosphate. E, UWGM4558, a poorly preserved specimen which nevertheless shows some traces of segmentation and limbs. F, UWGM2796, an extensively deformed specimen; the posterior on the left side of the sample is largely articulated (white arrow with black outline), but the anterior is discombobulated on the right. *Abbreviations*: ga, great appendage article; mb, muscle block. All scale bars represent 5 mm.

(Figs 1H, 5C, G); UWGM2801; UWGM2803 (Fig. 2C); UWGM 2827, part and counterpart (Fig. 10A); UWGM 2854, part and counterpart (Figs 1F, G, 6F, 7I, 9A–C, E); UWGM2857, part and counterpart (Figs 1D, E, 3C, 4A, B, 7C, E, 8E, 10C); UWGM2858, part and counterpart (Fig. 10B); UWGM2885, part and counterpart (Figs 1I–J, 6E, 7H, 8G, 9D); UWGM4558 (Figs 2E, 4C); and UWGM4718.

Rediagnosis. A great appendage-bearing arthropod with a transversely wide ovoid body outline and two cephalic appendages. First cephalic appendage, the great appendage, is uniramous with four articles. First article has highly reduced, broadly y-shaped sclerotized portion, second article roughly trapezoidal, third article is the largest and longest, fourth article is smaller, pointed, and projects at a nearly 90° angle to the long axis of the third article. Second cephalic appendage is biramous, and both exopod and endopod are considerably smaller than the great appendage; exopod may be distally setose. Axial region of the head is trapezoidal in dorsoventral view with compound eyes preserved in anterolateral corners of the trapezoid. A larger, faint, semicircular(?) head shield with anterolaterally directed posterior margins covers the axial region. Trunk consists of 14 somites. Axially, two pseudotagmata (*sensu* Lamsdell 2013) are evident: the first 10 somites form a broad pear-shaped preabdomen, while the last 4 somites form a posteriorly tapering

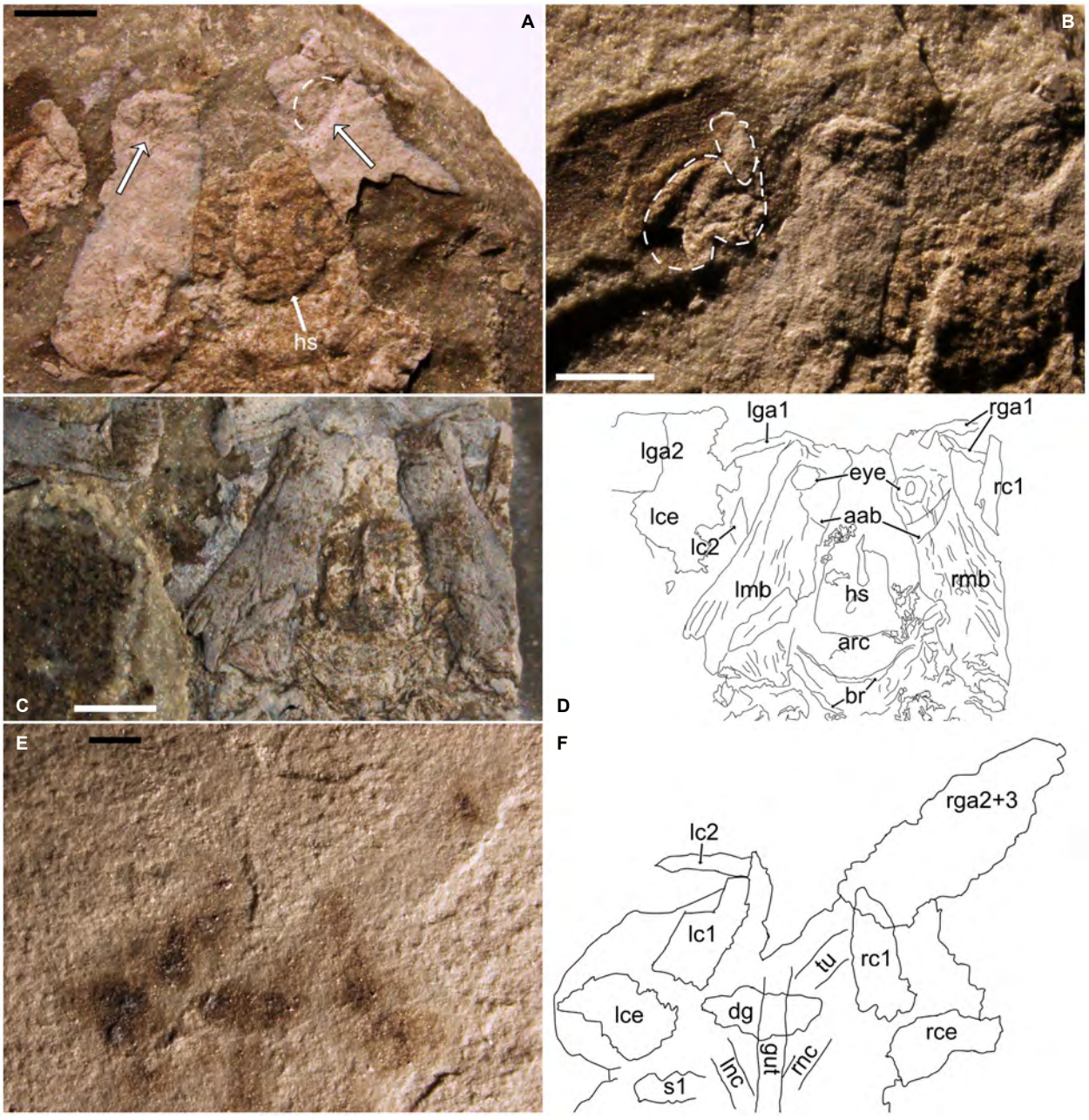

FIG. 3. Features of the head of *Parioscorpio venator*. A, head of UWGM2793; white arrows with black outlines point to the posterior of the depressions interpreted as the great appendage insertion points; dashed white arc highlights the anteromedial half of the eye, which appears as an oval with a dotted outline (the dark areas may represent facets). B, low angle light photograph of the upper left corner of the head and cephalic appendages of UWGM2793; the dashed white lines trace the second cephalic appendage rami, including the first segment of the endopod (smaller, anteriorward trace) and the exopod (larger, posteriorward trace). C–D, photograph and interpretive drawing of the head of paratype UWGM2857a; the striations in the trapezoidal muscle blocks are particularly well preserved in this specimen; these are interpreted as muscle fibres and suggest a complex arrangement of multiple muscles within the blocks. E–F, photograph and interpretive drawing of the head of paratype UWGM2764; preserved as a film, different from most other available specimens. *Abbreviations*: prefix r or l, indicates right or left of some elements; aab, appendage articulation boundary, i.e. of the great appendage; arc, arcuate structure; br, brace-like structures; c, cephalic appendage endopod podomere (1 or 2; r/l); ce, cephalic appendage exopod (r/l); dg, early digestive structure associated with the anterior of the gut; ga, great appendage element (1–3; r/l); hs, hypostome; mb, muscle block (r/l); nc, nerve cord (r/l); s1, cuticle of segment 1; tu, indeterminate tube. All scale bars represent 1 mm.

subrectangular postabdomen. Pleural regions of the trunk typically faint. The anterior two (or more) tergopleurae are anterolaterally directed, with subsequent tergopleurae directed first laterally, then increasingly posterolaterally. The first 12 trunk somites have a complex biramous limb with multiple filamentous elements that can be lobose, sub-lanceolate, to lanceolate in shape. The final two trunk somites with fan-shaped, filamentous primary rami and an indeterminate number of smaller, filamentous, fan-shaped elements; filaments are elongate and originate from indistinct rami. Terminal segment bears an anus and two lateral spines separated from tergite by a transverse, rounded suture; a small telson dorsal to the lateral spines extends posteriorly to about their length.

Redescription. The axial portion of *Parioscorpio venator* measures between 16.43 and 28.03 mm in length and between 5.41 and 11.34 mm in width (Anderson *et al.* 2021, tables S1, S2). Specimens UWGM2857 (Fig. 1D, E) and 2885 (Fig. 1I, J) are the smallest of those measured while UWGM2785 (Fig. 1B) and 2854 (Fig. 1F, G) are the widest (the length of both is incomplete and cannot be accurately assessed) and UWGM2764 (Fig. 1C) the

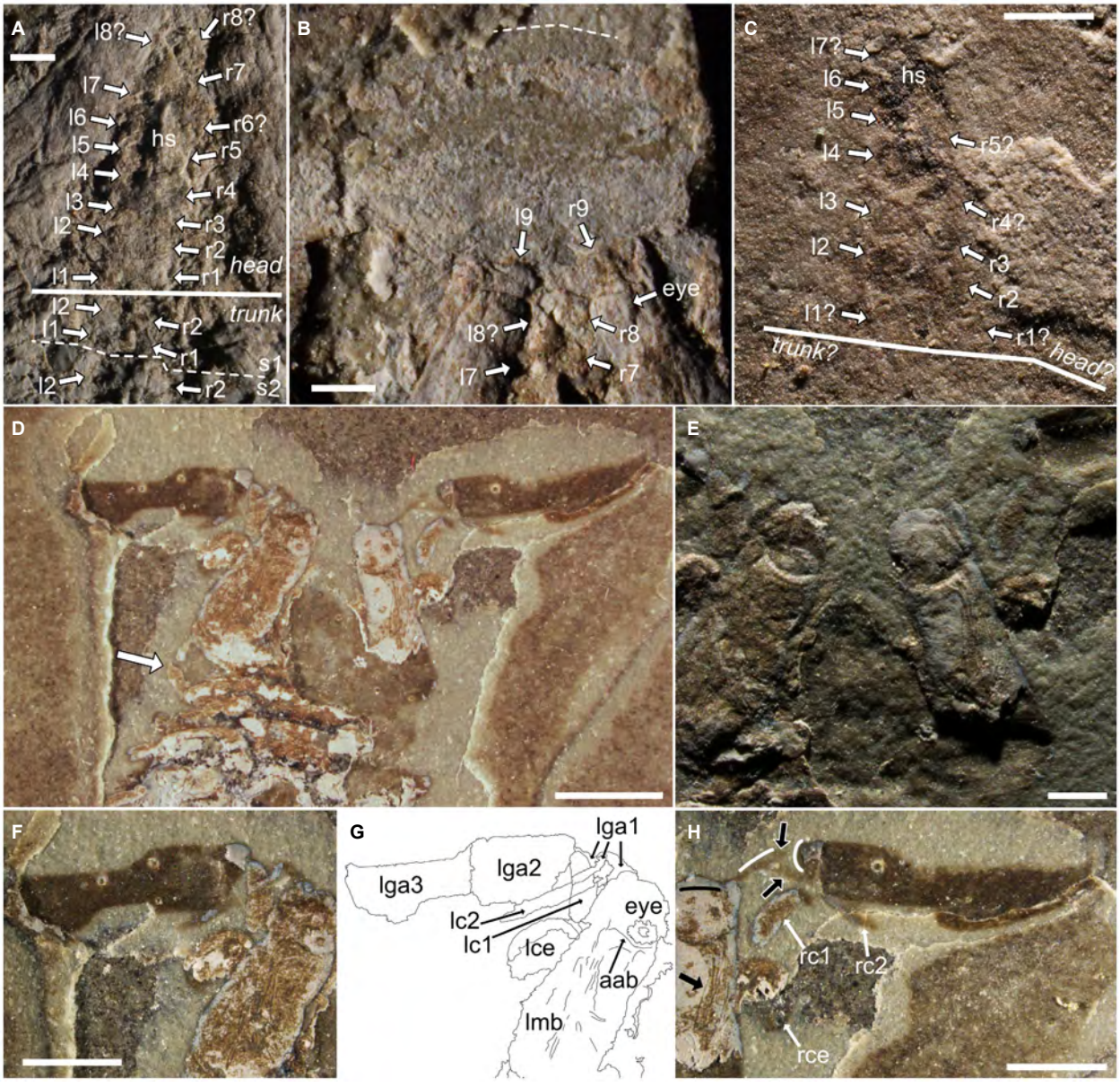

FIG. 4. Further features of the head and cephalic appendages of *Parioscorpio venator*. A–C, paired circles or rings of unknown function seen in the head and trunk of multiple specimens, indicated by arrows and sequentially labelled from posterior to anterior. A–B, rings of UWGM2857a: A, rings of the posterior head (1–9) and anterior trunk (1 or 2); those by the brace structures (see Fig. 3C–D) are the most discernible, but anteriorward they are partially obscured by the hypostome; posteriorward, there appear to be two pairs of circular structures per trunk somite; B, the seventh to ninth pairs of rings, anterior to the hypostome and highlighted due to a different lighting angle; the dashed line denotes the discernible anterior boundary of a broad, flat, lightly mineralized surface interpreted as the (possibly partially displaced) head shield. C, circles or rings of UWGM4558, most strongly developed just posterior to the hypostome and with three pairs apparently overprinting the hypostome, as in UWGM2857. D–H, the head and cephalic appendages of UWGM2785: D, overview of the head and anterior trunk segments; the arrow indicates the single clawed terminus of the walking portion of the first trunk leg; E, low angle light photography of the head, revealing the depressions marking the insertion zones for the great appendages; F–G, photograph and interpretive drawing of the left muscle block and cephalic appendages; for the sake of clarity, only the outline of the many overlapping elements of the great appendage and second cephalic appendage rami are traced; note that the second cephalic appendage's second endopod podomere (lc2) may end flush with the right edge of the first podomere (lc1) or just medial to it; H, right muscle block and cephalic appendages; black arrows with white outlines point to the distal branches of the y-shaped first great appendage article; the white arc to their right indicates the angled anteroproximal corner of the second great appendage article, which would have been rotated counterclockwise in life to lie flush with the distal branches of the first great appendage article; the left white arc and black arc show the estimated placement of the first great appendage article and its insertion zone under the head, respectively; the solid black arrow indicates fibres within the muscle block. *Abbreviations*: prefix r or l, indicates right or left of some elements; aab, appendage articulation boundary, i.e. of the great appendage; c, cephalic appendage endopod podomere (1 or 2); ce, cephalic appendage exopod; hs, hypostome; lga, left great appendage element (1–3); lmb, left muscle block; 1–9, ring structures in the head (1–9; r/l) or trunk (1 or 2; r/l); ?, dubious ring structures. Scale bars represent: 0.5 mm (A); 1 mm (B–C, E); 3 mm (D); 2 mm (F, H).

longest. Differences in major morphological details, like segment number, are not evident between smaller and larger specimens. Proportion differences in finer details, such as the length:width ratios of the great appendage articles, are minor and more likely to be natural within-species variation or taphonomic than a reflection of ontogeny or taxonomy.

Morphology of the head. The axial portion of the head containing soft tissue is roughly trapezoidal in outline with rounded corners, with a length between 3.12 and 4.84 mm and a width between 4.55 and 7.24 mm (Anderson *et al.* 2021, table S1). The lateral portions of the axial head are dominated by two trapezoidal blocks (Fig. 3A, C, D). They may show extensive striations (Figs 3C, D, 4D–H). Depressions are visible under raking light at the anterolateral corner of each trapezoidal block (Figs 3A, B, D, 4E–H, 5A, B, G). On UWGM2793 a partial, oval-shaped, dotted outline probably represents the eye (Fig. 3A, B); on other specimens a simple circular to sub-circular ring denotes the eye (Figs 3C, D, 4B, D, F, G, 5F).

The depressions were probably the insertion points for the great appendages (cf. Liu *et al.* 2007, fig. 3b; Haug *et al.* 2012*b*, fig. 3d) which in all observed specimens have been displaced laterally from the head to some extent (e.g. Fig. 4F, H). The striated trapezoidal structures are here interpreted as muscle blocks (see Features of the Head, below). UWGM2778 and 2787 (Fig. 5E, F), a part/counterpart pair, preserve different aspects of the muscle blocks' anatomy. On UWGM2778, two kite-shaped depressions (white dashed outlines on Fig. 5E) are seen in the trapezoidal muscle blocks which expand anteriorly and terminate near or just anterior to the eyes (eyes not readily evident in Fig. 5E). The centre of the kite-shaped depressions corresponds in location to a pair of pits posterior to the eyes on UWGM2787 (white dashed outlines in Fig. 5F). The kite-shaped depressions of UWGM2778 are interpreted as units of muscle that originally passed through the ventral pits on UWGM2787 and articulated with the now-displaced great appendages (the first articles of which are labelled in Fig. 5E, F). Depressions in UWGM2787 are not directly beneath the eye as they appear to be in other specimens (Figs 3A, B, D, 4D–H; 5G); it may be a taphonomic effect.

In UWGM2793 and 2857 (Fig. 3A, C, D) a pear-shaped, topographically elevated structure is located on the sagittal midline of the head centred a little over halfway along the length of the muscle blocks. This structure's posterior is marked by a convex arc (arrow labelled 'hs' in Fig. 3A; 'arc' in Fig. 3D). Based on the shape of the head, this arc lies just anterior to a transversely elongated oval in UWGM2764 which overprints an elongate, parallel-sided structure that terminates anterior to the oval (Fig. 3E, F) and runs posteriorly along much of the length of the body (Fig. 1C). The parallel-sided structure is interpreted as a simple gut, with the dark oval interpreted as an initial digestive structure (Fig. 3F). The pear-shaped structure is thus the hypostome.

Paired circular features along the axis of the head are seen on several specimens, usually only under low-angle light. They are usually most strongly expressed posteromedially in the head and appear to overprint features like

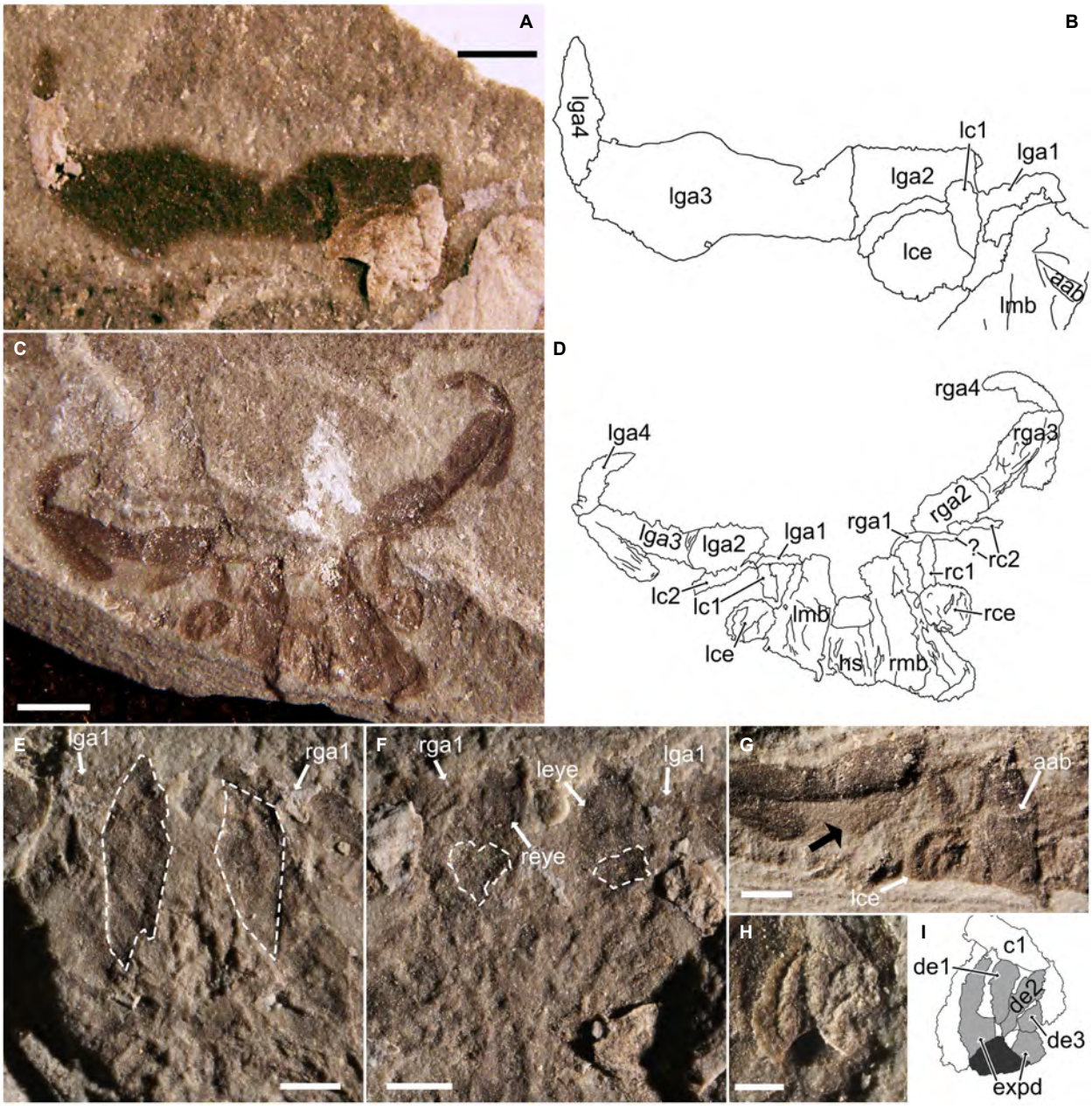

FIG. 5. Features of the cephalic appendages of *Parioscorpio venator*. A–B, photograph and interpretive drawing of the great appendage and second cephalic appendage of UWGM2793. C–D, photograph and interpretive drawing of UWGM2798, which preserves the cephalic appendages exquisitely; note the split in the cuticle along the length of the third great appendage articles. E–F, UWGM2778 and UWGM2787, part and counterpart, which provide evidence of the mechanical operation of the great appendages by the muscle blocks in the head; white dashed outlines indicate the mouldic outline of a muscle block pair in E and the insertions of the great appendages in F. G, left second cephalic appendage of UWGM2798; black arrow points to the distal edge of the endopod, the arrowhead's width reflecting the breadth of its potentially setose terminus. H–I, photograph and interpretive drawing of the left second cephalic appendage exopod of UWGM2793, also seen in Figure 3B; I, for ease of interpretation, pertinent exopod units are lightly shaded and pertinent phosphate removed by erosion is darkly shaded. *Abbreviations*: prefix r or l, indicates right or left of some elements; aab, appendage articulation boundary, i.e. of the great appendage; c, cephalic appendage endopod podomere (1 or 2; r/l); ce, cephalic appendage exopod (r/l); de, distal element (1–3); expd, exopod podomere; eye, eye (r/l); ga, great appendage element (1–4; r/l); hs, hypostome; mb, muscle block (r/l). Scale bars represent: 1 mm (A, E–G); 2 mm (C); 0.5 mm (H).

the hypostome (Fig. 4A, C). There may be at least nine (Fig. 4A, B) or as few as five (Fig. 4C) and they appear to extend into the trunk with up to two pairs per segment (Fig. 4A). Other structures are preserved in the head, but the interpretation of most is dubious; such as a pair of curious brace-like structures in UWGM2857a (labelled 'br' in Fig. 3D). These are axially oriented posteriorly, in contrast to ventral features such as the legs, which are oriented anteriorly, and may represent the preservation of a dorsal feature, like head segmentation.

The great appendage consists of only four articles (Fig. 5A–D). The first segment preserves only a small amount of material and when complete is roughly y-shaped (Figs 3C, D, 4F, G), with the open end of the 'Y' pointing toward the second article (Fig. 4H). The second article may appear either rectangular (Fig. 5A, B) or trapezoidal, with rounded anteromedial corners (Figs 4F–H, 5C, D). If length is considered to be the axis perpendicular to the main body's length, the article's length (range 1.51–2.17 mm) is slightly greater than the width (range 0.94–1.40 mm; Anderson *et al.* 2021, table S1). This article was apparently well-sclerotized, as it sometimes shows cracking patterns consistent with brittle fracture (e.g. Fig. 3B). The third article is the largest, between 2.21 and 3.86 mm in length and between 0.82 and 1.63 mm in width, and resembles a kitchen knife in outline. Basally is a rectangular 'handle,' which distally expands posteriorly into a 'blade.' Distal to this expansion, the posterior side of the article curves anteriorly towards its termination (Figs 4D, H, 5A–D). This termination is concave, and the convex base of article 4 articulates with it (Fig. 5B, D). Article 4 is small, between 1.48 and 1.87 mm long and 0.57–0.69 mm wide, with a conical outline and a mesial bulge more pronounced on its inner side than its outer (Fig. 5A–D). The conical tip appears straight in UWGM2793 (Fig. 5A, B), but bends inward toward the body axis in UWGM2798 (Fig. 5C, D).

The second cephalic appendage is much smaller than the first (Figs 3B, 4D, F–H, 5A–D, G) and is biramous, although the endopod is often displaced anteriorly to the exopod (Figs 4F–H, 5C, D, G). The endopod is composed of at least two segments, the first preserved somewhat three-dimensionally and considerably longer than wide (Anderson *et al.* 2021, table S1) and may have gentle longitudinal striations visible (Fig. 4F). The second podomere is as long as, or longer than, the first, but is narrower (Figs 4F–H, 5C, D, G) and often does not preserve well (Fig. 3C–F), if at all (Fig. 5A, B). There is limited evidence of setae extending along and beyond this podomere on UWGM2798 (Fig. 5G). The exopod is curled in on itself and under higher-angle incident light assumes an oval outline (Figs 4F–H, 5A–D). Under low-angle raking light, a more complex structure becomes visible (Figs 3B, 5G–I) which consists of a banana-shaped podomere that arcs from an anteromedial to posteromedial position and has two or three processes anterior to its distal tip. The length is simply measured as the long axis of the overall oval shape, and its width the short axis. Its length ranges between 1.07 and 1.60 mm and its width between 0.65 and 1.25 mm.

Whilst not apparent in all specimens, the second cephalic appendage is inserted ventrally below the trapezoidal muscle blocks, much like the great appendage, approximately halfway or posterior to halfway along the muscle blocks' length. In UWGM2785, bundles of striations in the muscle blocks, here interpreted as relict muscular fibres, lead to the second cephalic appendage exopod, which is just lateral to the head approximately halfway along its length (Fig. 4F–H). A pair of dark stains, of roughly the same shape as the first podomere of the endopod and the exopod, are visible in the anterior and posterior halves of the head, respectively, in UWGM2764 (Fig. 3E, F). These carbonaceous stains are interpreted as the compressional remnants of the endopod and exopod of the second cephalic appendage.

Pleural and dorsal regions of the head shield are poorly preserved in the observed specimens. UWGM2857a (Fig. 4B) exhibits a thin, lightly mineralized sheet accompanied by a distinctly flat region anterior to the axial features of the head. It is not clear if it is compressed or was displaced from the body in this instance. The posterior margin of the head shield appears to cover the anteriormost trunk, either to the first (e.g. UWGM2436 in Wendruff *et al.* 2018, fig. 1e–f) or second (e.g. UWGM2764, Fig. 6D; there are no clear tergopleural demarcations anterior to the posterior boundary of segment 2) trunk segment.

Morphologies found on both head and trunk. Two major features cross the boundary between the head and trunk. As mentioned above, in UWGM2764 a dark oval interpreted as digestive glands overprints on a simple, elongate gut (Fig. 3E, F). This bends off to the right and becomes ambiguous posterior to segment 6 (Fig. 6A). It is faintly seen again under raking light in the terminal segments (Fig. 6B), still a straight, simple tube. The digestive tract is not evident in any of the other available specimens. Along the length of the gut tract, small paired patches may be found, one or two for each segment, and with one pair behind the main digestive glands in the head (white arrows in Fig. 6A). These could either be small diverticulae or the compressional version of the paired circles or rings seen in Figure 4A–C.

The second feature is a pair of parallel, tube-like structures oriented on the midline of most of the available specimens. These structures are slightly nodulose in the anterior segments (black arrow in Fig. 7E), but are simple cords in the posterior segments (Fig. 7F). They are best

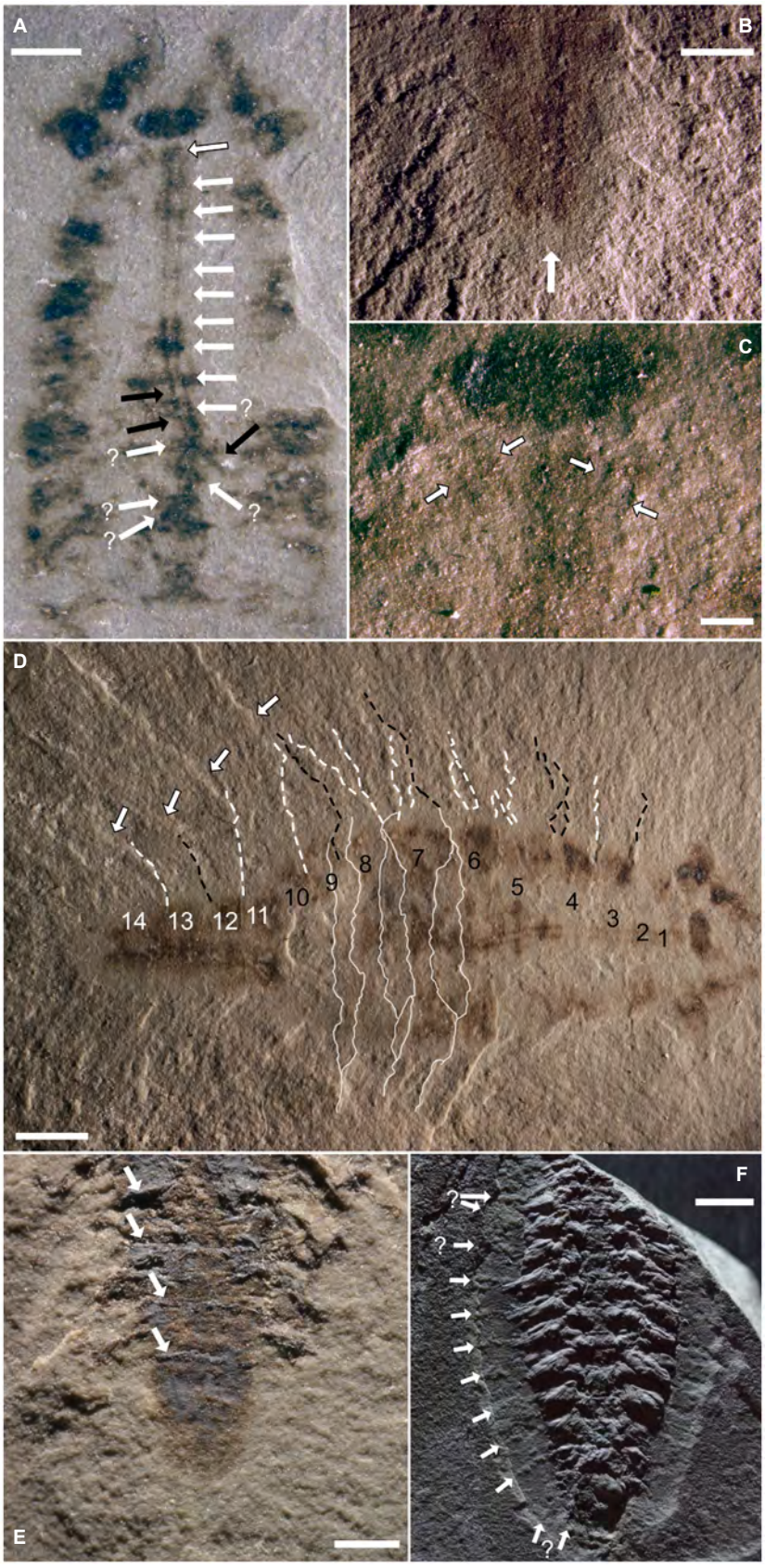
A
B
C
D
14
13
12
11
10
9
8
7
6
5
4
3
2
1
E
F

FIG. 6. Features that cross the head and trunk of *Parioscorpio venator* and of axial and tergopleural segmentation. A–D, features of the nearly flattened UWGM2764 with dark film preservation: A, head and anterior trunk showing the continuation of the gut beyond the head (Fig. 3E–F); white arrows in the trunk and a white arrow with a black outline in the head point to pairs of darkened patches that may be equivalent to the circles or rings in Figure 4A–C, or may represent digestive diverticulae; they become increasingly dubious posterior to the bend in the gut; black arrows point to this divergence to the right, probably severed during decay, posterior to the sixth segment; B, termination of the gut at the posterior of the specimen, visible as a faint mouldic impression under very low angle incident light; arrow points up the gut from its terminus; C, photograph taken under low angle light, showing the divergence of the putative nerve cords at the posterior head and anterior trunk; white arrows with black outlines point to the right and left boundaries of the right and left nerve cords; D, photograph taken under low angle light to demonstrate the tergopleurae of the trunk and how their width and structure relate to changes in the axial trunk's morphology; numbers indicate segment number, with those in the preabdomen black and those in the postabdomen white; plausible segment boundaries continuing into the tergopleurae are traced on the left side of the specimen by dashed lines (black lines indicate the posterior boundary of even-numbered segments while white lines indicate the posterior boundary of odd-numbered segments); arrows indicate putative pleural spines; because the specimen was not compressed perfectly perpendicular to bedding, there may appear to be multiple transverse divisions within a segment; these are traced in solid white on the boundaries between segments 6–9; this is also likely to account for the ambiguity of many tergopleural boundaries. E, posterior of UWGM2885a, demonstrating the relative length of the terminal axial segments; arrows demarcate the anterior boundaries of segments 11–14. F, low angle light photograph of UWGM2854a, showing the segmentation of the tergopleurae beyond the three-dimensionally preserved axial body; tergopleural boundaries on the left flank are indicated with arrows, and those that are less clear (three anteriorly, two posteriorly) are marked with '?'. Scale bars represent: 2 mm (A–B), 0.5 mm (C), 3 mm (D, F) and 1 mm (E).

seen in UWGM2793 (Fig. 7A, B), the part of UWGM2857 (Fig. 7C, D) and are visible in the flattened UWGM2764 (Fig. 6C). The width of the tubes matches trends in the width of the trunk somites: narrower anteriorly and posteriorly and widest medially (Anderson *et al.* 2021, table S2). These structures diverge anteriorly in the vicinity of the first trunk segment and continue into the posterior of the head (Figs 6C, 7G). Given their paired, ventral nature, we cautiously interpret these structures as nerve cords.

Morphology of the trunk. The axial region of the trunk of *Parioscorpio venator* consists of 14 somites, the shape of which is partly obscured in most of the specimens by the legs, which are usually three-dimensionally mineralized. Morphological features of the trunk itself are best preserved in one specimen, UWGM2764 (Figs 1C, 3E–F, 6A–D). In this specimen, no legs are preserved and the structure of the axial segment divisions are thus visible (Figs 1C, 6A, D). It is clear that trunk segment 1 is the shortest and transversely its axial portion is narrower than the head. Successive axial segments are wider and longer (segment 2 is 1.16 mm long and 6.66 mm wide), although the increase in size is subtle after segment 3, and maximum width for both the axial trunk and the entire axial body is achieved in the vicinity of somites 6 and 7 (segment 7 is 2.55 mm long and 10.08 mm wide; Anderson *et al.* 2021, table S2). The axial lengths of segments 8–13 are roughly equal, though shorter than segment 7 (segment 11 is 1.67 mm long). Transversely, the axial portion of segment 8 is narrower than 7, and the axial portions of segments 9 and 10 have lateral margins that are directed posteromedially (Figs 1C, 6D). The axial portion of the final four somites is considerably narrower than that of somites 1–10 (segment 11 is 5.34 mm wide). Segment 14 appears to be the longest on both UWGM2764 (Fig. 6B, D) and UWGM2885 (Fig. 6E), both of which are unobscured by legs on this final somite. Other specimens with legs show similar axial segment length and width trends, but the transverse contraction after somite 8 appears more gradual (e.g. Fig. 1A, B, E–G).

The dorsoventral shape of the axial body appears ovoid based on ring-shaped structures, probably representing unevenly compressed segment boundaries, seen in the middle trunk of UWGM2764 (Fig. 6D). Differentiating the tergites from the sternites, however, is difficult. On some specimens, spindle-shaped units with crescentic lateral boundaries may represent the sternites (Fig. 7H–I; Wendruff *et al.* 2018, fig. 1i; Wendruff *et al.* 2020*a*, fig. 2a). If so, they would be considerably narrower than the overlying tergites.

The pleural field is visible in several of the specimens, although it is usually subtle and without clear lateral margins. The tergopleural divisions between segments are best seen in UWGM2764 (Fig. 6D) and UWGM2854a (Fig. 6F) under low angle light, and also in UWGM2436 (Wendruff *et al.* 2018, fig. 1e–f), UWGM2437 (Wendruff *et al.* 2018, fig. 1l) and UWGM2575 (Wendruff *et al.* 2018, fig. 1i). They generally show increasing posterolateral deflection on successive segments. Unlike the sharp contraction in axial segment width seen between somites 8–11 in UWGM2764, the contraction in width of the pleural fields appears more gradual (Fig. 6D; Wendruff *et al.* 2018, fig. 1e–f) There is some suggestion of spines projecting posterolaterally off the tergopleural margins of posterior segments in UWGM2764 (Fig. 6D) and UWGM2436 (Wendruff *et al.* 2018, fig. 1f).

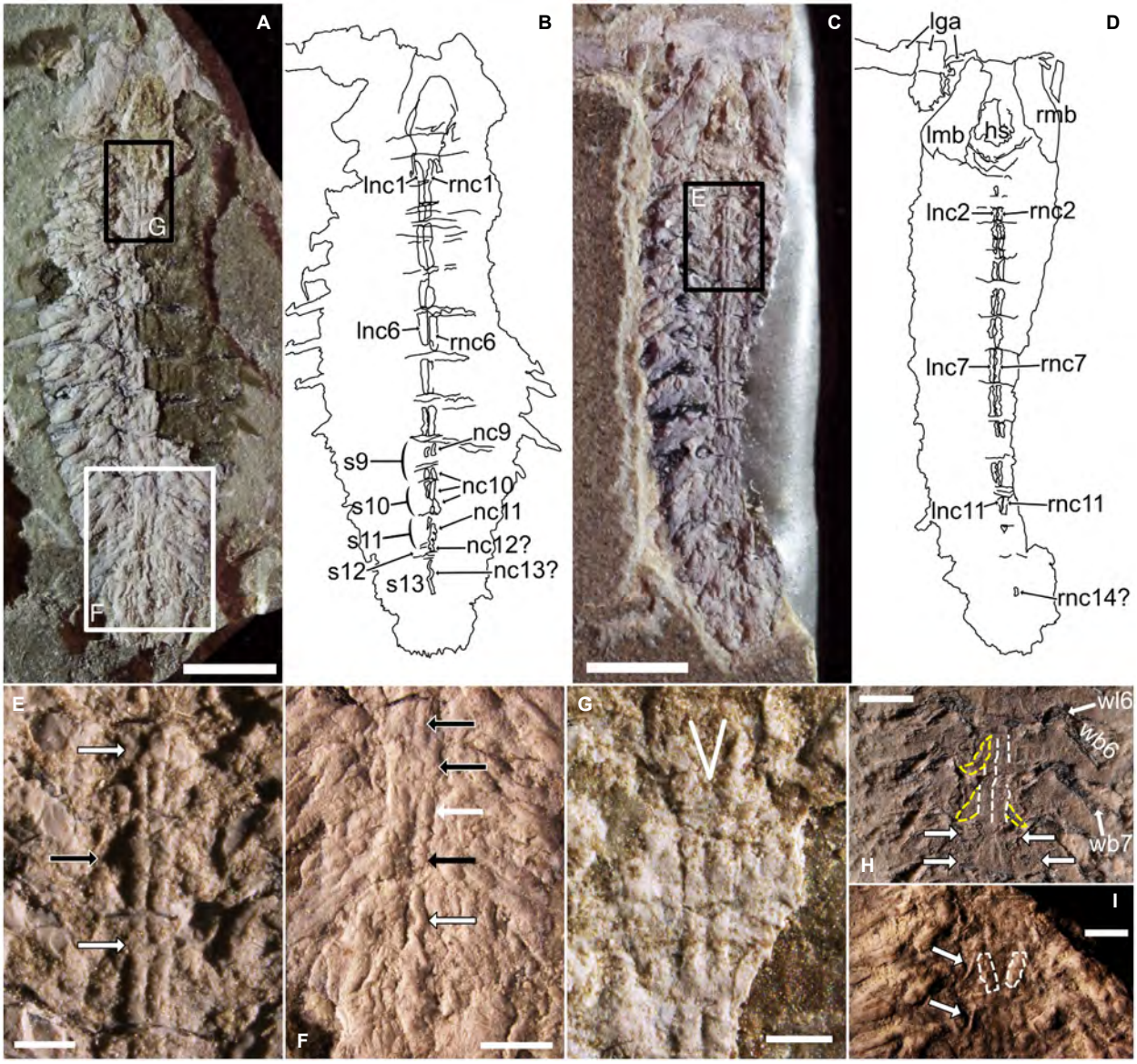

FIG. 7. Features of the nervous system and medial axis of *Parioscorpio venator*. A–B, photograph and interpretive drawing of UWGM2793, positions of enlargements F and G indicated on A. C–D, photograph and interpretive drawing of UWGM2857a; position of enlargement E indicated on C. E, paired nerve cords of segments 2–4; black arrow with white outline indicates slight anterior bulge interpreted as a pair of ganglia; white arrows with black outlines indicate where the ganglia should be but have been effaced, perhaps because of their slightly higher relief. F, nerve cords in the posterior of UWGM2793; the right cord appears better preserved and is traced out by arrows on segments 10 (black arrows with white outlines), 11 (white arrow), 12 (black arrow) and 13 (white arrow with black outline), becoming highly dubious posterior to this. G, anterior end of the nerve cords in UWGM2793; a white 'V' shows their divergence in the first segment, indicating the posterior of a possible oesophageal foramen. H, central trunk of UWGM2885b, demonstrating multiple types of impression on a single axial trunk segment, with the walking portions of some of the legs labelled for reference; on segments 6 and 7, the discernible impressions of the nerve cords (white dashed outlines) and crescentic-shaped structures (yellow dashed outlines) are highlighted, but they are visible on segments anterior and posterior to these, too; on segment 8, two pairs of circular or ring-like structures also observed in the head and anterior trunk are indicated (white arrows with black outlines; see Fig. 4A–C). I, anterior trunk of UWGM2854a with subparallel strap-like structures unlikely to be nerve cords highlighted (white dashed outline) on segment 3; crescentic structures that may indicate the borders of the sternites are indicated (white arrows with black outlines) and may be uncompressed homologues of the structures highlighted in H. *Abbreviations*: prefix r or l, indicates right or left of some elements; hs, hypostome; lga, left great appendage elements; mb, muscle block (r/l); nc, nerve cord of segment (1–14; ? indicates less confident assignment to segment; r/l); s, segment (9–13); wb, walking leg bundle (6, 7); s, segment (9–13); wl6, walking leg 6. Scale bars represent: 3 mm (A, C), 0.5 mm (E, G), 2 mm (F) and 1 mm (H–I).

The trunk legs are visible and preserved to varying degrees in most specimens (Figs 1, 2, 8, 9). They are usually three-dimensionally mineralized, often robustly so, to the point that their structure can be difficult to determine and smaller or less-mineralized components of the legs are obscured. The legs of somites 1–12 have the same basic components. Basally the leg has a basipod, which may consist of a single solid unit (Fig. 8A, B), or it may have one to several lobes along its length (legs 6–8 in Fig. 9B, C, legs 3, 5–7 in Fig. 9E). Towards its distal end, the basipod has an endite bearing a series of relatively short filaments, forming a bundle with a lobose shape (legs 2–9 in Fig. 8A, B; legs 10–12 in Fig. 8C, D; legs 4–8 in Fig. 9B, C; legs 3–6 in Fig. 9E).

Distal to the basipod, the leg then splits into an exopod and an endopod. The number of podomeres on the exopod is difficult to determine (there may be at least 10, based on leg 4 in Fig. 9E), and in many cases the exopod appears as a simple rod (leg 2 in Fig. 8A, B; leg 12 in Fig. 8C, D; legs 5–7 in Fig. 9B, C). In a few legs, distally the exopod bears anterolaterally to posterolaterally oriented filaments in one or multiple bundles (legs 6 and 7 in Fig. 8A, B; probably legs 4 and 8 in Fig. 9B, C). More typically, the exopods may bear grooves along their length (legs 10 and 11 in Fig. 8C, D; legs 4–6 in Fig. 9E). Whether these grooves are elongate filaments or a preservational artefact is difficult to determine.

The endopod is complex and consists of a series of podomeres, presumably used for walking, and a basal exite that forms the most distinctive component of the leg. The walking portion of the endopod is usually largely hidden by other components of the legs (legs 6 and 7 in Fig. 8A, B) or is simply poorly preserved (e.g. legs 10–12 in Fig. 8C, D). On UWGM2885, however, the walking portions of the endopods are clearly visible (legs 3–7 in Fig. 8G; legs 3–7 in Fig. 9D). There appear to be around six or seven podomeres, but the number is not clear. The trend of the walking endopods is roughly perpendicular to the body axis, with a sharp posterior bend in the terminal one or two podomeres. The walking leg tip is generally not well preserved, but when it is (Fig. 4D), it terminates in a single, stout claw. On many of the walking legs, a filamentous bundle seems to originate on the second or third podomere and expands posterolaterally. Preserved in UWGM2885 as a black film with thin bluish coats (Figs 8G, 9D) these bundles are preserved in three-dimensions in other specimens, even if the walking legs to which they correspond are not. This is especially evident in UWGM2854 (legs 4–7 in Fig. 9B, C; legs 3–6 in Fig. 9E), where the filamentous bundle can be seen largely tucked behind components of the endopod exite.

The endopod exite has three filamentous bundles, although its segmentation or annulation is dubious. The basal bundle is longest and projects beyond the axial margins of the trunk, particularly in legs 5–8 (Figs 8A, B, 9A–C, E). These filamentous bundles are racemose in shape and the apical tip is occasionally broken off (legs 3–7 in Fig. 8A, B). Alternatively, some of these could be displaced walking leg tips (e.g. legs 4–6 in Fig. 9B, C; perhaps legs 6–7 in Fig. 9E). The racemose bundles are both distinct in shape and often preserved, so their transverse width makes for a good proxy of total leg size for somites 1–12 (e.g. compare the 'racemose bundle width' values for UWGM2793 and 2854 in Anderson *et al.* (2021, table S2) to the trends in leg size seen in Fig. 8A–D for UWGM2793 and Fig. 9A for UWGM2854a). Like the legs themselves, the racemose bundles increase in size quickly to leg 3, then increase in size slowly to a maximum width between somites 6–8, then decrease in width to somite 12.

The two apical bundles are sublanceolate to lanceolate in shape and 'sheath' around the racemose bundle. The first, the anterior sheathing bundle, is quite small, often poorly preserved and directed anterolaterally (legs 4, 6–8 in Fig. 8A, B). The second, larger and more prominent posterior sheathing bundle is directed posterolaterally (legs 3–4, 6–9 in Fig. 8A, B; perhaps legs 10–12 in Fig. 8C, D; legs 4–8 in Fig. 9B, C; legs 3–7 in Fig. 9E).

The structure of legs 13 and 14 (Fig. 8E) appear to consist of a primary ramus of two ranks of parallel, posteriorly directed filaments (Fig. 8F, p#). Towards the base of the legs are at least two accessory rami with two ranks of smaller filaments directed perpendicular or subperpendicular to the ramus axis (Fig. 8F, a#).

Another feature of the legs worth mentioning is the presence of small straps of material that cross posterolaterally from the body axis adjacent to the nerve cords towards the trunk legs. Sometimes, a secondary, anterolaterally trending set is also present. These are seen on multiple specimens, but are best developed on UWGM2793 (Fig. 8A, B, labelled 'lt' on Fig. 8B). Whether they originate on the body axis and extend into the legs, or vice versa, is unclear, although when they are preserved they can be highly distinctive.

The caudal termination of *Parioscorpio venator* may be buried, obscured by legs, or simply poorly preserved (Figs 1A, B, D–G; 2A, B, E; 7A–D; 8E, F). When evident, the terminus appears as either a simple semicircle (Figs 1C, I, J; 6D, E) or as a distinct, three-pronged apparatus (Figs 2F, 9F; Wendruff *et al.* 2018, fig. 1e–f, i, k–l). The three processes are of approximately equal length, with the central process separate from and dorsal to the two lateral processes (Fig. 9F). The central process is probably the true telson, while the lateral processes are separated from the fourteenth segment by a curving suture (Fig. 9F). Since segment 14 lacks pleural spines (Fig. 6D), these lateral processes may reflect the posteriorly directed tergopleurae of the terminal somite, rather than furcae or caudal rami (*sensu* Aria & Caron 2017*a*).

Remarks. Though *Parioscorpio venator* is not a rare component of the Waukesha biota, its morphology is sufficiently chimerical (Fig. 11) that, even with evidence from multiple specimens, its characters defy ready homologization with established arthropod groups. Before proceeding to elemental analysis of the fossils' composition and phylogenetic analysis of the species' affinities, we first present an overview of the preservational habits of *P. venator*, then consider some of the more unusual morphologies of the organism in greater detail. We examine

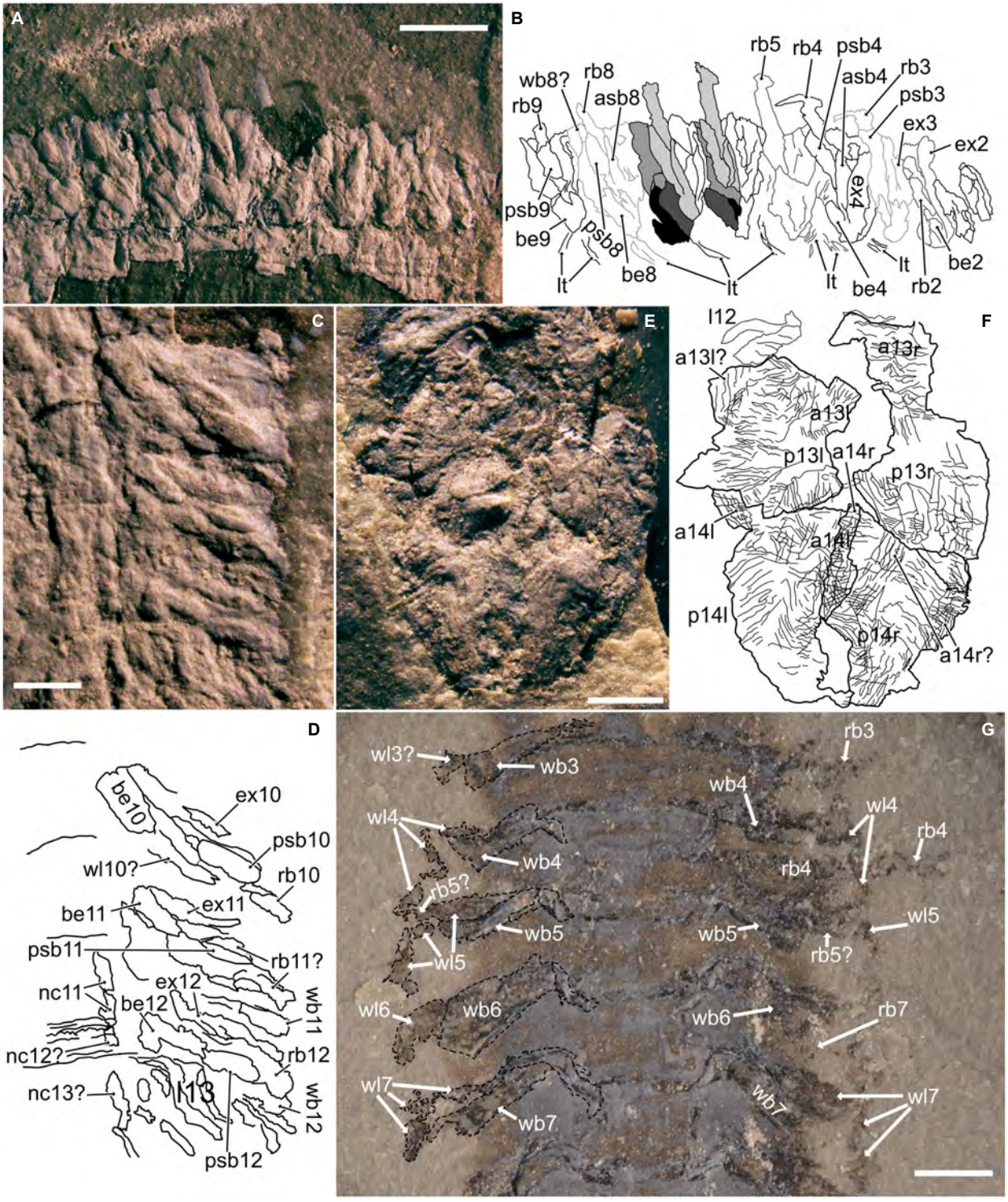

FIG. 8. Features of the legs of *Parioscorpio venator*. A–B, photograph and interpretive drawing of the first nine left trunk legs of UWGM2793; B, key units are labelled in legs 2–5, 8 and 9, with successive legs outlined in different shades of black and grey to aid in differentiation; legs 6 and 7 are shaded according to leg unit: black shading denotes the basipod, dark grey the basipod endite, medium grey the walking portion of the endopod, light grey the endopod exite, and white the exopod. C–D, photograph and interpretive drawing of right legs 10–12 of UWGM2793; some structure of leg 13 appears visible, but is ambiguous. E–F, photograph and interpretive drawing of hind legs 13 and 14 of UWGM2857a; heavy outline denotes the boundary of the legs and their respective filaments; the thinner lines denote filaments of primary and accessory rami. G, photograph of legs 3–7 of UWGM2885a, which preferentially preserves the walking portions of the endopods; the left flank is traced with major units labelled, while the more poorly preserved right flank only has easily discernible major units labelled. *Abbreviations* r or l, as suffix, indicates right or left of some elements; a, accessory filamentous ramus of posterior leg 13 or 14 (r/l); asb, anterior sheathing bundle of leg (4 or 8); be, basipod endite of leg (2–12); ex, exopod of leg (2–12); l, leg elements of somite (12 or 13); lt, potential tendon or muscle of legs; nc, nerve cord of segment (11–13); p, primary filamentous ramus of posterior leg (13 or 14; r/l); psb, posterior sheathing bundle of leg (3–12); rb, racemose bundle of leg (2–12); wb, walking leg bundle (3–12); wl, walking leg (3–10); ?, uncertain assignment of leg or nerve cord unit. Scale bars represent: 2 mm (A), 0.75 mm (C, E) and 1 mm (G).

alternative interpretations of these morphologies where appropriate in an attempt to resolve where in the arthropod family tree this species may fit and where it cannot. Consequently, we also evaluate how the morphology of *P. venator* is incompatible with its initial placement in Scorpiones by Wendruff *et al.* (2020*a*).

The preservational pathways expressed in the specimens vary somewhat, even within individuals. Many specimens preserve considerable quantities of soft tissue as a partially three-dimensional, white to blue material (e.g. Fig. 1A) previously interpreted as calcium phosphate (e.g. Jones *et al.* 2015). On companion pieces, or when removed by erosion, these leave dark coloured mouldic depressions (compare Fig. 1D, E). A separate preservation habit of limited patches of shiny, black, compressional material (best seen in Fig. 1A, D, J) has been interpreted as being carbonaceous (e.g. Wendruff 2016). Specimens with a substantial phosphatic composition may be somewhat three-dimensional (Figs 1A, B, D–H, 2A, B, D, F) or slightly three-dimensional (Figs 1I, J, 2C, E). On the other hand, phosphate-poor specimens, such as UWGM2764 (Fig. 1C), which is preserved as a dark film with virtually no phosphate, are nearly completely flattened.

Features of the head. The first morphology to consider is probably the most noticeable aspect of the animal: the great appendages projecting forward from the body. The notion of what constitutes a 'great appendage' has shifted with time (see the introduction of Aria & Caron 2015) and despite attempts to create a scenario of homology for the spectrum of great appendages (Haug *et al.* 2012*a*), it is becoming increasingly evident that at least some 'great appendages' are analogous to one another (e.g. Fu *et al.* 2011; Cong *et al.* 2014; Aria & Caron 2015). They can even evolve *de novo* in lineages, as in the artiopod *Kodymirus vagans* Chlupáč & Havlíček, 1965 (Lamsdell *et al.* 2013). If 'frontalmost pairs of appendages' that are 'more spinose and prehensile . . . [are] broadly referred to as "great appendages"' (Aria & Caron 2015, p. 2), then the first appendages of *P. venator* may certainly be thought of as great appendages, although they are unusual in bearing only four articles, a single sub-chelate termination and a reduced, y-shaped first article (Figs 4D–H, 5A–D, 11B, 12A).

The reason for this shape is a consequence of its function: rather than being optimized for articulation against succeeding elements within an appendage, as in most great appendages (Haug *et al.* 2012*a*), the great appendages of *P. venator* articulated toward one another, probably to hold prey in a vice (Fig. 12B). The entire structure of the head and great appendage has been modified to facilitate this movement. If the great appendage is reconstructed such that the reduced first article is just anterior to the oval depressions underneath the trapezoidal muscle blocks (Figs 4H, 11A), then this article can serve as an articulation point for the muscles held in the head (Fig. 5E, F). In fact, the observed y-shaped first article is probably just the sclerotized portion of a more extensive and membranous first element that escaped preservation in the available specimens (Fig. 11B). The membranous portion would have stretched from the posterior end of the oval depressions and loosely enveloped the sclerotized y-shaped structure. A membranous cuticle would be necessary to facilitate the broad range of movement needed to bring the great appendages together (Fig. 12B); when the muscles contracted against the medial portion of the first article, the entire great appendage would swing inward. When the muscles were contracted against the distal portion of the first article, the appendages would swing back out. A range of movement of at least 90° would be easily possible, and when working with the subchelate motion of the terminal and penultimate articles (Fig. 12A), the great appendages would be capable of quickly and effectively seizing prey items.

The closest analogues to these raptorial appendages are not found in the great appendage arthropods of the Cambrian, but in the true bugs of Nepomorpha (Borror & White 1970; Carver *et al.* 1991), specifically the giant water bugs (Belostomatidae), water scorpions (Nepidae),

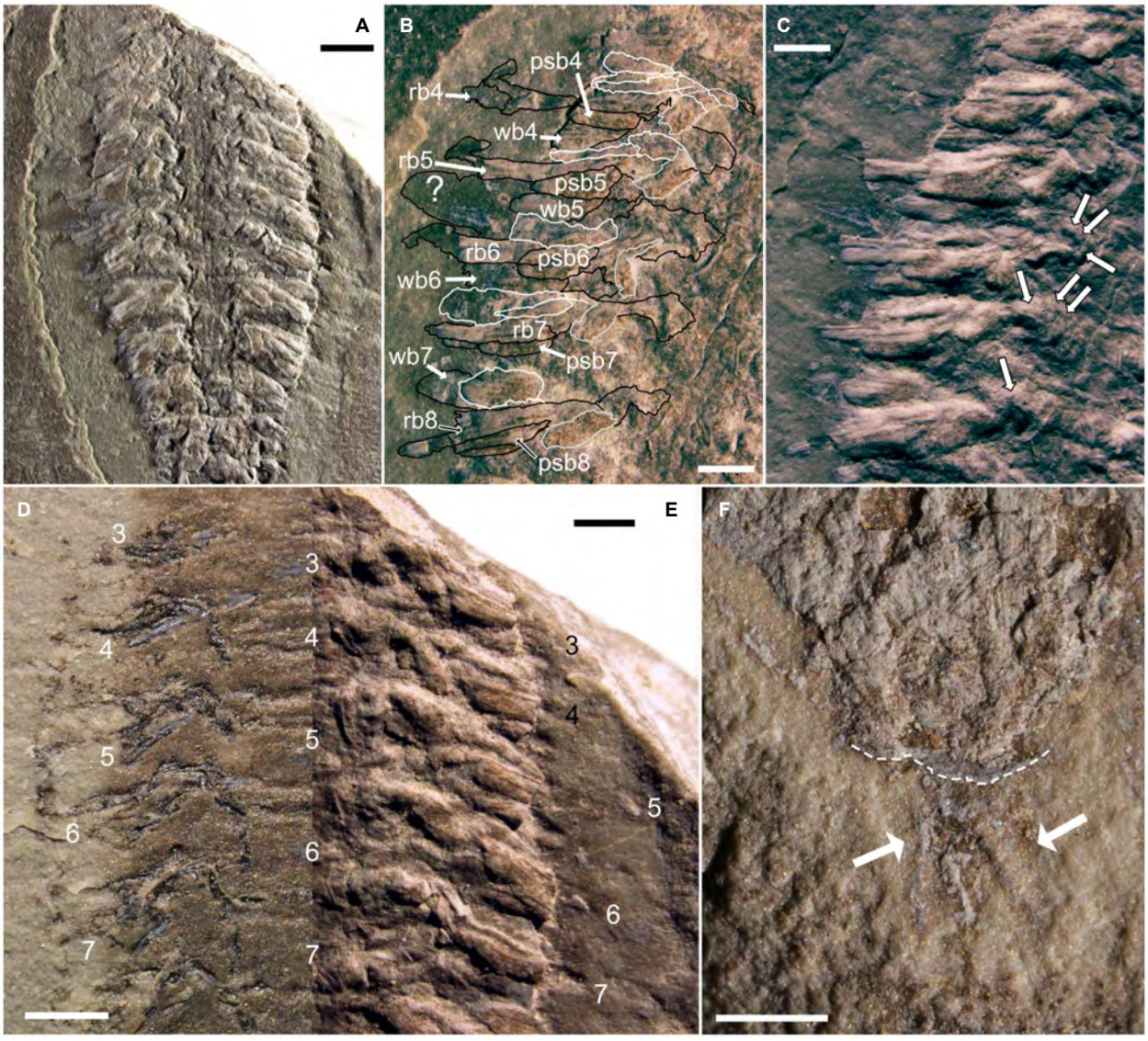

FIG. 9. Features of the legs and posterior terminus of *Parioscorpio venator*. A–C, preservation of the highly three-dimensional legs of UWGM2854a: A, overview of the specimen; B–C, photographs of left legs 4–8 in normal and low-angle incident light, respectively; B, with shading-coded outlines of the major leg units superimposed: black indicates the basipod and all portions of the endopod (major units of the endopod labelled), light grey indicates the basipod endite, white indicates the exopod, and the black outline with a '?' in its centre is an anomalous unit which may be displaced from elsewhere; C, arrows point to lobes in the basipods. D–E, photographs that contrast legs 3–7 of UWGM2885b, which preferentially preserves the walking portions of the endopods, and UWGM2854a, which preferentially preserves the filamentous bundles of the legs; numbers indicate segment number (centre rank), the best-preserved portion of the indicated leg (left rank), or the racemose bundle of the indicated leg (right rank); for the right rank, the number is to the right of the racemose bundle tip for legs 3–5 and between a break in the length of the racemose bundle for legs 6 and 7. F, features of the posterior of UWGM2796, including the trifurcate caudal apparatus and the fan-like filaments of appendage 14 that flank the anus; dashed white line highlights the suture separating segment 14 from the lateral processes; arrows indicate the lateral processes themselves. *Abbreviations*: rb, racemose bundle of leg (4–8); psb, posterior sheathing bundle of leg (4–8); wb, walking leg bundle (4–7). Scale bars represent: 2 mm (A) and 1 mm (B–F).

toad bugs (Gelastocoridae) and creeping water bugs (Naucoridae). In Nepomorpha it is the first thoracic appendage that has evolved to be a typical insect raptorial appendage (Gullan & Cranston 2010, p. 346) with the third and fourth podomeres (that is, the femur and tibia) designed to articulate against one another to grasp prey. At rest, the raptorial appendages are held out laterally in front of the head in a position similar to *P. venator*. Most

of these true bugs are moderately dorsoventrally flattened ambush predators in ponds and lakes, and use their raptorial appendages to catch insects, or even vertebrates (Borror & White 1970). The analogous development of body shape and raptorial appendages between *P. venator* and Nepomorpha can reasonably be inferred to reflect adaptation to a predatory lifestyle in a vertically restricted aquatic environment, that of the former being a marine to brackish intertidal setting (Kluessendorf 1990).

Oversized cephalic appendages do not always function for predatory purposes; for instance, the large, sexually dimorphic antennae of male anostracans (McLaughlin 1982) are used for clasping onto females. Of the specimens of *P. venator* with a well-preserved anterior head, all appear to have the great appendages. However, although they appear to be more slender on some of the smaller specimens (e.g. compare Figs 2C and 10A to 2D), our sample size is simply not large enough to determine if this is dimorphic, allometric or taphonomic in nature. For example, comparing the head dimensions and great appendage article dimensions of UWGM2793, 2798 and 2857 (Anderson *et al.* 2021, table S1) reveals little evidence for consistent size relationships.

A second matter for consideration is the head somite to which the great appendage belongs, as this has significant bearing on the arthropod clades to which *P. venator* may be associated. Among extant arthropods, the chelicerae of Chelicerata and the antennule antennae of Mandibulata have been conclusively demonstrated to be deutocerebral (e.g. Strausfeld 2012). Accepting the hypothesis of Chen *et al.* (2004) and Haug *et al.* (2012*a*) that chelicerae are modified short-great appendages, Megacheira bear deutocerebral appendages too. The supposed deutocerebral innervation of the great appendage of *Alalcomenaeus* sp. demonstrated by Tanaka *et al.* (2013) has supported this hypothesis for the megacheirans, but brain-based evidence is, understandably, rare in the fossil record (Ortega-Hernández 2015) and not without controversy (Liu *et al.* 2018).

A suitable proxy is the placement of the great appendage with respect to the mouth, or the hypostome that covers it, as the mouth is associated with the deutocerebrum and tritocerebrum, such that appendages anterior or anterolateral to the mouth are deutocerebral, and those that are immediately posterior or posterolateral to the mouth are tritocerebral (Scholtz & Edgecombe 2005; Yang *et al.* 2013). Thus, the first limbs of species like *Oelandocaris oelandica* have confidently been assigned as 'antennular' (i.e. deutocerebral; Stein *et al.* 2005), the 'specialized post-antennal appendages' of *Fuxianhuia* and *Chengjiangocaris* as tritocerebral (Yang *et al.* 2013; but see Budd 2002 for an alternative interpretation) and the great appendages of the artiopod *Kodymirus vagans* as tritocerebral (Lamsdell *et al.* 2013). Appendages that insert anterior to even the eyes may be interpreted as protocerebral (Yang *et al.* 2013; Cong *et al.* 2014; Aria & Caron 2017*a*). In the case of *P. venator*, the insertion point for the great appendages appears to be either beneath the eyes (Figs 3A–D, 4D–H) or just posterior to them (Fig. 5E, F), but in either case are anterior or anterolateral to the hypostome. This suggests strongly that the anteriormost great appendages are, in fact, deutocerebral.

The placement of the lateral eyes is another morphological feature that merits discussion, as it is difficult to tell whether the eyes of *P. venator* are anteriorly oriented above the great appendages but below the head shield, or embedded within the head shield and expressed dorsally. Dorsally embedded eyes occur throughout Arthropoda, but tend to be typical of the artiopods and chelicerates (Scholtz & Edgecombe 2005; Lerosey-Aubril *et al.* 2017) and are not found among the megacheirans (Hou & Bergström 1997). Since no specimens of *P. venator* have yet been found preserved laterally, it is not possible to determine their placement precisely. The reconstruction of Fig. 11A is purposefully ambiguous in this regard, suggesting that the eyes may leave an impression in the head shield, but not necessarily be embedded within it. Not even the ring of ommatidia in UWGM2793 (Fig. 3A) presents a conclusive interpretation. This ring may be suggestive of laterally oriented 360° vision that would only be useful if the eyes were above the level of the body, or a ventrolaterally oriented eye could have been compressed into a lateral position during taphonomic compaction.

A final feature of the head involves the number of somites that constitute the head tagma, and whether it even is a true tagma. With the possible exception of *Fuxianhuia* and its relatives (Yang *et al.* 2013), euarthropods have at least five cephalic somites: an ocular somite and four posterior ones that, at least plesiomorphically, bear appendages (Scholtz & Edgecombe 2005; Stein 2013; Liu *et al.* 2016; Dunlop & Lamsdell 2017). *Parioscorpio venator* seemingly defies this by preserving only two appendages on its head, which, assuming an ocular anteriormost somite, brings the total to three. Although we prefer a biramous interpretation, it is possible that the second cephalic appendage is actually two uniramous appendages, as there is no definitive evidence of a basipod and, with the possible exception of UWGM2793 (Figs 3A–B, 5A–B), there is little convincing evidence of much overlap between the two elements, as would be expected of rami sharing a basipod (unless they have separated insertions, as in the prosomal endopods and exopods of *Offacolus kingi* and *Dibasterium durgae* Briggs *et al.*, 2012; Sutton *et al.* 2002; Briggs *et al.* 2012). Even so, this would only bring the total somites up to four. However, as noted in the Redescription, above, there is a possibility that the cephalic shield extends over the first


A
B
C
1
2
3
4
4
D
E

FIG. 10. Additional specimens and perspectives of interest of *Parioscorpio venator*. A, UWGM2827a, a relatively poor-quality specimen preserved in a thicker bed of dolosiltstone, unusual for *P. venator*; the cephalic muscle blocks and great appendages appear to be more slender than in many specimens. B, UWGM2858a, an incomplete and highly selectively preserved specimen whose overall size and segment dimensions are compatible with better-preserved specimens of *P. venator*; the curved, kerogenized straps, in particular, bear a striking similarity to the potential leg muscles or tendons shown in Figure 8A–B (lt); presumed anterior oriented up. C, the filamentous fan-like rear limbs of UWGM2857a, illuminated from a different angle than in Figure 8E; the primary filamentous rami are outlined (boundary hidden in shadow traced with a dashed line). D–E, UWGM2764 and UWGM2163, respectively; UWGM2163 was designated the paratype of *P. venator* by Wendruff *et al.* (2020*a*) and UWGM2764 was subsequently found to be its counterpart; D, all noticeable boundaries outside the axial body traced (compare to Fig. 6D) with the likely pleural field border marked by a heavy trace (dashed where uncertain); arrows point to pigment patches, the accompanying numbers indicating the segment to which they belong; E, reproduced from Wendruff *et al.* (2020*a*) with noticeable boundaries traced (axial body in white, pleural field in heavier black line, tergopleural segment boundaries in dashed black line); black arrows with white outlines indicate the two segments counted in Wendruff *et al.* (2020*a*) as a single segment; white arrow with black outline indicates the posteromedial corner of a feature seen as a rectangular coxa in Wendruff *et al.* (2020*a*, fig. 1d); as can be seen, the 'rectangle' is made of several components occupying slightly different topographical levels (black lines lateral to arrow). Scale bars represent: 5 mm (A), 2 mm (B–C), and 4 mm (D–E).

one or two trunk segments (Figs 6D, F, 11A), such that they may belong to the 'head'. Indeed, the legs of the first two 'trunk' somites appear to be smaller versions of those on subsequent trunk somites, a feature seen in the post-great-appendage head limbs of Megacheira (e.g. Liu *et al.* 2007). If the first two trunk-like somites are incorporated into the head, this would probably require the head to be interpreted as a pseudotagma (*sensu* Lamsdell 2013), as there is no differentiation in limb series between the head and trunk, excepting the great appendage and its following appendage (an allowable exception; e.g. Lamsdell 2013, fig. 1b).

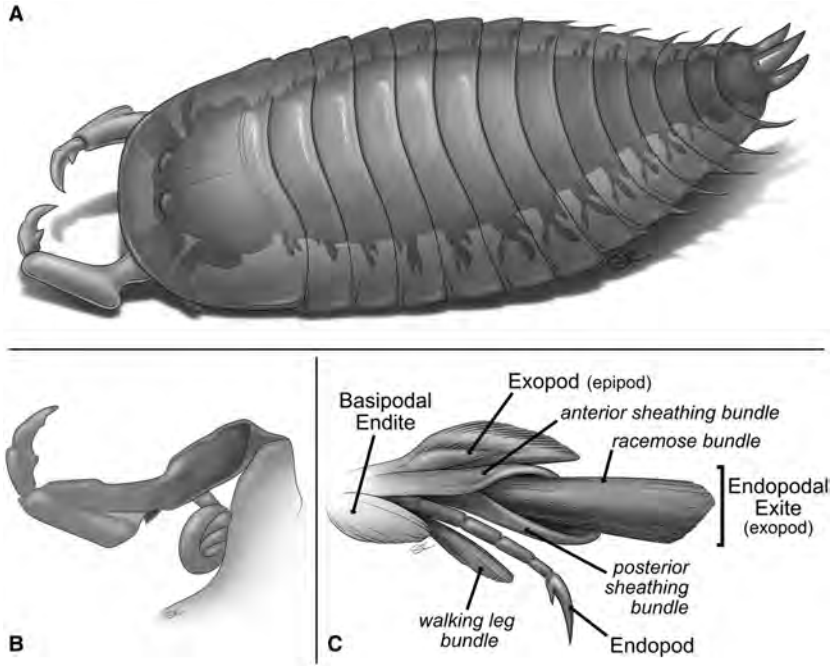

FIG. 11. Reconstructions of the morphology of *Parioscorpio venator*. A, whole body, from a three-quarters dorsal view; note that the limbs can be seen through the thin, translucent tergopleural cuticle; the tentative preservation of the tergopleurae in most specimens raises this possibility. B, focus on the great appendage and second cephalic appendage and their attachment to the head; the reconstruction shows slight lateral displacement of the limbs to better envision their bases; note that the sclerotized portion of the first article of the great appendage is contained within a translucent membrane. C, illustration showing our reconstruction of a standard trunk limb; limb rami are labelled in roman (with alternative interpretations in smaller font), while individual filamentous bundles on the endopod and endopodal exite/exopod are labelled in italics; the exact proportions of the limb components vary based on the limb's placement on the body; this illustrated limb, with the racemose filamentous bundle considerably longer than the exopod/epipod or the walking portion of the endopod, is from the middle of the trunk.

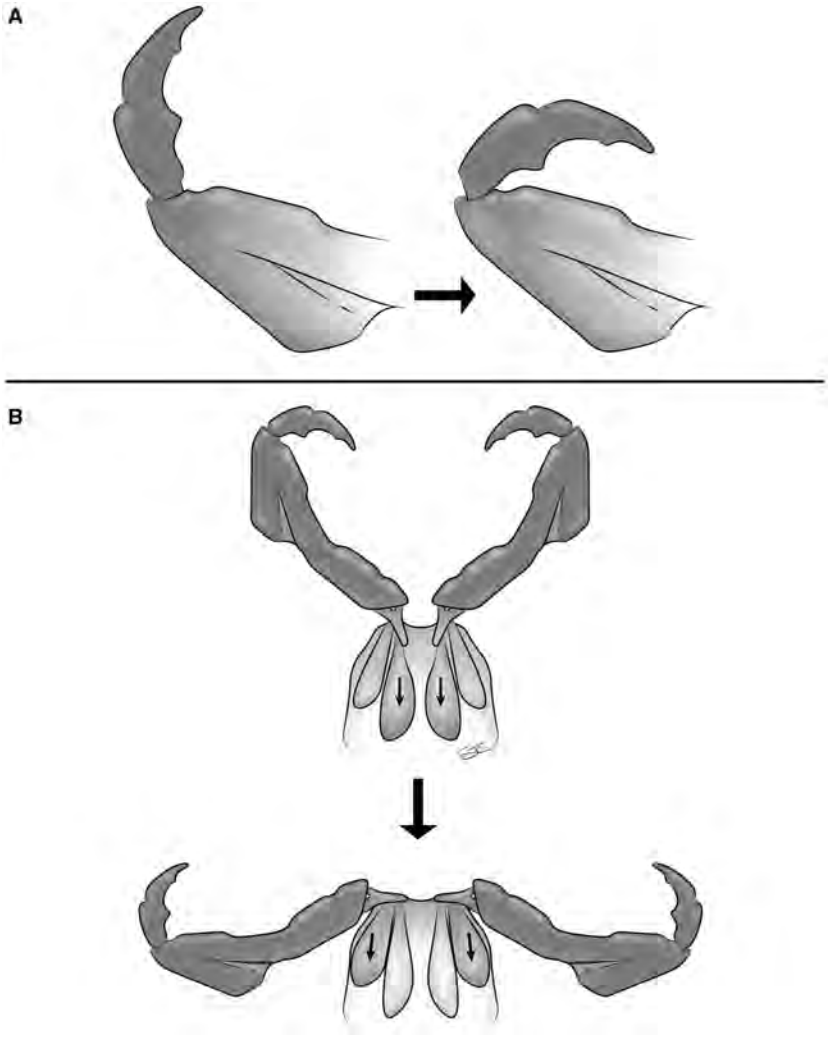

FIG. 12. Reconstructions showing operation of the components of the great appendage. A, subchelate function of the fourth great appendage article against the third great appendage article; this action may have been useful in adjusting the grip on captured food items. B, an illustration of the main raptorial motion of the great appendages, coming together in front of the head beyond the margin of the head shield; flexion of the head muscles on the inner edge of the first great appendage article causes the great appendage to swing forward and adaxially; flexion of the head muscles on the outer edge of the first great appendage article causes the great appendage to swing backward and abaxially.

Nonetheless, because the axial segmentation remains distinct in the first two trunk-like somites, we prefer to consider them part of the trunk and analyse them as such. A clue to the fate of the other cephalic limbs may be found in the circular structures that can be seen in the head and the trunk segments of some specimens (Figs 4A–C, 7H). These may be impressions of internal muscle attachment sites or apodemes. Indeed, the locations of the anterior pair of circles in the trunk segments (Figs 4A, 7H) matches closely to the origins of the posterolaterally directed straps preserved in some specimens (Figs 8A–B, 10B). These latter features compare favourably to the 'apodemal rods' of *Apankura machu* Vaccari *et al.*, 2004 (Vaccari *et al.* 2004, fig. 1), and thus could be interpreted as tendons or apodemal extensions related to movement in the legs or to flexure of the body, anchored to the circular structures.

Within the head, there may be between five to nine pairs of circular structures along the axis between the two muscle blocks. Assuming two per somite, as in the trunk (Fig. 4A), this would suggest structures that belonged to 2–4 original head somites. The 'extra' pair may belong to a reduced somite; notably, the two 'brace structures' seen as the impression of a head tergite have only one pair of circles between them (Figs 3C–D, 4A). Although not definitive evidence, these paired circular structures suggest there were ancestrally more cephalic segments in *P. venator*, in line with what is expected in a euarthropod. The boundaries of these somites, excepting those defined by the brace structures, may have been obliterated due to the enlargement and specialization of the muscle blocks that operate the great appendage. This would also mean the head is a true tagma, defined by extensive modification of the first two limbs and their musculature and loss of the subsequent ones. Nonetheless, because the total number of head somites cannot be conclusively determined, this character is coded ? in the phylogenetic matrix (Anderson *et al.* 2021, appendix S1).

Features of the trunk. The trunk legs are arguably the most specialized morphology in *Parioscorpio venator*. For many stem-group euarthropods, while there are minor variations in traits like endopod armature, exopod setae shape and podomere number between clades, the post-frontalmost legs appear broadly similar: the exopod consists of a broad, lobose or rod-like ramus with few podomeres, the endopod is well-developed, often spiny and with many podomeres, and the shared basipod is usually gnathiferous (Edgecombe & Ramsköld 1999; García-Bellido & Collins 2006; Liu *et al.* 2007; Haug *et al.* 2012*a*; Stein 2013). The anterior trunk appendages of *P. venator* retain their biramous nature (Fig. 11C) but show modifications more akin to the panoply of forms found in Crustacea (e.g. McLaughlin 1982; Siveter *et al.* 2017) and can potentially be interpreted in a manner more typical of crustaceomorph taxa. For example, the basipod subdivision in UWGM2854 (Fig. 9C) would constitute strong evidence in favour of a crustaceomorph interpretation (Aria & Caron 2017*a*), although it is not clear that these are authentic features. They are not preserved in, for example, UWGM2793 (Fig. 8A, B). The basipod endite is unusual for an endite in that it bears filaments that form a setose bundle (best seen in Fig. 8A–D), rather than stout setae or dentition (Aria & Caron 2017*a*, fig. 2d, f–g). It also does not appear to originate on the ventral side of the basipod, but rather posteroventrally (Fig. 9B, C; note how the tilted limbs make them appear almost dorsal on Fig. 9E).

Distally, the anterior trunk legs contain a further four rami, and it is not certain whether the next-distal ramus constitutes the exopod (our preferred interpretation, and labelled as such on Figs 8, 9), or a large, distally oriented epipod (Fig. 11C). For an epipod, its origin would be fairly distal on the basipod, but this is found in extant crustaceans (e.g. the 'pseudepipod' of Cephalocarida, McLaughlin 1982, fig. 9e), as are epipods comparable in size to the 'main' rami (e.g. Boxshall & Jaume 2009, fig. 4; Siveter *et al.* 2017, fig. 3). Such an interpretation would allow for the endopodal exite to be seen as an exopod instead. This would make for an unusual exopod: stenopodous with sheathing bundles of filaments and a long racemose bundle made of stiff filaments terminating beyond the lateral edge of the body axis. Yet, seeing this ramus as an endopodal exite is an unusual feature too; the sausage-shaped exites on the limbs of *A. pisiformis* offering a rare comparison (Müller & Walossek 1987, fig. 4; pl. 24, fig. 1).

Determining which of these interpretations is correct, exopod/endopod exite or epipod/exopod, is contingent on resolving the nature of the separation of the endopod exite/exopod from the walking portion of the endopod. If the former splits from the latter, an endopod exite interpretation is supported, but if both split from the basipod, then they are clearly different rami and the exopod interpretation is supported. Unfortunately, only the tips of a few racemose bundles are distinctly preserved on UWGM2885, which preserves the best walking legs, and so the nature of their joining cannot be discerned (Figs 8G, 9D). On legs 6 and 7 of UWGM2793, it appears that the base of the walking leg and the endopod exite/exopod diverge distal to the basipod and would originate at about the same point on the basipod, (Fig. 8A, B), supporting an endopod exite interpretation, but this is not unequivocal. What does appear clear is the emergence of a final, ventrally-oriented filamentous bundle emerging as an endite on the walking legs (best developed in Figs 8G, 9D). This is an unusual feature and its purpose is not immediately apparent; it may have served a tactile sensory function.

The final two somites of the trunk bear appendages that are very different from the rest of the body, and the fan-like shape assumed by the filaments of their rami (Figs 8E, F, 10C) bears a striking resemblance to the uropods of some malacostracans. However, there are few other features on *P. venator* that would suggest an affinity with a clade as advanced as Malacostraca. Instead, this is more likely to be a case of convergence similar to the remarkably uropod-like limbs on the last 'abdominal' somite of *Sidneyia inexpectans* (Bruton 1981). In malacostracans, uropods vary in number and form, but usually serve a locomotory function, particularly for making quick escapes (McLaughlin 1982). We suspect that the final two pairs of limbs served a similar role in *P. venator*, perhaps in making sudden lunges to capture prey or elude predators. The partial overlap of the final limb pair on the anus suggests they may have helped to clear away fecal material as well (Fig. 9F).

The division of the trunk into further tagmata or pseudotagmata is problematic, in spite of these uropod-like posteriormost limbs, as distinctive changes in the structure of the limbs and exoskeleton do not align in somite placement. First, although the fan-like limbs show a significantly different morphology to the anterior trunk limbs, they probably do not define a third tagma since they are confined to the two posterior somites (Lamsdell 2013). Additionally, although there is a marked constriction in the transverse width of the axis from trunk somites 8 to 11, such that somites 11 to 14 are markedly narrower, we only tentatively designate this as a pseudotagma, since the constriction in width through these segments is much more gradual in the tergopleurae (Fig. 6D). Finally, the first appearance of potential pleural spines does not coincide with either the axial constriction or the fan-like posterior limbs, and may be found as anteriorward as segment 7 or 8 (Wendruff *et al.* 2018, fig. 1e).

The final feature on the trunk for which an alternative interpretation may be considered is the pair of lateral

processes flanking the telson. Above, we interpreted these as the backward-bent and more heavily sclerotized pleural spines of the final trunk somite, with the median telson as a separate entity. However, it is possible that all three processes are part of a single telsonic complex, separated from the final trunk segment by the suture marked in Figure 9F. The lateral processes could then be interpreted as furcae, but not caudal rami (*sensu* Aria & Caron 2017*a*; see their remarks on char. 204) as the latter are derived from limbs. Since the anal segment bears the second pair of uropod-like limbs, there are no further somites from which limbs could be modified into caudal rami. We see the furcal interpretation as possible, but less likely, since the median process appears separate and dorsal from the lateral processes. As with the relative placement of the eyes in dorsoventral profile, a laterally preserved specimen of *P. venator* would resolve this ambiguity.

Features of the nervous system. Perhaps the most intriguing aspect of the morphology of *Parioscorpio venator* is that most of the studied specimens preserve a pair of ventral cord-like structures down their midline, which we interpret as nerve cords. This allows for the nodular bulges in the anterior segments to be seen as ganglia (Fig. 7E) and the divergence of the nerve cords in the first trunk segment (Fig. 7G) to be interpreted as the posterior margin of the oesophageal foramen (Strausfeld 2012). The fact that the cords are paired makes an interpretation of a gut or heart untenable, and their immediate adjacency makes it unlikely that they are digestive glands paralleling the tract of the gut. Indeed, in UWGM2764, where the gut is well preserved, the nerve cords can be seen diverging posterolateral to the anterior digestive gland (white arrows in Fig. 6C).

While the number of Cambrian arthropod genera with fossilized brain structure has slowly increased (Ma *et al.* 2012; Tanaka *et al.* 2013; Cong *et al.* 2014; Ortega-Hernández 2015) evidence of the nerve cords posterior to the brain has remained very rare, confined to *Alalcomenaeus* sp. (Tanaka *et al.* 2013), *Chengjiangocaris kunmingensis* Yang *et al.*, 2013 (Yang *et al.* 2016) and, perhaps, the anterior nerve cords of *Lyrarapax unguispinus* Cong *et al.*, 2014. While convincing evidence of a brain has yet to be found for *P. venator*, the nerve cord structure compares favourably with the general chelicerate bauplan (Strausfeld 2012) and can also be compared to the putative nervous system of the megacheiran *Alalcomenaeus* (Tanaka *et al.* 2013) and the fuxianhuiid *C. kunmingensis* (Yang *et al.* 2016). For example, the oesophageal foramen of *P. venator* appears to close in the vicinity of the first trunk segment boundary (Figs 6C, 7G), posterior to its position in *Alalcomenaeus* but comparable to that of larval *Limulus* (Tanaka *et al.* 2013, fig. 4a–b), while the anterior transition from the nerve cord to the brain is not preserved at all in *C. kunmingensis* (Yang *et al.* 2016, fig. s3).

Posterior to their joining, the nerve cords remain tightly coupled (Fig. 7A–D) as in *Alalcomenaeus* (Tanaka *et al.* 2013, fig. 1f–g). In both *Alalcomenaeus* (Tanaka *et al.* 2013, fig. 1e) and *C. kunmingensis* (Yang *et al.* 2016, fig. 2b–e), the ganglia are robustly developed, dominating the structure of the nerve cord. In *P. venator*, however, the ganglia have a more subtle appearance (Fig. 7E), and the paired nature of the nerve cords dominates the preservation, more comparable to the structure of the modern remipede and grasshopper nerve cords featured in Yang *et al.* 2016 (fig. s5c–d). The nerve cords continue to trunk segment 14 in UWGM2857a (Fig. 7C, D), which is similar to modern *Limulus* (Tanaka *et al.* 2013, fig. 4b) and *C. kunmingensis* (Yang *et al.* 2016, fig. 1b), but stands in contrast to *Alalcomenaeus*, where the segments after trunk segment 8 were apparently innervated with anterior neurons in a manner similar to a scorpion (Tanaka *et al.* 2013, fig. 4a, c).

Unfortunately, the relatively coarse nature of the phosphatization of *P. venator* makes it difficult to determine if missing small-scale features of the nerve cords reflect biology or taphonomy. For example, no ganglia appear to be developed posterior to segment 10 in UWGM2793 (Fig. 7F), but they may simply have been homogenized into the preserved structure of the nerve cords, as the ganglia were also noted to grow smaller posteriorly in *C. kunmingensis* (Yang *et al.* 2016). Similarly, there is no evidence for the commissure connecting ganglia or for peripheral nerves, although these should both have been present in the living organism (compare to Yang *et al.* 2016, figs 2d–e, 3).

In light of the critique of Liu *et al.* (2018), it is also wise to consider alternative interpretations of the preservation of labile morphologies like nervous systems. Indeed, in some specimens, the nerve cords appear flattened or discontinuous between segments and could more conservatively be interpreted as ventral muscles or tendons (e.g. Fig. 7I). These could be related to the tendons sometimes seen at the base of the legs (e.g. 'lt' in Fig. 8B; Fig. 10B). In some specimens, these could also be the crescentic borders of the potential sternites, impressed onto the axial body. Flattened structures also sometimes appear preserved side-by-side with the nerve cords (e.g. Fig. 7H). Thus, there may be a spectrum in the preservation of ventral elements: nerve cords, muscles or tendons, sternal impressions, or a superimposed combination of these features.

Interpreting Parioscorpio *as a scorpion.* Wendruff *et al.* (2020*a*) described *Parioscorpio venator* as the earliest known scorpion, supposedly with elements of a respiratory tract indicative of possible terrestrialization.

However, description of the species was based on only two specimens, neither of which preserved chelicerae, a full telson, or a full suite of prosomal limbs. As the present rediagnosis and redescription of 19 specimens has demonstrated, there are few unequivocal features to support inclusion of *P. venator* within crown-group Chelicerata, as necessitated by a scorpion affinity. In fact, *P. venator* only superficially resembles a scorpion in certain taphonomic circumstances. Problems associated with an assignment to Scorpiones stem from considerations of the following characters: (1) the total number and structure of somites; (2) the structure of the frontal-most appendage; and (3) the number and morphology of the post-frontal appendages.

Examination of UWGM2764, paratype and counterpart to UWGM2163, reveals a total of 14 post-cephalic segments, not 12 as Wendruff *et al.* (2020*a*) counted. These are indicated by patches of darker kerogen (Fig. 10D) that are usually accompanied by transverse divisions under low-angle light (Fig. 6D). As detailed in the Redescription, above, there are 10 somites anterior to the axial constriction and 4 posterior. The two anterior segments were not counted (Figs 6D, 10D) and the two segments anterior to the constriction were counted as a single segment (Fig. 10E) by Wendruff *et al.* (2020*a*). This count of 14 is matched among other complete specimens in the available collection.

Specimen UWM2764 also shows the pleural field adjacent to the axial body (Fig. 10D). In fact, the pleural field is visible in UWGM2163, too (Fig. 10E; Wendruff *et al.* 2020*a*, fig. 1c), on the right side of the body. Constriction of the axial body at their sternite 7 is the basis of their division of the trunk into a mesosoma and metasoma, technically the preabdomen and postabdomen, key pseudotagmata in the body of Scorpiones (Kjellesvig-Waering 1986; Lamsdell 2013), but it is clear that this is not reflected in the width of the pleural fields. Furthermore, a metasoma bearing tergopleurae is incompatible with a scorpion affinity (Kjellesvig-Waering 1986).

Another key apomorphy of total group scorpions is the presence of a stinger (Dunlop & Lamsdell 2017). Wendruff *et al.* (2020*a*, fig. 1a–b) contended its presence in the holotype UWGM2162, although a stinger with a poison bulb was never demonstrated in any of our specimens. Instead, the terminus of the animal, when present, manifests as a tridentate structure, consisting of a short, triangular telson flanked on either side by short spines of similar length (Fig. 9F). We interpret these lateral spines as the tergopleurae of the ultimate somite, as detailed in the Redescription, above. The 'poison vesicle' observed by Wendruff *et al.* (2020*a*) is more likely to be a flattened gap between the phosphatized remnants of the ultimate trunk legs. A similar gap is present at the posterior of the final limbs of UWGM2857 (Figs 8E, F, 10C).

Neither chelicerae nor antennae are preserved on any of our specimens. The limbs interpreted as pedipalps by Wendruff *et al.* (2020*a*) are the great appendages, and interpreted here as deutocerebral. In specimens with a well-preserved anterior, the great appendage can be seen as an unusual limb with four podomeres (Fig. 5A–D), which somewhat resembles an enlarged, rotated version of the specialized post-antennal appendage of fuxianhuiids (Yang *et al.* 2013; see Affinities with Fuxianhuiids and Mandibulates, below). The small, terminal podomere lies at nearly a right angle to the penultimate podomere, and there is no evidence for an additional 'free finger' (Fig. 5A, C). However, even if these appendages are chelate, this would not necessarily indicate a scorpion pedipalp, as chelate great appendages have evolved numerous times within Arthropoda (e.g. Lamsdell *et al.* 2013; Aria & Caron 2017*a*).

Posterior to the great appendage, we interpret either one biramous appendage or, potentially, two uniramous appendages in the head (Figs 4F–H, 5C, D, G), consistent with what is actually preserved in the holotype (Wendruff *et al.* 2020*a*, figs 1a–b, 3). What they term the 'trochanter', 'femur' and 'patella', though, appear to be the broken endopod of the second cephalic appendage. The exopod of the second cephalic appendage is labelled '?' to the left of the left muscle block in the head (Wendruff *et al.* 2020*a*, fig. 1b). However, the four 'coxae' posterior to the 'pedipalp' (actually the great appendage, see Fig. 3F) in UWGM2163 are unconvincing. For example, what is indicated as the fourth coxa on the right (Wendruff *et al.* 2020*a*, fig. 1d) appears to be multiple components that can resemble a rectangular shape at certain light angles (Fig. 10E). As a member of the clade Prosomapoda (Lamsdell 2013), arachnids and scorpions should have a set of six limbs on their prosoma, the first five being uniramous and the sixth variable in ramification. In *P. venator*, there is only evidence for two or, at most, three (Figs 3B–F, 4D–H, 5A–D, G) limbs in the head.

Euchelicerata, inclusive of Prosomapoda, is comprised of chelicerates bearing only platy or otherwise highly reduced or modified limbs in their opisthosoma (Dunlop & Lamsdell 2017). Book gills/lungs are among these platy appendages, and were not identified by Wendruff *et al.* (2020*a*) As detailed in the Redescription, above, most of our specimens do indeed preserve legs on the trunk (Figs 8, 9), and those on somites 1–12 have the appearance of a biramous arthropod limb. Although the structure of these limbs is quite complex, both setose ramus and ambulatory endopod components are present (Fig. 9D, E). The final two limb pairs, located on somites 13 and 14, have a platy appearance with filamentous fans (Figs 8E, F, 10C) similar to those of some artiopods (see Affinities with *Sidneyia*, Artiopods, and the Status of *Xus yus*, below). Thus, we can confidently say that *P. venator* is not a member of Euchelicerata either.

The other major morphological consideration of Wendruff *et al.* (2020*a*) involves supposed features of the pulmonary–cardiovascular system. We advocate for the consideration of alternative interpretations of these morphologies. For example, the hourglass-shaped feature interpreted as the pericardium (Wendruff *et al.* 2020*a*, fig. 2a) could be muscles or tendons associated with the body axis, or they could be the preserved sternites of the trunk somites (Fig. 7H, I). Additionally, the hourglass-shape could be imparted as a consequence of the overlying 'pulmo-pericardial sinuses' truncating an otherwise square or rectangular morphology (Wendruff *et al.* 2020*a*, fig. 2a). The 'sinuses' themselves may be muscles or tendons, as observed in other specimens (Figs 8A, B, 10B), or they may simply be taphonomically effaced legs (compare to Fig. 9A–C). Surprisingly labile tissues have been preserved in fossil arthropods before (Kjellesvig-Waering 1986; Manning & Dunlop 1995; García-Bellido & Collins 2006; Yang *et al.* 2016) and we have already interpreted the presence of nerve cords on *P. venator* (Figs 6C, 7A–G). Thus, it is not outside the realm of possibility that the pulmonary–cardiovascular system interpretation of Wendruff *et al.* (2020*a*) is correct. Regardless, this does not indicate that *P. venator* could breathe on land. The respiratory and circulatory systems of xiphosurids and scorpions closely resemble one another (Göpel & Wirkner 2015; Wendruff *et al.* 2020*a*), but this does not necessitate that extant scorpions can respire underwater.

The consideration of the clade to which *Parioscorpio venator* does belong is presented in Phylogenetic Analysis and Affinities, below. What can be said with confidence at this point, however, is that *P. venator* is not a member of crown-group Arachnida, or even crown-group Euchelicerata.

FOSSIL PRESERVATION PATHWAYS

As mentioned in the Remarks, above, there are several preservational habits that typify *Parioscorpio venator* fossils. White to blue–white phosphatic material preserves morphologies either three-dimensionally or as sheets with slight elevation, which, when removed, leaves dark-coloured impressions. Some areas are preserved as black, presumably carbonaceous, compressions, either as solid sheets (e.g. between segments and legs in Figs 7A, C, 8A, E, and walking legs and walking leg bundles in Figs 8G, 9D) or with a distinct 'speckled' appearance (racemose filamentous bundles 'rb3,' 'rb4' and 'rb7' in Fig. 8G). Finally, small, golden deposits or cubes of pyrite can stud the impressions left behind by removed white to blue–white material (e.g. Figs 4D, F, H, 5E, F), although these are never dense enough to imitate morphology.

Generally, these preservational habits are similar to what has been previously described for other arthropod fossils from the Waukesha. Mikulic *et al.* (1985*a*, *b*) postulated that the white to blue–white material was fluorapatite, which was later endorsed as 'phosphatic' by energy dispersive x-ray spectroscopic (EDS) analysis of *Venustulus waukeshaensis* (Moore *et al.* 2005, p. 243). Similarly, Jones *et al.* (2015) demonstrated a calcium phosphate composition for the white material in *Ceratiocaris papilio*, although the interpretation of the 'dark brown carbon film', equivalent to our dark impressions, could not be substantiated with their EDS (Jones *et al.* 2015, p. 1017). They further identified 'aggregates of minute, interlocking pyrite crystals' and larger pyrite cubes cutting across the white material and the dark impressions (Jones *et al.* 2015, p. 1017). The white to blue–white material was referred to as calcium phosphate and the black compression habit an 'organic carbon film' by Wendruff *et al.* (2020*b*, p. 9).

Our analysis shows that the white phosphatic material, dark impressions, golden pyritic deposits, and black compressions are all distinguishable phases in backscattered electron (BSE) SEM imaging (Fig. 13B); although the dark impressions, while optically visible, are largely indistinguishable from the host-rock matrix in BSE imaging (Figs 13B, 14A). The brightest (or highest greyscale) in BSE imaging (indicating high average atomic weight) are the golden pyritic deposits. As indicated by Jones *et al.* (2015), these materials do indeed correspond to pyrite as indicated by enrichment in iron and sulfur (Fig. 13C). The next brightest phase (Fig. 13B), corresponding to the nerve cords and legs in the trunk (Fig. 13A, B) and the muscle block in the head (Figs 13A, 14A), shows elevated concentrations not only of calcium and phosphorous (Figs 13D, 14C), but also of sodium and sulfur (Figs 13C, E, 14B, D). A slightly elevated carbon signal is also noticeable (Figs 13G, 14F). These results suggest that the white to blue–white material is indeed a phosphate, probably francolite, whose general formula of $(Ca, Mg, Sr, Na)_{10}(PO_4, SO_4, CO_3)_6F_{2–3}$ can accommodate the observed elemental distributions.

The dark impression phase shows an enrichment in aluminium, with occasional spots that show strong enrichment in silicon (Fig. 13F). These silicon spots correspond to grains of a relatively light phase in the BSE images (Fig. 13B). This is exactly the same pattern seen in the matrix (Fig. 14E), and strongly suggests that the dark impression phase is not a distinctly separate preservation pathway as proposed by Jones *et al.* (2015), but is instead the mouldic impression of the francolite phase in the argillaceous matrix. The small areas of silicon enrichment would correspond to silt grains found in the matrix. It is possible that there is a diffuse amount of organic carbon in these impressions, which would explain its darker colour while still escaping EDS detection. A similar phenomenon has been seen on *Ottoia* fossils from

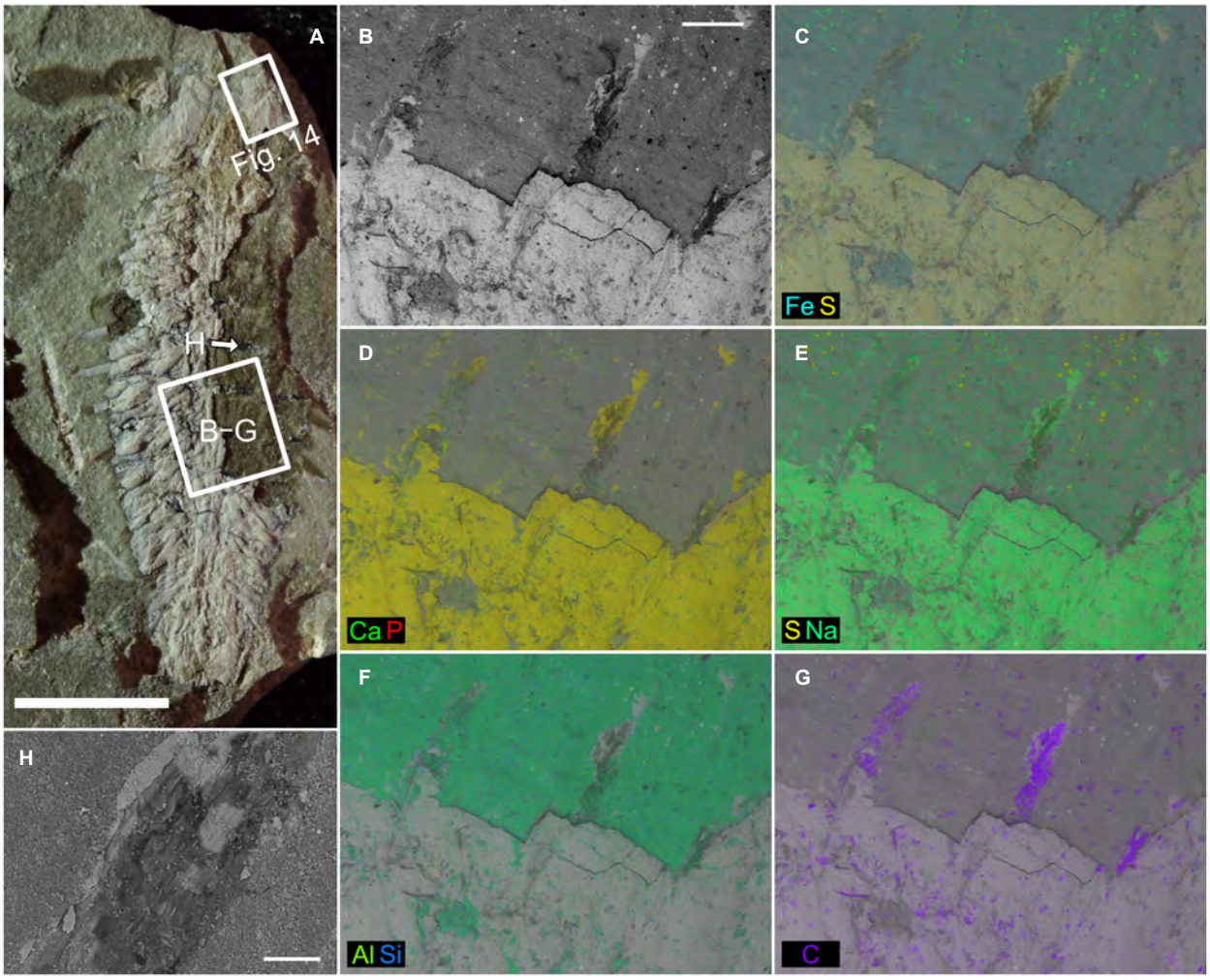

FIG. 13. Scanning electron microscopy (SEM) images and energy dispersive x-ray spectroscopy (EDS) maps identifying the preservational habits of *Parioscorpio venator*. A, overview of UWGM2793; positions of enlargements B–G and area analysed in Figure 14 indicated. B–G, hybrid SEM images (composed of mixed back scattered electron and secondary electron signals) and EDS maps of the middle trunk of UWGM2793: B, base image; C, with iron (Fe) and sulfur (S) EDS maps superimposed; D, with calcium (Ca) and phosphorous (P) EDS maps superimposed; E, with S and sodium (Na) EDS maps superimposed; F, with aluminium (Al) and silicon (Si) EDS maps superimposed; G, with carbon (C) EDS map superimposed. H, image focusing on the waxy, blistered preservation of the kerogen at the division of two trunk segments. Scale bars represent: 5 mm (A), 0.5 mm (B) and 100 μm (H).

Burgess-Shale-type deposits (Broce & Schiffbauer 2017) and in the patchy light kerogenization of visibly carbonaceous discoidal fossils from the early Cambrian Carrara Formation (Lieberman *et al.* 2017). Indeed, attempts to elementally map the composition of the dark film of UWGM2764 (Fig. 1C) returned no appreciable carbon signal, and the fossil was indistinguishable from the argillaceous matrix.

Finally, the black compression habit is also the darkest greyscale phase seen in the BSE image (Fig. 13B), indicating the substance has a low average atomic number. Indeed, this habit appears to be made purely of carbon (Fig. 13G) and under closer inspection has the waxy, blistered appearance typical of mature kerogen (Fig. 13H). Unexpectedly, small flecks of carbonaceous material could be seen scattered about other areas of the fossil under the SEM (Fig. 14A, F). It is not clear if these are the remnants of originally more widespread carbonaceous material associated with the specimen, unassociated bits of organic debris deposited with the fossil or post-exhumation contamination.

Thus, *P. venator* has at least three pathways of preservation associated with it: phosphatization (*sensu* Xiao & Schiffbauer 2009; Schiffbauer *et al.* 2014*a*) and keroginization (i.e. carbonaceous compression) that preserve tissue-level detail, and pyritization that forms a 'dusting' around

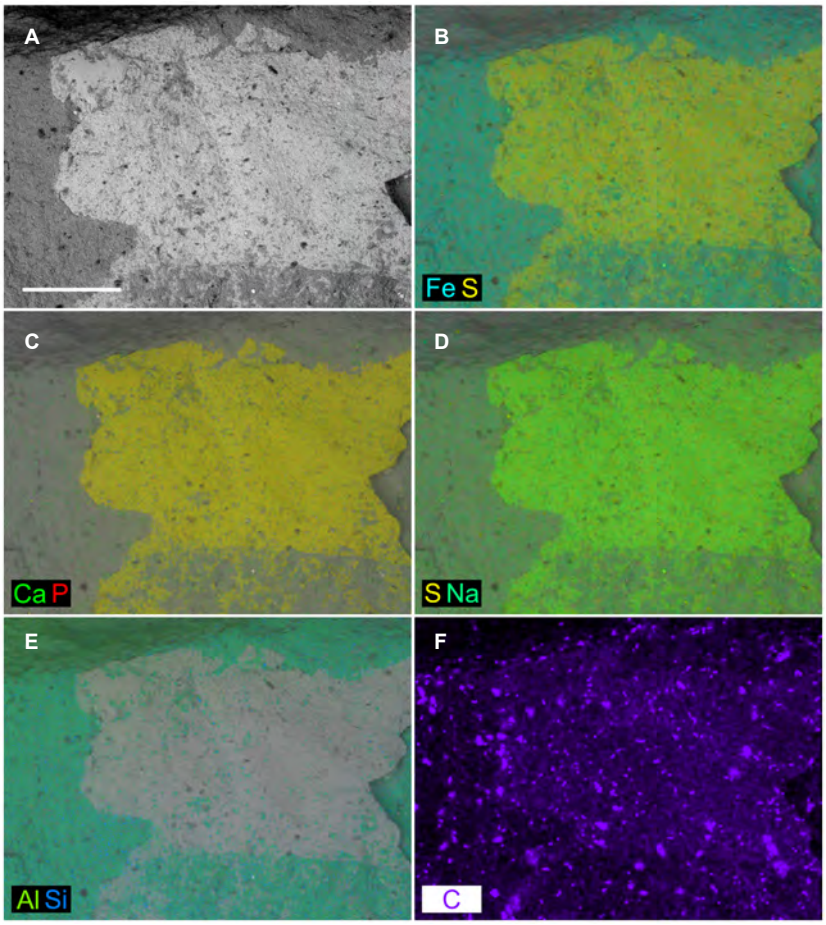

FIG. 14. Hybrid scanning electron microscope (SEM) images (combining secondary electron and back scattered electron signals) and energy dispersive x-ray spectroscopy (EDS) maps of the head of UWGM2793, further displaying the preservational habits of *Parioscorpio venator*. A, base image on the anterior right side of the head; location with respect to the entire organism shown in Figure 13A. B–E, base image with element EDS maps superimposed: B, iron (Fe) and sulfur (S); C, calcium (Ca) and phosphorous (P); D, S and sodium (Na); E, aluminium (Al) and silicon (Si). F, carbon (C) EDS map showing its faint presence in the head muscle block. Scale bar represents 0.5 mm.

the preserved cuticle. Of these three pathways, the former two appear to be taphonomically constructive, whereas pyritization is rather only accessory mineralization. Such mixed taphonomic mineralization pathways are a common phenomenon associated with many soft-bodied fossil deposits (e.g. *Chuaria* carbonaceous fossils, Anderson *et al.* 2011; fossils of the Gaojiashan lagerstätte, Cai *et al.* 2012; Schiffbauer *et al.* 2014*b*), probably due to complex geochemical gradients and microbial zonation in the burial environment (Muscente *et al.* 2017). There does not appear to be a strong correlation between lithology and preservation pathways, though the sample size is admittedly small. Phosphatization, kerogenization and pyritization are present in *P. venator* preserved in both thicker beds of calcilutite and finely alternating laminae of calcilutite and dolosiltstone. The one specimen preserved in a thicker bed of coarser dolosiltstone shows relatively poor preservation quality, consistent with trends observed by Wendruff *et al.* (2020*b*), but it too is phosphatized, though evidently lacking compressed carbonaceous materials (Fig. 10A). These preservation pathways confirm and expand on what has been observed previously in Waukesha fossils (Mikulic *et al.* 1985*a*; Moore *et al.* 2005; Jones *et al.* 2015; Wendruff *et al.* 2020*b*) and are common to the arthropods of the Waukesha.

While the dominance of arthropods at Waukesha may warrant palaeoecological comparisons with any standard Burgess-Shale-type deposit (Briggs *et al.* 1994), the taphonomy bears a closer resemblance to the obrution/stagnation deposits of Solnhofen and Holzmaden (Seilacher *et al.* 1985; Etter 2002; Etter & Tang 2002). More specifically, Burgess-Shale-type deposits are primarily kerogenous with secondary contributions from pyritization and aluminosilicification (Anderson *et al.* 2011; Gaines 2014), and phosphatization plays a relatively minor role, usually confined to digestive tracts (Orr *et al.* 1998; Butterfield 2002). On the other hand, phosphatization and kerogenization are the primary preservational pathways at Waukesha, similar to Solnhofen and Holzmaden (Barthel *et al.* 1990; Etter & Tang 2002). Perhaps the closest analogue to a dominantly phosphatized deposit with the animal component comprising abundant arthropods may be the coastal plain, estuarine and marginal marine deposits of the Mississippian of Scotland (Briggs & Clarkson 1989; Cater *et al.* 1989). The Granton

Shrimp Beds and related deposits differ from the Waukesha, though, in the much greater siliciclastic input of the former.

PHYLOGENETIC ANALYSIS AND AFFINITIES

As detailed in the Material and Method, above, the phylogenetic analysis herein was based on the character list and character table of Aria & Caron (2017*a*). For some characters multiple interpretations were plausible (Table 1). The characters which changed between coding for the exopod/endopodal exite and epipod/exopod interpretations of the main trunk limbs (see Features of the Trunk, above) are listed in Table 2. Our primary phylogenetic analysis is presented in Figure 15, with analyses where alternative states were considered for both the exopod/endopodal exite and epipod/exopod interpretations in Anderson *et al.* (2021, fig. S1).

Many character traits were shared between *Parioscorpio venator* and the comparison taxa (Anderson *et al.* 2021, appendices S1–S2) but only a handful could be considered to be synapomorphies uniting *P. venator* with a stem-group taxon or clade (Table 3). More often, shared characters were plesiomorphies for the arthropods in general, or defined broadly inclusive nodes featuring many stem- and crown-group taxa. These were of little use in determining the precise taxonomic placement of *P. venator*.

Thus, although the affinities between *P. venator* and the comparison taxa warrant discussion, these affinities are usually not straightforward. This is not unexpected when relating a stem-group taxon to a larger clade when most of the known members of the clade are considerably more derived or more basal, or if the taxon under consideration is a specialized member of a stem group. But, it also means that multiple scenarios through which characters are transformed to relate *P. venator* to a comparison taxon may need to be considered. As a result, the sections

TABLE 1. Characters of *Parioscorpio venator* incorporated into the phylogenetic analysis for which alternative interpretations of their states are feasible.

Character number	Brief description	Alternative states*	Contingency?†
19	Median eyes present?	**0 (no)** or ? (unknown)	No
20	Median eye number	**- (inapplicable)** or ? (unknown)	Yes: 19 (0,-) or (?,?)
27	Eyes embedded in tergal shield?	0 (no) or **? (uncertain)** or 1 (yes)	No
28	Ophthalmic ridges?	**0 (no)** or ? (unknown)	No
39	Articulation between head shield and first trunk segment	**0 (tergal overlap)** or ? (uncertain)	No
67	Ocular lobes?	**0 (no)** or ? (unknown)	No
133	Serial repetition of post-cephalic digestive structures?	0 (no) or **? (uncertain)** or 1 (yes)	Yes: 132
134	Shape of post-cephalic digestive structures	- (inapplicable) or ? (uncertain) or **0 (reniform)**	Yes: 133 (0,-) or (?,? or 0) or (1,0)
135	Striations on post-cephalic digestive structures	- (inapplicable) or **? (uncertain)**	Yes: 133 (0,-) or (?,?) or (1,?)
136	Branching of post-cephalic digestive structures	- (inapplicable) or **? (uncertain)**	Yes: 133 (0,-) or (?,?) or (1,?)
137	Differentiated cephalic digestive structures?	0 (no) or **? (uncertain)** or 1 (yes)	Yes: 132
160	Podomere count in tagma II?	0 (7) or 1 (<7) or **? (uncertain)**	No
178	Proximal lamellae?	0 (no) or **? (uncertain)**	Yes: 176
179	Internalized proximal lamellae?	- (inapplicable) or **0 (no)**	Yes: 178 (0,-) or (?,0)
182	Main trunk exopod type	**2 (rodiform)** or 3 (annulate)	Yes: 181
187	At least one pair of exopods annulated?	**? (uncertain)** or 1 (yes)	Yes: 182 (3,1) or (2,?)
189	Attachment segment for a lobate exopod?	0 (no) or **? (uncertain)**	Yes: 181
192	Is endite a latero-distal projection on endopod podomeres?	0 (no) or **? (uncertain)** or 1 (yes)	No
196	Endopod podomeres with short spines?	**0 (no)** or ? (uncertain)	No
206	Presence of furcae?	**0 (no)** or 1 (yes)	No

All characters and character states were derived from the analysis of Aria & Caron (2017*a*).

*The state in **bold** represents the preferred interpretation, used in the analysis whose cladogram is shown in Figure 15.

†Indicates if a character's state is dependent on the state of a sovereign character. If the sovereign character also has alternative interpretations, the relations of the sovereign state to the contingent state for *P. venator* are listed as such: (sovereign, contingent).

TABLE 2. Character states affected when alternating between interpreting the two anteriormost rami of the main trunk limbs (as preserved in the fossils; in life probably dorsally oriented on the leg) as exopod and endopodal exite (the standard interpretation, shown in Figs 8–9) and as epipod and exopod (the alternative interpretation).

Character number	Brief description	Exopod/endopodal exite interpretation state*	Epipod/exopod interpretation state
178	Proximal lamellae?	0 (no) or **? (uncertain)**	? (uncertain)
179	Internalized proximal lamellae?	- (inapplicable) or **0 (no)**	0 (no)
182	Main trunk exopod type	**2 (rodiform)** or 3 (annulate)	2 (rodiform)
187	At least one pair of exopods annulated?	**? (uncertain)** or 1 (yes)	0 (no)
190	Ornamentation type on exopods	0 (setae)	1 (lamellae)
191	Epipods present?	0 (no)	1 (yes)

*When alternative character interpretations are presented, the state in **bold** is the one used in the phylogenetic analysis shown in Figure 15 (see Table 1 for more details).

'Affinities with Comparison Taxa' (and its subsections) and 'Comparisons with *Marrella* and *Agnostus*', below, are abbreviated versions of the full considerations. Supplementing considerations are contained in Anderson *et al.* (2021, appendix S2).

The primary phylogenetic analysis retained only 20 most parsimonious trees with a length of 901. The small number of trees leads to a high degree of resolution in the strict consensus tree (Fig. 15), as well as some taxonomic placements which may be somewhat spurious. For example, Hymenocarina resolve as the sister group of Hexapoda, with Xenocarida as sister to both of these. *Opabinia* and *Isoxys* resolve together as a sister group to Radiodonta. *Yicaris*, an early Cambrian taxon which displays multiple advanced crustacean features (Zhang *et al.* 2007), resolves as the basal-most artiopod. *Parioscorpio venator* itself resolves towards the base of the euarthropod tree, more basal than Megacheira, but one node above *Fuxianhuia*, *Shankouia*, *Chengjiangocaris* and Euthycarcinoidea *sensu stricto*. Other analyses have resolved *Fuxianhuia* and its relatives in a basal euarthropod position (e.g. Legg *et al.* 2013) but in this analysis it also remains tightly coupled to Euthycarcinoidea *s.s.*, as in Aria & Caron (2017*a*), despite the fact that the latter group bears mandibles (e.g. Vaccari *et al.* 2004) and, in light of recent discoveries, seems likely to actually represent stem myriapods (Edgecombe *et al.* 2020; see Affinities with Fuxianhuiids and Mandibulates, below). In spite of these oddities, most of the crown groups (e.g. Hexapoda, Malacostraca, Chelicerata, Myriapoda) and major stem-group clades (e.g. Artiopoda, Megacheira, Radiodonta) remain intact (Fig. 15), though individual taxa may form local polytomies.

Branch support analyses reveal relatively low levels of support for many clades, and for the topologies that relate larger clades to one another (Fig. 15). The most strongly supported clades are consistently those enforced by the backbone constraints inherited from Aria & Caron (2017*a*), which apply to some extant taxa (Anderson *et al.* 2021, appendix S1). Small fossil clades may show stronger support (e.g. *Branchiocaris* + *Tokummia*, *Sidneyia* + *Emeraldella* and *Offacolus* + *Dibasterium*), as do fossil taxa closely allied to or embedded within clades supported by the backbone constraints (e.g. *Eothele*, Phosphatocopina and *Arthropleura*). The node supporting *Parioscorpio* collapsed in the first step of Bremer analysis (Fig. 15) and was not resolved in bootstrap or jackknife support analyses at all, instead resolving as the sister to Euthycarcinoidea *s.l.* (Aria & Caron 2017*a*) with very weak support (4 for bootstrap and 7 for jackknife). Bremer support analysis with alternative states returned similar trends and results (Anderson *et al.* 2021, fig. S1).

Analyses with the consideration of alternative states would move around the placement of *P. venator*, and often other arthropod clades as well. In all the proceeding cases,

FIG. 15. Cladogram demonstrating the placement of *Parioscorpio venator* in the arthropod tree, using the character matrix of Aria & Caron (2017*a*) as a basis. This analysis uses only the preferred interpretations of characters (see Table 1) and incorporates the exopod/endopodal exite interpretation of the main trunk limbs (see Features of the Trunk and Table 2; for cladograms illustrating alternative character states and interpretations of the main trunk limbs, see Anderson *et al.* 2021, fig. S1). Major monophyletic clades within Arthropoda are labelled, and the placement of *P. venator* is highlighted in yellow. Roman and italic script numbers to the upper left of each node are Bootstrap and Jackknife support values, respectively ('-' indicates that the node was not resolved in a particular branch support analysis; values in parentheses indicate that nodes in a branch support analysis matched the primary analysis in the taxa contained, but not in topology). Bold numbers to the lower left of each node are Bremer support values. *Abbreviations*: Art., Artiopoda; Meg., Megacheira; Eu., Euthycarcinoidea *sensu lato*; Rad., Radiodonta.

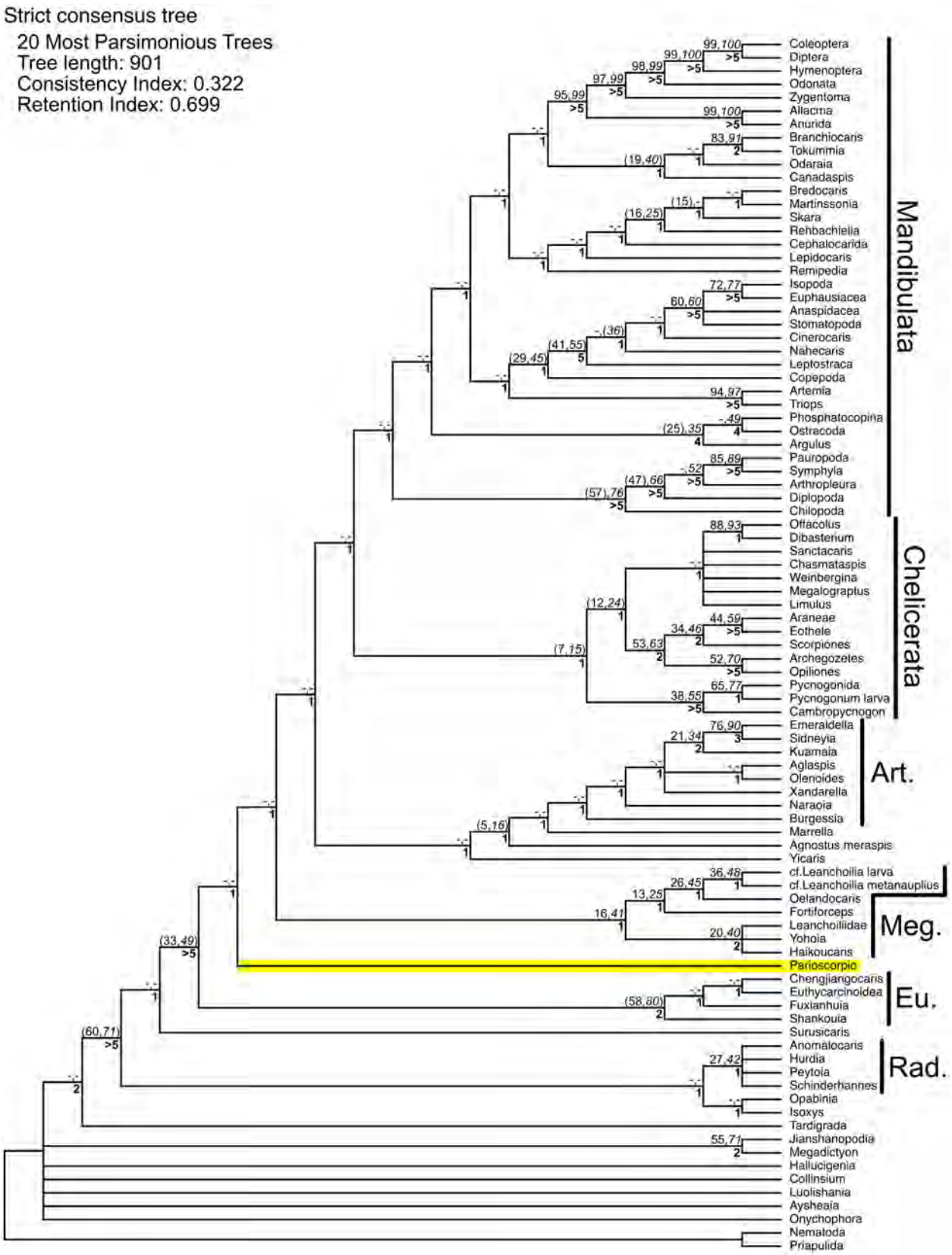
Strict consensus tree
20 Most Parsimonious Trees
Tree length: 901
Consistency Index: 0.322
Retention Index: 0.699
Coleoptera
Diptera
Hymenoptera
Odonata
Zygentoma
Allacma
Anurida
Branchiocaris
Tokummia
Odaraia
Canadaspis
Bredocaris
Martinssonia
Skara
Rehbachiella
Cephalocarida
Lepidocaris
Remipedia
Isopoda
Euphausiacea
Anaspidacea
Stomatopoda
Cinerocaris
Nahecaris
Leptostraca
Copepoda
Artemia
Triops
Phosphatocopina
Ostracoda
Argulus
Pauropoda
Symphyla
Arthropleura
Diplopoda
Chilopoda
Mandibulata
Offacolus
Dibasterium
Sanctacaris
Chasmataspis
Weinbergina
Megalograptus
Limulus
Araneae
Eothele
Scorpiones
Archegozetes
Opiliones
Pycnogonida
Pycnogonum larva
Cambropycnogon
Chelicerata
Emeraldella
Sidneyia
Kuamaia
Aglaspis
Olenoides
Xandarella
Naraoia
Burgessia
Marrella
Agnostus meraspis
Yicaris
Art.
cf.Leanchoilia larva
cf.Leanchoilia metanauplius
Oelandocaris
Fortiforceps
Leanchoiliidae
Yohoia
Haikoucaris
Meg.
Parioscorpio
Chengjiangocaris
Euthycarcinoidea
Fuxianhuia
Shankouia
Eu.
Surusicaris
Anomalocaris
Hurdia
Peytoia
Schinderhannes
Opabinia
Isoxys
Rad.
Tardigrada
Jianshanopodia
Megadictyon
Hallucigenia
Collinsium
Luolishania
Aysheaia
Onychophora
Nematoda
Priapulida

TABLE 3. Potential synapomorphies between *Parioscorpio venator* and the ten stem-group taxa with which it was compared.

Shared character and state (potential synapomorphy)	Comparison taxon	Broadest clade sharing the character†
28(0): Lack of ophthalmic ridges	*Fuxianhuia*	Euthycarcinoidea *sensu lato*
72(1): Frontalmost appendage is chelate	*Offacolus kingi*	Chelicerata (including Pycnogonida)
86(0): All cephalic limbs are not walking limbs	*Tokummia katalepsis*	*Branchiocaris* + *Tokummia* (other hymenocarines code ?)
94(1): Reduced post-antennular appendage with a strongly clawed terminus	*Fuxianhuia*	*Fuxianhuia* + *Shankouia* + *Chengjiangocaris* (i.e. paraphyletic Fuxianhuiida)
141(1): Metameric ganglia on nerve cord present	*Fuxianhuia*	*Fuxianhuia* + *Shankouia* + *Chengjiangocaris* (probably plesiomorphic for Arthropoda; a taphonomic artefact in these taxa)
171(0): Precoxa is not a whole pre-coxal podomere	*Oelandocaris oelandica*	*Oelandocaris* (this trait is unresolved in most fossil taxa, and thus probably not truly synapomorphic with *Oelandocaris*)
182(2): Main trunk exopods rodiform	None‡	*Naraoia* or *Olenoides* or *Xandarella*
190(0): Exopod ornamentation setiferous	*Agnostus* meraspis	*Agnostus* meraspis

Only characters shared between *P. venator* and one of the comparison taxa, and the single largest clade to which that comparison taxon belongs that also bears the character (e.g. Euthycarcinoidea *s.l.* for *Fuxianhuia*), are listed here. There are shared traits but no potential unique synapomorphies shared with *Marrella splendens*, *Surusicaris elegans*, *Sydneyia inexpectans*, Leanchoiliidae or *Yohia tenuis*.

Shared missing or ambiguous (?) or inapplicable (-) states are not considered (though shared missing or ambiguous states are highlighted in green in Anderson *et al.* 2021, appendix S1).

Potential synapomorphies are assessed based on the preferred interpretation of characters for *P. venator* (see Table 1) and the exopod/endopodal exite interpretation of the anterior trunk leg rami (see Table 2).

†The 'broadest clade' sharing the synapomorphy is defined in terms of the clades in Figure 15.

‡This character is included as it is shared with only *Naraoia*, *Olenoides* and *Xandarella* in the character matrix. These taxa are scattered within the Artiopoda in Figure 15, but have resolved together as members of a monophyletic Trilobitomorpha in other analyses (e.g. Lerosey-Aubril *et al.* 2017).

the discussed relationships refer to the strict consensus trees, which are figured in Anderson *et al.* (2021, fig. S1). For both exopod/endopodal exite and epipod/exopod interpretations when alternative states are recorded as ?, *P. venator* resolves as the basal-most member of a clade uniting Hymenocarina and Euthycarcinoidea *s.l.* at the base of Mandibulata, which in turn forms a polytomy with Lamellipedia (Artiopoda + *Marrella*, *sensu* Stein 2013, fig. 1d) and Chelicerata (Anderson *et al.* 2021, fig. S1a–b).

When alternative states are coded as absent or the smaller possible number of a repeating morphology, *P. venator* resolves as part of a broad euarthropod polytomy (although in the epipod/exopod interpretation, Crustacea, Megacheira and Myriapoda are still intact; Anderson *et al.* 2021, fig. S1d). When alternative states are coded as present or the largest possible number of a repeating morphology for the exopod/endopodal exite interpretation, very little can be said of the placement of *P. venator*, as it is part of a large euarthropod polytomy (Anderson *et al.* 2021, fig. S1e). For the epipod/exopod interpretation, *Parioscorpio* is again part of a large euarthropod polytomy (Anderson *et al.* 2021, fig. S1f), but in this case only the non-arachnid Euchelicerata and Euthycarcinoidea *s.l.* have completely collapsed and Megacheira remains intact.

Despite being topologically resolved at the base of clades in all the phylogenetic analyses and associated with nodes that collapse readily in branch support analyses (Fig. 15; Anderson *et al.* 2021, fig. S1), there are few characters which could be considered autapomorphic for *Parioscorpio venator* in the character matrix. These include characters 101, 102, 104–110 and 112–119 which code for the third, fourth and fifth cephalic appendages and, following the examples of *Surusicaris* and *Cambropycnogon* in the matrix, are recorded as inapplicable, since *P. venator* does not have cephalic appendages beyond the second, by our preferred interpretation. Bearing only two anterior cephalic appendages may be an autapomorphy, but it is not a particularly strong one, as the loss of cephalic appendages occurs in many arthropod taxa (as discussed in considerations of the comparison stem-group taxa).

Character 100, in which the 'exopod of the post-antennular appendage' is a paddle ([3]) is another potential autapomorphy for *P. venator*, particularly if it is a basal arthropod taxon as depicted in Figure 15. Only Remipedia and several malacostracan taxa also display this character state in the matrix, and the construction of the 'paddle' in *P. venator* is highly distinctive. It is not a single unit, but formed by the close association of an arcing banana-shaped podomere and its distal processes (Fig. 5H–I). These are

always found preserved close together, and appear to have functioned as a unit (Figs 3B, 4F–H, 5A–D, G–I). Other compelling candidates for autapomorphies were not specifically coded for in the character matrix of Aria & Caron (2017*a*). These include the lateroventrally directed 'walking leg bundle' of the main trunk legs (Fig. 8G), the multi-segmented endopodal exite with apparently lamellate setae forming a 'racemose bundle' (Figs 8A, B, 9B, C) and the filamentous uropod-like legs on the final two somites that immediately follow the 'normal' trunk legs (Figs 8E, F, 10C). In combination, the two-limbed head, paddle-like second appendage exopod, four-segmented great appendage and longitudinally elongate muscle blocks that operate them may also form a unique suite of characters.

Affinities with comparison taxa

The following discussion considers all of the comparison taxa listed in the Material and Method and highlighted in Anderson *et al.* (2021, appendix S1) except for *Marrella splendens* and *A. pisiformis*. These two are detailed in the subsequent section, as they were deemed unlikely to be related to *Parioscorpio venator*, but nevertheless have interesting traits which are worth comparing. In this section, a few comparison taxa are considered within their own subsections when they warrant extra discussion. Supplementary text for these sections may be found in Anderson *et al.* (2021, appendix S2).

There are no potential unique synapomorphies between *Surusicaris elegans* and *P. venator*, and most shared characters are plesiomorphic for the arthropod bauplan (i.e. char. 31[1]: a somital head tagma; char. 180[0]: lack of trunk endopod reduction). One shared trait of interest is character 74[1] (a reduction in segment number of the 'frontalmost arthrodized appendage'), which is a key 'great appendage trait' shared between *Surusicaris*, *Isoxys* and *Parioscorpio*. It is also found in the comparison taxa Leanchoiliidae, *Yohoia*, *Oelandocaris* and *Offacolus*. Indeed, while this trait may be found scattered throughout the phylogenetic analysis character table, it is common to all listed megacheirans and chelicerates (Anderson *et al.* 2021, appendix S1). Character 74 serves mostly to highlight how great appendages may emerge convergently (or perhaps may even be plesiomorphic; e.g. Scholtz & Edgecombe 2005). Notably, no species of *Surusicaris* or *Isoxys*, which was resolved as the sister to *Surusicaris* by Aria & Caron (2017*a*), has yet been found with great appendages similar to *P. venator*, despite the variety of great appendage forms found in *Isoxys* (Vannier *et al.* 2009; Stein *et al.* 2010; Fu *et al.* 2011; Aria & Caron 2015). Hence, there is no reason to believe they are closely related (Fig. 15).

When the material of *P. venator* was initially restudied, we hypothesized that the animal was a megacheiran due to its frontal-most appendage being a 'great appendage' and a lack of evidence for primary or secondary antennae (Scholtz & Edgecombe 2005). However, our analysis indicates there are no unique synapomorphies shared between the megacheiran taxa examined (Leanchoiliidae and *Yohoia*) and *P. venator*. *Oelandocaris oelandica*, which resolves with Megacheira in our analyses (Fig. 15; Anderson *et al.* 2021, fig. S1a–b, d, f), and *P. venator* do share character 171[0], as neither of the species have a precoxa which constitutes an entire precoxal podomere (Table 3). However, this is likely to be a taphonomic artefact, as most of the other comparison taxa simply code ?. While *P. venator* does share a 'reduced segmentation of frontalmost arthrodized appendage' (char. 74[1]) with Megacheira, it does not share key character state 69[1]: the presence of a 'branching frontalmost appendage'. Thus, our phylogenetic analysis does not indicate a strong affinity with the megacheirans and *Oelandocaris* (Fig. 15; Anderson *et al.* 2021, fig. S1).

Yet, in many respects *P. venator* aligns with the definition of Megacheira put forth by Hou & Bergström (1997) modified by the understanding that the 'great appendage' is deutocerebral and homologous to the antennule (Tanaka *et al.* 2013): they bear schizoramous appendages (Figs 8, 9), the first limb pair developed as a great appendage (Figs 4D–H, 5A–D), a pleural fold (i.e. pleural fields adjacent to an axis; Figs 2C, 6D, F, 10D, E), an elongated last tergite (Fig. 6D, E) and a lack of furcae (by our interpretation, Fig. 9F). Although the legs of *P. venator* are primarily directed laterally (Figs 8, 9) and not pendent, and the eyes may or may not be anterior (Table 1; Figs 3A–D, 4F, G, 5F), these traits could easily be seen as ecological innovations to a primarily benthic life habit in an intertidal environment. We consider inclusion of *P. venator* in Megacheira a distinct, though unproven, possibility (see Anderson *et al.* 2021, appendix S2 for further discussion).

Observation of *Oelandocaris oelandica*, one of the stem-group comparison taxa, offers some insight on this morphological disconnect, particularly as it relates to how the trunk limbs of standard megacheirans could be altered to the form seen in *P. venator*. *Oelandocaris oelandica* is generally considered to be a basal crustacean (i.e. Stein *et al.* 2005; Stein *et al.* 2008) despite having been more recently interpreted as a megacheiran (Aria *et al.* 2015; Aria & Caron 2017*a*), probably due to frontal appendages that at least superficially resemble those of *Leanchoilia* (Stein *et al.* 2008, fig. 4b). Regardless, *O. oelandica* displays a remarkable set of appendages with morphologies that straddle those of basal arthropods and derived crustaceomorphs. For the largest instar yet known, the limbs from head appendage 4 posteriorward appear similar to those of many stem-group arthropods, with a strong basipod, spiny, multisegmented endopod and lobose exopod (Stein

et al. 2008, fig. 7d–f). However, head limb 2 has a crustacean-like appearance, with a short endopod and stenopodous exopod bearing long setae, or insertions for them (Stein *et al.* 2005, fig. 3c).

Head limb 3 on *O. oelandica* is stranger still; in the smallest instar known, it appears similar to the antennal limb (i.e. head segment 2; Stein *et al.* 2008, fig. 9c, g). However, in larger instars, it bears an exopod which is lobate towards its base and stenopodous with long setae distally (Stein *et al.* 2008, fig. $5a_1$), presenting perhaps an intermediate form between a lobate and stenopodous exopod. In contrast, the exopod of the third head limb of the analysed *Leanchoilia* 'metanauplius' of Liu *et al.* (2016, fig. 3d) appears very similar to the crustaceomorph antenna and early-instar third limb of *O. oelandica* (although segmentation of the former cannot be discerned with the resolution of their figured data), but this limb matures to a 'standard' stem-group arthropod limb (compare to 'h2' in Liu *et al.* 2016, fig. s4). This is not to suggest that *O. oelandica* should be seen as a somewhat more-derived megacheiran, but rather as evidence in support of the hypothesis of Aria & Caron (2017*a*) that features typical of crustacean adults may be found in unrelated larval forms, and that adult crustaceans acquired some of these morphologies through paedomorphosis. For example, head limb 3 on *O. oelandica* also bears a small proximal endite, but was seen as a potential precursor to a crustacean coxa by Stein *et al.* (2005). It also invites comparison to the unusual basipod endites of the trunk limbs of *P. venator* (Figs 8A–D, 9B, C, E). Paedomorphic retention or heterochronic modification of juvenile features may explain why the leg morphologies in *P. venator* differ so substantially from 'standard' megacheirans, or other arthropod groups in general. Admittedly, a combination of heterochronic trends would probably be necessary to derive the full suite of rami on the main trunk limbs of *P. venator* from a megacheiran ancestor (Fig. 11C). However, without more information from ancestors or relatives, we are reluctant to speculate on the sequence of these changes at this point.

In some respects, *Parioscorpio venator* compares favourably for a relationship to Chelicerata, and may be seen as amenable to the short-great-appendage-to-chelicerae hypothesis of Haug *et al.* (2012*a*) and Chen *et al.* (2004); a hypothesis recently supported by the confirmation of reduced labra in the adults of both megacheirans and chelicerates (Liu *et al.* 2020). Importantly, *P. venator* bears a chelate frontal-most appendage (char. 72[1]), a synapomorphy common to *Offacolus kingi* (Table 3) and indeed to all chelicerates. Within the schema of Haug *et al.* (2012*a*), the four great appendage elements (Fig. 5A–D) would place it in the same morphological step as Pantopoda, which had split from Euchelicerata by the late Cambrian (Waloszek & Dunlop 2002) at the latest, and one step above the megacheiran *Haikoucaris ercaiensis* (Haug *et al.* 2012*a*, fig. 11), which would suit both a placement in the chelicerate stem and a potential bridge to Megacheira. The structure of the last two trunk limbs of *P. venator* could offer another chelicerate connection: interpreted here as uropod-like rami useful in locomotion, their relatively delicate nature compared to the filamentous bundles of the more anterior limbs (Fig. 8) could indicate a respiratory function (Suzuki & Bergström 2008).

Nonetheless, at this point, character affinities are simply not strong enough to confidently assign *P. venator* to the chelicerate stem. There are several key chelicerate characters that *P. venator* does not possess, among them characters 89, 180 and 183. Character 89, 'proximo-distal differentiation of endopod podomeres in head', is shared by all chelicerate taxa in the character matrix, except the larval form of *Cambropycnogon*. The latter two characters code for the tagmatization of limbs optimized for locomotion and food manipulation in the prosoma and limbs modified for respiration and reproduction in the opisthosoma, which are key trends in the evolution of Euchelicerata (Dunlop & Lamsdell 2017) that are simply not developed in *P. venator*. The shared trait of a chelate frontal-most appendage between *P. venator* and Chelicerata (Table 3) is not unambiguous, either. Technically, the operation is subchelate in *P. venator* (Fig. 12A), as it is in the 'clasp-knife' operation of the chelicerae of Araneae (Dunlop & Lamsdell 2017). Nonetheless, Araneae scores 'present' for character 72 in Aria & Caron (2017*a*), so we consider it reasonable to do the same for *P. venator*, although this does not guarantee homology with the chelicerate chelicerae. Finally, the robust hypostome of *P. venator* (Figs 3A, C, D, 4A, 5C, D) is not consistent with the synapomorphy of a reduced labrum uniting Megacheira and Chelicerata, as proposed by Liu *et al.* (2020). This morphology would have to be seen as a reversion to the ancestral state (Liu *et al.* 2020, fig. 3) if *P. venator* is a stem-group chelicerate.

If *P. venator* is a member of the chelicerates, it would be placed far back on the stem, perhaps in a similar position to Habeliida (Aria & Caron 2017*b*), although it is unlikely that these are closely related to *P. venator* (Anderson *et al.* 2021, appendix S2). For these same reasons, placement of *P. venator* within crown Euchelicerata, as proposed by Wendruff *et al.* (2020*a*), is untenable, as described with greater detail in Interpreting *Parioscorpio* as a scorpion, above.

Affinities with Sidneyia*, artiopods, and the status of* Xus yus. When comparing *Parioscorpio venator* to *Sidneyia inexpectans*, there are no unique potential synapomorphies between the two species. Some apparent similarities do not hold under closer inspection. For example,

the trunk limbs of *S. inexpectans* bear a large, crescentic basipod and a three-segmented exopod (see the reconstruction in Stein 2013, fig. 9), which is somewhat atypical compared to most artiopods. Nevertheless, they bear little resemblance to the trunk legs of *P. venator*. Additionally, the last two somites of *S. inexpectans* also show a major change in limb morphology, as in *P. venator*; however, the penultimate somite of *S. inexpectans* bears no limbs at all, and the uropod-like limbs of the final somite do not resemble those of *P. venator* (Bruton 1981).

Nonetheless, the general body shape of *P. venator* does conform to that of an artiopod, with tergopleurae that extend out laterally (char. 154[0]) and potentially dorsally expressed eyes (char. 27[?]; Table 1), true of many artiopods like Aglaspidida (Van Roy 2006; Lerosey-Aubril *et al.* 2017) and Trilobita (Whittington 1997). Our preferred interpretation of the exopods as rodiform (char. 182[2]) is an unusual trait shared in the phylogenetic analysis character table only with the trilobitomorphs *Olenoides*, *Naraoia* and *Xandarella* (Table 3). Previously, some specimens of *P. venator* had been interpreted as cheloniellids, first in the dissertation of Wendruff (2016) as *Latromirus tridens*, then in an unpublished but publicly available manuscript with the placeholder name of *Xus yus* Wendruff *et al.*, 2018. While some specimens of this unofficially described taxon, including the putative holotype UWGM2439 (Wendruff *et al.* 2018, fig. 1a–c) and one of the putative paratypes, UWGM2345 (Wendruff *et al.* 2018, fig. 1d), may indeed be cheloniellids, or at least vicissicaudatans, others (UWGM2436, 2437 and 2575; Wendruff *et al.* 2018, fig. 1e–l) more closely resemble *Parioscorpio venator*, and we reassign them as such.

The prior assignment of these three specimens to the same species as UWGM2439 and 2345 was probably due to an erroneous homogenization between what appear to be eyes in the putative holotype (Wendruff *et al.* 2018, fig. 1c) with the second cephalic appendage exopod of *P. venator*, which is of a similar shape in normal light and in a similar position on the head (e.g. Figs 4D, 5A, C). The actual eyes of *P. venator* are, however, anterior and relatively medial on the head, overlapping the muscle blocks (e.g. Fig. 3A–D). The segment count, relative width of the tergopleurae and the structure of the three-pronged tail apparatus appear to be different between *P. venator* and the proposed holotype of *L. tridens*/*X. yus*. The latter also lacks great appendages, bearing instead a short appendage with a coarsely setose terminus (Wendruff *et al.* 2018). The preservation quality of the 'raptorial appendages' on UWGM2345 (Wendruff *et al.* 2018, fig. 1d) is too poor to determine what they actually are: they could represent raptorial appendages, the 'small anterior appendage' of UWGM2439, or stout antennae.

Taphonomically, Wendruff *et al.* (2018) asserted that UWGM2439 and 2345 are dorsally preserved while UWGM2436, 2437 and 2575 are ventral equivalents of the same species. Dorsal preservation would explain the lack of legs on UWGM2439 and 2345. However, there is no reason the pleural fields should not also be well-preserved in the ventral specimens, as they are in UWGM2439 as sheets of phosphate and in UWGM2345 as carbonaceous compressions or kerogen-rich dark impressions after the removal of francolite. In *Parioscorpio venator*, the pleural fields are either not preserved or preserved tenuously (Figs 2C, 6D, F, 10D, E; Wendruff *et al.* 2018, fig. 1e–f, h, j–l); only in UWGM2575 do they show some substantial phosphatization (Wendruff *et al.* 2018, fig. 1i). Due to these morphological and taphonomic differences, *Parioscorpio venator*, including UWGM2436, 2437 and 2575 are a separate species from *L. tridens*/*X. yus*, represented by UWGM2439 and 2345.

On a technical note, it is prudent to emphasize here that *Xus yus* is not considered to be an available name under the code of the International Commission of Zoological Nomenclature (ICZN) for several reasons. First, the name had an initial, unpublished ZooBank entry associated with an article submitted to *PLoS One*, but the article was never published and the corresponding ZooBank entry has since been deleted. Second, the manuscript was made available through *bioRχiv*, which does not have an ISSN registered to ZooBank, nor does it list an intended online archive on ZooBank. Finally, within the manuscript available on *bioRχiv*, there is no mention of either ZooBank or an LSID. However, because UWGM2439 and 2345 were not available for physical examination, it is beyond the scope of this article to alleviate their taxonomic conundrum.

Could *P. venator* still be a cheloniellid, or at least an artiopod? The greatest obstacle to an artiopodan affinity is not the presence of great appendages, but its lack of antenniform antennules. Although rare, a few artiopods have developed a specialized anterior appendage comparable to a great appendage. These include a small pair of potentially raptorial appendages in *Cheloniellon calmani* Broili, 1932 (Stürmer & Bergström 1978) and a large pair of clearly raptorial appendages in *Kodymirus vagans* (Lamsdell *et al.* 2013). In both these cases, though, the raptorial limbs are posterior to the preserved antennules, and can even be seen in *K. vagans* inserting in the standard tritocerebral position on the posterolateral side of the hypostome (Lamsdell *et al.* 2013, fig. 5a–b). In contrast, the great appendages of *P. venator* insert far anteriorward on the head (Figs 3A–D, 4D–H, 5E–G) in a position more compatible with a deutocerebral interpretation.

At this point, we consider it unlikely that *P. venator* bears a strong affinity to Artiopoda, as major changes to both the anteriormost appendage and the trunk limbs (compare Edgecombe & Ramsköld 1999; Mayers *et al.*

2019 to Figs 8, 9) would be required for an artiopod ancestor to be directly related to *P. venator*. However, the unexpected finding of the vicissicaudatan *Kodymirus vagans* and its large raptorial appendages (Lamsdell *et al.* 2013) and the hints of morphological variety seen in the trunk limbs of more derived Vicissicaudata (Stürmer & Bergström 1978; Briggs *et al.* 1979; Hesselbo 1992) point to the potential of limb disparity in this still-enigmatic group (Lerosey-Aubril *et al.* 2017). The discovery of a transitional form between *P. venator* and a species like *S. inexpectans* would certainly prompt a reevaluation of our conclusion.

Affinities with fuxianhuiids and mandibulates. There are several potential synapomorphies between *Parioscorpio venator*, *Fuxianhuia*, and its relatives (Table 3), which include *Chengjiangocaris*, *Shankouia* (together, the fuxianhuiids, in a paraphyletic sense) and the Euthycarcinoidea *s.s.* in both Aria & Caron (2017*a*) and our analyses (Fig. 15). These include lacking ophthalmic ridges (char. 28[0]), bearing a reduced 'post-antennular appendage' with a strongly clawed terminus (char. 94[1]) and having 'metameric ganglia on [the] nerve cord' (char. 141 [1]). The first character is unlikely to be of much significance, as only *Limulus* and *Olenoides* score a 1 for an ophthalmic ridge, it being inapplicable or absent for other taxa. The absence of character 141 in most taxa is almost certainly a taphonomic effect, although it is curious that *P. venator* (Fig. 7A–H), *Fuxianhuia protensa* Hou, 1987 (Ma *et al.* 2012) and *Chengjiangocaris kunmingensis* Yang *et al.*, 2013 (Yang *et al.* 2016) all have the potential to preserve this tissue which is vanishingly rare in other taxa.

Character 94, which codes 1 for 'the specialized post-antennal appendage (SPA)' in *Fuxianhuia* (Yang *et al.* 2013) and the endopod of the second cephalic appendage in *P. venator* (Figs 4F–H, 5C, D, G) is the most compelling synapomorphy due to the unusual structure of the short, claw-like appendage. Even so, it is difficult to homologize the structure between the taxa. *Fuxianhuia* and its relatives bear antenniform antennules (char. 74 [0]) although they are fairly robust (char. 75[0]). Homologization to the great appendages of *P. venator* would, as in the artiopod case, require a major transformation of the antennule form.

A potential synapomorphy not specifically coded for in the character table of Aria & Caron (2017*a*) concerns the tagmatization of fuxianhuiids' anterior somites. The 'head', such as it is, consists of a small anterior sclerite and a larger posterior sclerite that collectively bear the eyes, antennules and SPAs. This creates a three somite 'head' with two limb pairs, a condition which does not have a specific state for character 32, the number of 'somites defining [the] anteriormost tagma'. Thus, character 32 was coded ? for *Fuxianhuia*, *Shankouia* and *Chengjiangocaris* by Aria & Caron (2017*a*) and, by inheritance, our character table (Anderson *et al.* 2021, appendix S1). This three-somite head also bears an interesting resemblance to the minimalist interpretation in *P. venator*, where what appears to be the head only has two limb sets: the great appendage and the second cephalic appendages. The reduced first two 'trunk' appendages in *P. venator* would then complete the plesiomorphic arthropod head (e.g. Chen *et al.* 2004) that is not explicitly expressed in the head tagma of the adult. Interestingly, the first two 'trunk' limbs of *C. kunmingensis* are also quite diminutive (Yang *et al.* 2013, fig. 3), though like those of *P. venator*, they imitate the structure of the full-sized trunk legs.

The surprising number of potential synapomorphies between *Fuxianhuia* and *P. venator* led us to consider one final alternative state analysis, in which several features of the head of *P. venator* were considered homologous to Fuxianhuiida (Fig. 16). Specifically, we interpreted the great appendage, not the second cephalic endopod, as the SPA, where the muscle blocks (Figs 3A, C, D, 4D, E) form the first element of the SPA, elements 2 and 3 of the great appendage together form element 2 of the SPA (Figs 4F–H, 5A, B), with the y-shaped first element of the great appendage representing an apodeme connecting SPA element 1 to element 2 (Figs 4F–H, 5C, D) and great appendage element 4 represents SPA element 3. The SPA is thus a three-segmented structure as it is in *Fuxianhuia* and *Chengjiangocaris* (Yang *et al.* 2013), but flipped forward and much enlarged. Indeed, the muscle blocks often appear very similar to the great appendages when they are dark impressions (e.g. Fig. 2A, C, D, F), and would allow for the SPA of *P. venator* to still be seen as tritocerebral as they are for the fuxianhuiids (Ma *et al.* 2012; Yang *et al.* 2013), inserting posterolateral to the hypostome (Figs 3A, C, D, 5C, D). Functionally, though, the first article of the SPA would probably not be very mobile (Fig. 16B) and would serve as an articulation base for the second article, much as it did when seen as a cephalic muscle block for a deutocerebral great appendage (Figs 12B, 16A).

Other morphological changes include reinterpreting the endopod of the second cephalic appendage as a much-reduced antennule (Figs 4D, F–H, 5C, D, G), akin to what occurs in the nepomorph true bugs (Carver *et al.* 1991), the similarity of their raptorial appendages to the great appendage of *P. venator* having been discussed in Features of the Head, above. The exopod of the second cephalic appendage would then be seen as a lateral eye, the banana-shaped podomere representing the visual surface (Figs 4D, F–H, 5A–D, G–I). They would be slightly pedunculate and lateroventral (Fig. 16B), and not dorsally embedded in the head shield, as presumed for *Xus yus* (Wendruff *et al.* 2018). This would mean that the eyes

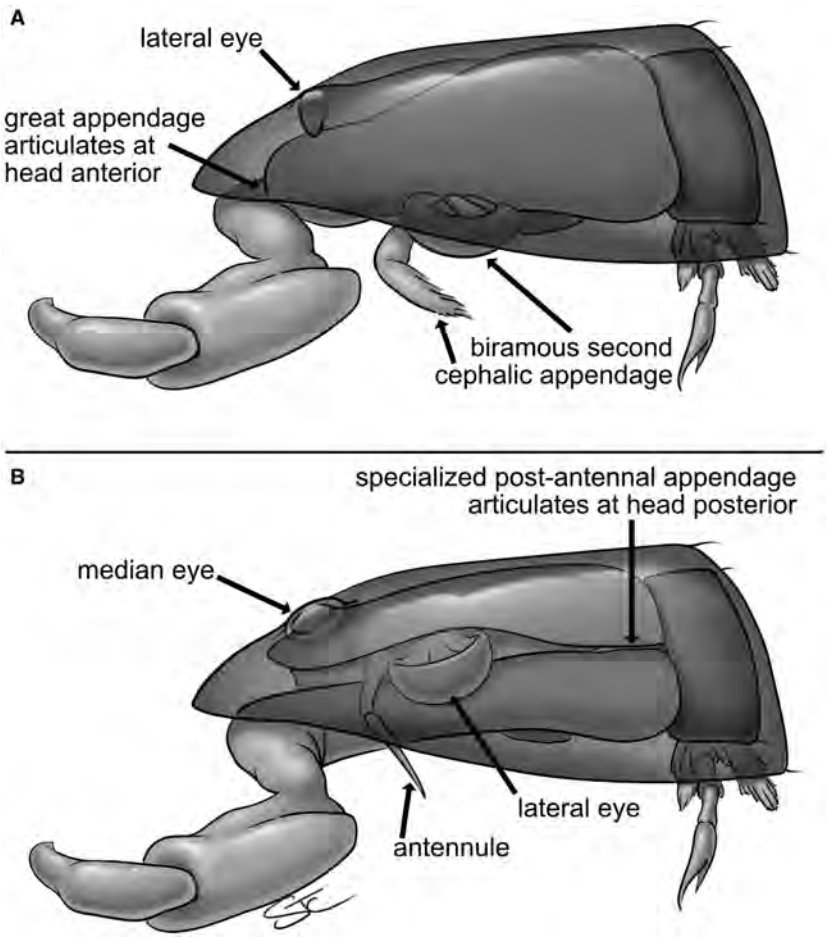

FIG. 16. Reconstructions of the head and first trunk segment of *Parioscorpio venator* from a lateral perspective, according to two morphological interpretations. A, the preferred, standard interpretation where the great appendage is operated by a muscle block in the head and the second cephalic appendage is biramous. B, an alternative 'Fuxianhuiid-head' interpretation, where the great appendage is a specialized post-antennal appendage (*sensu* Yang *et al.* 2013), inserted behind the hypostome; the second cephalic appendage endopod is seen as an antennule, and the former second cephalic appendage exopod is reinterpreted as a lateral eye, the former lateral eye now rising as a large, turret-like median eye on the dorsal surface of the head.

seen in multiple specimens (Figs 3A–D, 4B, D, F, G, 5F) would represent large median eyes.

Although these reinterpretations offer more conventional explanations for some features; namely that the strange curled second cephalic appendage exopod is just an eye, and the large cephalic muscle blocks are large, muscular appendage articles (Fig. 16), they also raise other morphological questions. What of the apparent faceting in UWGM2793, seen in Figure 3A, which is now seen as a median eye? What became of the anterior sclerite, typically seen in fuxianhuiids (Yang *et al.* 2013; Ortega-Hernández 2015)? Finally, what is the significance of the ring-like structures seen in the head of *P. venator* if they are not associated with relict head segmentation (Fig. 4A–C)? Regardless, a fuxianhuiid interpretation of the head features in *P. venator* is compelling, and we altered the coding for *Parioscorpio* in our character matrix accordingly (see the yellow-highlighted characters for the 'Fuxianhuiid-head interpretation' row in Anderson *et al.* 2021, appendix S1).

The phylogenetic analysis was run as it was for the primary and alternative character state analyses, except that the taxon 'Euthycarcinoidea' was removed. Despite the close association of Euthycarcinoidea *s.s.* with the fuxianhuiids in Aria & Caron (2017*a*, *b*) and this study (Fig. 15; Anderson *et al.* 2021, fig. S1a–b, e), the discovery by Edgecombe *et al.* (2020) of details of a tentorium and hypopharynx in the Devonian euthycarcinoid *Heterocrania rhyniensis* Hirst & Maulik, 1926 that closely resemble those of myriapods suggests a close relationship between the two (in addition to other characters, see Edgecombe *et al.* 2020, pp 8968–8969). This does not mean that euthycarcinoids and myriapods could not both be closely related to the fuxianhuiids, but some character states for Euthycarcinoidea *s.s.* should be changed or added to the matrix of Aria & Caron (2017*a*), a task beyond the scope of this study. For now, we simply exclude Euthycarcinoidea *s.s.* for this last analysis, which specifically seeks to compare *P. venator* to the fuxianhuiids.

The results (Fig. 17) show *Parioscorpio* to resolve not within Fuxianhuiida, but in a polytomy at the base of Euarthropoda, with the fuxianhuiids and remaining euarthropods forming the other two branches. The remaining euarthropods, in turn, resolve Megacheira as the sister group to the crown euarthropods and the artiopods,

which form a broad polytomy with little clade cohesion beyond those supported by the backbone. In the 50% majority rule tree, *Parioscorpio* resolves as the sister to all other euarthropods in 79% of the trees. Notably, at 891 steps, the 470 most parsimonious trees of this analysis are 9 steps shorter than any analysis including Euthycarcinoidea *s.s.* (Fig. 15; Anderson *et al.* 2021, fig. S1). Some clades are also surprisingly resilient in Bremer analysis when compared to many of the other phylogenies: Megacheira remain (albeit as a polytomy) until step 3, and the fuxianhuiid polytomy and resolved Arachnida persist until step 4.

Oddly, a closer association with Fuxianhuiida is found in some of our other alternative state analyses, where Euthycarcinoidea *s.s.* is included and the great appendage is not coded as the SPA. Phylogenetic analyses where alternative states were coded as uncertain (?) resolved a topology with *P. venator* as the sister to a clade containing Euthycarcinoidea *s.l.* and Hymenocarina in the strict consensus tree (Anderson *et al.* 2021, fig. S1a–b). This scenario, in which *P. venator* is related to both the fuxianhuiids and stem-group Mandibulata is actually rather compelling, as *P. venator* bears some characters typical of Mandibulata.

Parioscorpio venator shares one potential synapomorphy with the comparison taxon stem-mandibulate *Tokummia katalepsis* (Table 3), namely that no cephalic limbs appear to be adapted to walking (char. 86[0]), which is also shared with the closely-related *Branchiocaris* and most other members of Mandibulata (Anderson *et al.* 2021, appendix S1). *Parioscorpio venator* also does not have a 'repeated appendage morphology' in its head (char. 87 [0]) a state common in Mandibulata which is true for *P. venator* mainly because it has only two head appendages. Additionally, epipods are not known outside of Crustacea (Boxshall 2004), so the epipod/exopod interpretation of the main trunk limbs in *P. venator* (Table 2) would argue very strongly for inclusion within Mandibulata, as would multiple subdivisions seen in the trunk limb basipods of UWGM2854 (Fig. 9C), if they prove to be authentic (Aria & Caron 2017*a*).

If *P. venator* is a member of Mandibulata, though, it would have to be as a specialized stem species. Perhaps the most important mandibulate character set absent in *P. venator* is the intricate modification of the head limbs for food gathering and manipulation into a highly distinct head tagma (Walossek & Müller 1990; Scholtz & Edgecombe 2005; Stein *et al.* 2005). Most head appendages appear to be missing, and it is only the great appendage, in the position of the antennule (or antenna, as a SPA), which is strongly adapted for food gathering. While the antennules (and antennae) of Mandibulata may bear few antennomeres and be employed for a variety of purposes (e.g. McLaughlin 1982; Walossek & Müller 1990; Boxshall 2004), the seizing capture of larger prey is not one of them (Fig. 12). Fortunately, hypothesized stem-mandibulates have been shown to accommodate a wide variety of body forms that do not show many of the characters typical of crown-group crustaceans and myriapods (e.g. Walossek & Müller 1990), and more head appendages may have been present in larval *P. venator* that are reduced to the point of absence in the adult forms.

The corollary to this is the hypothesis of Aria & Caron (2017*a*), in which the 'crustacean-like' morphologies common to many larval forms are synapomorphically maintained in adults in Mandibulata. Thus, the interpretation of mandibulate-like features in *P. venator* (e.g. non-lobate trunk exopods, the potential of epipods and sub-segmented basipods in the trunk limbs) must be done with caution when interpreting potential homologies. Nonetheless, the placement of *P. venator* in 'alternative state' phylogenetic analyses at either the base of a stem-mandibulate clade uniting Euthycarcinoidea *s.l.* and Hymenocarina (Anderson *et al.* 2021, fig. S1a–b) or at the base of Mandibulata in some 50% majority rule consensus trees (specifically, the 'negative certainty' interpretation analyses and the epipod/exopod interpretation of the 'positive certainty' analyses) leaves us to consider the alliance of *P. venator* to the mandibulates as a serious possibility.

Comparisons with Marrella *and* Agnostus

Marrella splendens was included as a comparison taxon because, like *Parioscorpio venator*, it has proven difficult to phylogenetically classify with confidence (e.g. Hou & Bergström 1997; Siveter *et al.* 2007; Lamsdell *et al.* 2013;

FIG. 17. Strict consensus tree cladogram demonstrating the placement of *Parioscorpio venator* in the arthropod tree using the character matrix of Aria & Caron (2017*a*) as a basis, but with the removal of Euthycarcinoidea and with various morphologies of the head of *P. venator* interpreted as being homologous with Fuxianhuiida (the fuxianhuiid-head interpretation). Namely, the great appendage is interpreted as a tritocerebral specialized post-antennal appendage (*sensu* Yang *et al.* 2013), the second cephalic endopods are interpreted as deutocerebral antennules, the second cephalic exopods are interpreted as lateral eyes, and the former lateral eyes are interpreted as median eyes. Major monophyletic clades within Arthropoda are labelled, the placement of *P. venator* is highlighted in yellow and bold numbers to the left of nodes are Bremer support values. *Abbreviations*: Hex., Hexapoda; Hym., Hymenocarina; Meg., Megacheira; Fux., Fuxianhuiida.

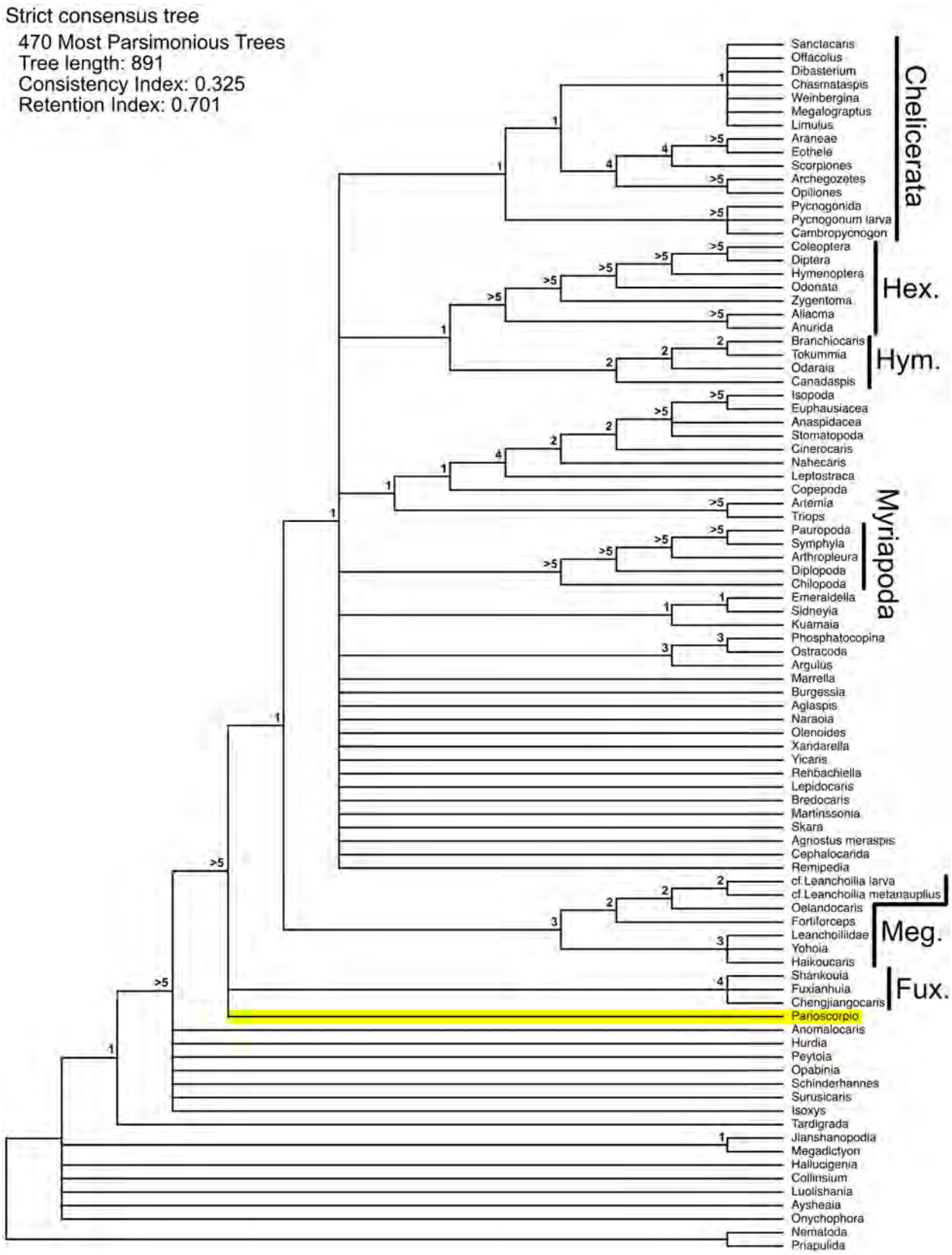
Strict consensus tree
470 Most Parsimonious Trees
Tree length: 891
Consistency Index: 0.325
Retention Index: 0.701
Sanctacaris
Offacolus
Dibasterium
Chasmataspis
Weinbergina
Megalograptus
Limulus
Araneae
Eothele
Scorpiones
Archegozetes
Opiliones
Pycnogonida
Pycnogonum larva
Cambropycnogon
Chelicerata
Coleoptera
Diptera
Hymenoptera
Odonata
Zygentoma
Allacma
Anurida
Hex.
Branchiocaris
Tokummia
Odaraia
Canadaspis
Hym.
Isopoda
Euphausiacea
Anaspidacea
Stomatopoda
Cinerocaris
Nahecaris
Leptostraca
Copepoda
Artemia
Triops
Pauropoda
Symphyla
Arthropleura
Diplopoda
Chilopoda
Myriapoda
Emeraldella
Sidneyia
Kuamaia
Phosphatocopina
Ostracoda
Argulus
Marrella
Burgessia
Aglaspis
Naraoia
Olenoides
Xandarella
Yicaris
Rehbachiella
Lepidocaris
Bredocaris
Martinssonia
Skara
Agnostus meraspis
Cephalocarida
Remipedia
cf.Leanchoilia larva
cf.Leanchoilia metanauplius
Oelandocaris
Fortiforceps
Leanchoiliidae
Yohoia
Haikoucaris
Meg.
Shankouia
Fuxianhuia
Chengjiangocaris
Fux.
Parioscorpio
Anomalocaris
Hurdia
Peytoia
Opabinia
Schinderhannes
Surusicaris
Isoxys
Tardigrada
Jianshanopodia
Megadictyon
Hallucigenia
Collinsium
Luolishania
Aysheaia
Onychophora
Nematoda
Priapulida

Legg *et al.* 2013; Aria & Caron 2017*a*). In the strict consensus trees of our analyses, it either stood alone as part of a broad euarthropod polytomy (Fig. 17; Anderson *et al.* 2021, fig. S1c–d) or resolved in the 'lamellipedian' position associated with Artiopoda (Fig. 15; Anderson *et al.* 2021, fig. S1a–b, e–f). Notably, any node supporting Lamellipedia always collapsed within a single step of Bremer analysis.

Morphologically, *Marrella* is unusual even for Marrellomorpha; like *P. venator*, it bears only two cephalic appendages (García-Bellido & Collins 2006), fewer than any other marrellomorph (*Xylokorys chledophilia* Siveter *et al.*, 2007 and *Vachonisia rogeri* Lehmann, 1955 have the most at five), although unlike *P. venator* they are both uniramous (excepting the fuxianhuiid-head interpretation). If the exopod setae of *Marrella* are not lamellate, but filamentous, as interpreted by Rak *et al.* (2013), then another trunk limb character is potentially shared between *M. splendens* and *P. venator*. The trunk exopods are clearly annulate in *Marrella* (García-Bellido & Collins 2006, fig. 13c–d), and if the annulation on the exopod ramus of *P. venator* specimen UWGM2854 is authentic (an alternative state in Table 1), this would indicate that *P. venator* and *M. splendens* share highly unusual annulate exopods with setiferous filaments. Despite these shared traits, we nonetheless do not consider *P. venator* to be particularly closely related to *M. splendens* or to any of the marrellomorphs. They do not resolve closely together in our phylogeny (Fig. 15) and *P. venator* does not have a multisegmented trunk (char. 149) or medially directed trunk appendage setae, present in Marrellomorpha (Rak *et al.* 2013). Further, although the cephalic limbs can be quite robust in some marrellomorphs (e.g. *Mimetaster hexagonalis* Gürich, 1931, discussed by Stürmer & Bergström 1976) no known marrellomorph ever approximates a great appendage on its antennule somite.

Like *Oelandocaris*, *A. pisiformis* has been considered a candidate for the larviform-appendages-as-crustaceomorph hypothesis of Aria & Caron (2017*a*), and is thus of great interest for comparison to the unusual limbs of *P. venator*. *Agnostus pisiformis* and the rest of the agnostids were long considered to be diminutive trilobites whose bauplan was achieved by paedomorphosis (Chatterton & Speyer 1997; Jell 1997) until the discovery of limbs by Müller & Walossek (1987) in meraspids and early holaspids of *A. pisiformis*. These limbs were seen as sufficiently crustacean-like that it was hypothesized that *A. pisiformis* was a stem-group crustacean (e.g. Walossek & Müller 1990; Stein *et al.* 2005), comparing particularly favourably to *Henningsmoenicaris scutula* Walossek & Müller, 1990. Both the phylogeny of Aria & Caron (2017*a*) and most of our phylogenetic analyses resolve *A. pisiformis* as artiopods, although not necessarily as the sister to the trilobite *Olenoides* (Fig. 15; Anderson *et al.* 2021, fig. S1a–b, e–f). As with *Marella*, the analyses where alternative states are coded as absent or the smallest possible number of a repeating morphology and the fuxianhuiid-head analysis only resolve *Agnostus* as part of a euarthropod polytomy (Fig. 17; Anderson *et al.* 2021, fig. S1c–d).

Agnostus pisiformis shares one potential synapomorphy with *P. venator* unique among the stem-group comparison taxa (Table 3): 'exopod ornamentation type' consisting of 'setae' (char. 190[0]). This trait is common in crown-group Crustacea, but it is also found on the leanchoiliid 'metanauplius' of Liu *et al.* (2016), supporting both the hypothesis of Aria & Caron (2017*a*) and the notion that some limb features of *P. venator* could be acquired through paedomorphosis. The bizarre 'club-shaped appendages' on the endopod podomeres of *A. pisiformis* (Müller & Walossek 1987, pl. 16, fig. 3) compare favourably to the racemose bundle-bearing endopodal exites of *P. venator* (Figs 8A–D, 9A–E), and is indeed the only example we could find of a comparable structure in the arthropod fossil record. We agree with Chatterton & Speyer (1997) that the limbs of *A. pisiformis* would have to represent a combination of heterochronic and innovative morphological changes, and this is likely to be the case for *P. venator* too.

Although *P. venator* and *A. pisiformis* share these specific traits and a general crustacean-like trend in limb morphology, we nonetheless do not support a close affinity between the two, as their morphology is considerably disparate in most other respects. Important characters to consider are the gradual change in limb shape across the head of *A. pisiformis* which is abrupt in *P. venator* (chars 86, 88), the small number of trunk segments in *A. pisiformis* (char. 147[4]), and the presence of a pygidium in *A. pisiformis* (char. 209[1]) while *P. venator* bears a telson (char. 201[1]). Nonetheless, it is encouraging to take note of the broad variety of limb morphologies found in stem-group arthropod taxa, even as it makes classification schemes an endeavour of great difficulty.

CONCLUSION

Parioscorpio venator is an unusual arthropod that is among the best-preserved and most character-rich of all the fossils at the Waukesha lagerstätte. Previously interpreted as a remipede, branchiopod (Mikulic *et al.* 1985*a*, *b*), cheloniellid (Wendruff *et al.* 2018) or a scorpion (Wendruff *et al.* 2020*a*), our redescription does not find a definitive affinity with any major euarthropod group (Figs 15, 17), although it shares individual potential synapomorphies with many clades, particularly the fuxianhuiids (Table 3). It is worth noting the unfortunate association of the generic name *Parioscorpio* with a taxon that is demonstrably

not a scorpion. This only clouds the affinities of this organism in the taxonomic literature going forward. *Parioscorpio venator* instead possesses a distinct and unusual morphology with large raptorial appendages with subchelate tips and large muscle blocks in its head that allowed for the great appendages to be forcefully brought together (Fig. 12). The much smaller, apparently biramous second cephalic appendages may have been useful in processing food or had a sensory function, since the animal apparently did not have antennae. Alternatively, the muscle blocks may be seen as the first article of a specialized post-antennal appendage like that of the fuxianhuiids, with short antennae and lateroventral eyes situated dorsal to this first article, about halfway along its length (Fig. 16B). The first articles would be relatively immobile, and the raptorial action of the distal articles would remain essentially the same in this alternative interpretation. Most of the trunk legs consist of an exopod and an endopod with a prominent endopodal exite, as well as numerous filamentous bundles that may have helped to keep the arthropod clean, respire or sense its environment. The last two trunk legs form paddle-like fans that may have been useful in keeping the posterior clean and in escaping from threatening situations, or they may have been directly used in respiration as in limulid and eurypterid gills (Dunlop & Lamsdell 2017; Suzuki & Bergström 2008). The axial, branchiopod-like body was enveloped by a broad, usually poorly-preserved tergopleural exoskeleton, whose posterior segments probably ended in spines.

While *P. venator* is not a scorpion, our understanding of the timing of scorpion evolution is fortunately only slightly affected, as the oldest occurrence of Scorpiones is *c.* 1 myr younger than the Waukesha (Laurie 1900; Wendruff *et al.* 2020*a*). On the other hand, the exploration of the potential lineages of this complex stem-group arthropod presented here can inform on the evolution of any of several stem-arthropod groups. In particular, if *P. venator* proves to be a member of Fuxianhuiida, it would extend the range of this group by tens of millions of years. Additionally, the diagnosis of *P. venator* and its present rediagnosis and redescription serve to emphasize the palaeontological and palaeobiological information that is stored in Laurentia's mid-Palaeozoic lagerstätten. Lacking the sheer outcrop size or taxonomic diversity of some of the great Cambrian deposits, these have often been understudied or dismissed since they do not contain a 'normal' open marine fauna. The preserved multiple tissue types of *Parioscorpio venator* argue against this interpretation, and these small middle Palaeozoic lagerstätten may represent palaeontology's best hope of tracing the passage of the Cambrian world into the Palaeozoic and the beginnings of the Modern fauna (Lamsdell *et al.* 2017). Recently, the Waukesha (e.g. Haug *et al.* 2014; Jones *et al.* 2015) and deposits like it (Vrazo *et al.* 2017), including the Winneshiek (e.g. Lamsdell *et al.* 2015*a*, *b*), Eramosa (e.g. von Bitter *et al.* 2007; LoDuca & Tetreault 2017), Manitoba (e.g. Rudkin *et al.* 2008; Rudkin *et al.* 2013) and Big Hill (e.g. Lamsdell *et al.* 2017; Lamsdell *et al.* 2019) lagerstätten, have attracted considerable palaeontological attention, and we hope this trend will continue. Ultimately, the resolution of the affinity of *P. venator* will probably be found amongst its relatives and predecessors in these deposits.

Acknowledgements. We thank Carrie Eaton, Museum Curator of the University of Wisconsin Geology Museum, for access to specimens, aid with processing the specimen loans, and for photographing UWGM2798 for Figure 1H and UWGM2779 for Figure 2D, Stacy Turpin Cheavens for professional illustrations featured in Figures 11, 12 and 16, Lauren Wright for assistance in tracing Figures 6D and 10D–E, Loren Babcock and Andrew J. Wendruff for valuable conversations, and Waukesha Lime and Stone Company for allowing and facilitating the initial collection of the specimens consulted in this study. We also thank Bruce Lieberman and two anonymous reviewers for comments that greatly assisted in the improvement of previous versions of this manuscript. This research was supported by National Science Foundation (NSF) Earth Sciences Postdoctoral Fellowship (EAR-PF) 1725762 (EPA) and NSF Sedimentary Geology and Paleobiology CAREER Award 1652351 (JDS). Instrumentation used for analyses was acquired through NSF Instrumentation and Facilities 1636643 (JDS).

DATA ARCHIVING STATEMENT

Data for this study (including tables of morphological measurements, the phylogenetic analysis character matrix with *Parioscorpio venator* and the comparison taxa highlighted and its associated nexus files, strict consensus trees for alternative state analyses, and further considerations of potential relationships between *P. venator* and the stem-group comparison taxa) are available in the Dryad Digital Repository: https://doi.org/10.5061/dryad.rn8pk0p5w

Editor. Xi-Guang Zhang

REFERENCES

ANDERSON, E. P., SCHIFFBAUER, J. D. and XIAO, S. 2011. Taphonomic study of Ediacaran organic-walled fossils confirms the importance of clay minerals and pyrite in Burgess Shale-type preservation. *Geology*, **39**, 643–646.

—— —— JACQUET, S. M., LAMSDELL, J. C., KLUESSENDORF, J. and MIKULIC, D. G. 2021. Stranger than a scorpion: a reassessment of *Parioscorpio venator*, a problematic arthropod from the Llandoverian Waukesha Lagerstätte. *Dryad Digital Repository*. https://doi.org/10.5061/dryad.rn8pk0p5w

ARIA, C. and CARON, J.-B. 2015. Cephalic and limb anatomy of a new isoxyid from the Burgess Shale and the role of "stem bivalved arthropods" in the disparity of the frontalmost appendage. *PLoS One*, **10**, e0124979.

—— —— 2017*a*. Burgess Shale fossils illustrate the origin of the mandibulate body plan. *Nature*, **545**, 89–92.

—— —— 2017*b*. Mandibulate convergence in an armoured Cambrian stem chelicerate. *BMC Evolutionary Biology*, **17**, 261.

—— —— and GAINES, R. 2015. A large new leanchoiliid from the Burgess Shale and the influence of inapplicable states on stem arthropod phylogeny. *Palaeontology*, **58**, 629–660.

BARTHEL, K. W., SWINBURNE, N. H. M. and CONWAY MORRIS, S. 1990. *Solnhofen: A study in Mesozoic palaeontology*. Cambridge University Press, 244 pp.

BORROR, D. J. and WHITE, R. E. 1970. *A field guide to insects: America north of Mexico*. The Peterson Field Guide Series. Houghton Mifflin Company, New York, 408 pp.

BOXSHALL, G. A. 2004. The evolution of arthropod limbs. *Biological Reviews*, **79**, 253–300.

—— and JAUME, D. 2009. Exopodites, epipodites, and gills in crustaceans. *Arthropod Systematics & Phylogeny*, **67**, 229–254.

BREMER, K. 1988. The limits of amino acid sequence data in angiosperm phylogenetic reconstruction. *Evolution*, **42**, 795–803.

BRIGGS, D. E. G. and CLARKSON, E. N. K. 1989. Environmental controls on the taphonomy and distribution of Carboniferous malacostracan crustaceans. *Transactions of the Royal Society of Edinburgh: Earth Sciences*, **80**, 293–301.

—— and COLLINS, D. 1999. The arthropod *Alalcomenaeus cambricus* Simonetta, from the Middle Cambrian Burgess Shale of British Columbia. *Palaeontology*, **42**, 953–977.

—— BRUTON, D. L. and WHITTINGTON, H. B. 1979. Appendages of the arthropod *Aglaspis spinifer* (Upper Cambrian, Wisconsin) and their significance. *Palaeontology*, **22**, 167–180.

—— ERWIN, D. H. and COLLIER, F. J. 1994. *The fossils of the Burgess Shale*. Smithsonian Institution Press, 238 pp.

—— SIVETER, D. J., SIVETER, D. J., SUTTON, M. D., GARWOOD, R. J. and LEGG, D. 2012. Silurian horseshoe crab illuminates the evolution of arthropod limbs. *Proceedings of the National Academy of Sciences*, **109**, 1–4.

BROCE, J. S. and SCHIFFBAUER, J. D. 2017. Taphonomic analysis of Cambrian vermiform fossils of Utah and Nevada, and implications for the chemistry of Burgess Shale-type preservation. *Palaios*, **32**, 600–619.

BROILI, F. 1932. Ein neuer Crustacee aus dem rheinischen Unterdevon. *Sitzungsberichte der Bayerischen akademie der Wissenschaften, mathematisch-naturwissenschaftliche Abteilung*, **1932**, 27–38.

BRUTON, D. L. 1981. The arthropod *Sidneyia inexpectans*, Middle Cambrian, Burgess Shale, British Columbia. *Philosophical Transactions of the Royal Society B*, **295**, 619–653.

BUDD, G. E. 2002. A palaeontological solution to the arthropod head problem. *Nature*, **417**, 271–275.

BUTTERFIELD, N. J. 2002. *Leanchoilia* guts and the interpretation of three-dimensional structures in Burgess Shale-type fossils. *Paleobiology*, **28**, 155–171.

CAI, Y., SCHIFFBAUER, J. D., HUA, H. and XIAO, S. 2012. Preservational modes in the Ediacaran Gaojiashan Lagerstätte: pyritization, aluminosilicification, and carbonaceous compression. *Palaeogeography, Palaeoclimatology, Palaeoecology*, **326–328**, 109–117.

CARVER, M., GROSS, G. F. and WOODWARD, T. E. 1991. Hemiptera. 429–509. *In* NAUMANN, I. D., CARNE, P. B., LAWRENCE, J. F., NIELSEN, E. S., SPRADBERY, J. P., TAYLOR, R. W., WHITTEN, M. J. and LITTLEJOHN, M. J. (eds). *The insects of Australia: A textbook for students and research workers*. Cornell University Press, 1138 pp.

CATER, J. M. L., BRIGGS, D. E. G. and CLARKSON, E. N. K. 1989. Shrimp-bearing sedimentary successions in the Lower Carboniferous (Dinantian) Cementstone and Oil Shale Groups of northern Britain. *Transactions of the Royal Society of Edinburgh: Earth Sciences*, **80**, 5–15.

CHATTERTON, B. D. E. and SPEYER, S. E. 1997. Ontogeny. 173–247. *In* KAESLER, R. L. (ed.) *Treatise on invertebrate paleontology. Part O. Arthropoda 1 (Revised)*. The Geological Society of America & University of Kansas. 536 pp.

CHEN, J., WALOSZEK, D. and MAAS, A. 2004. A new 'great-appendage' arthropod from the Lower Cambrian of China and homology of chelicerate chelicerae and raptorial antero-ventral appendages. *Lethaia*, **37**, 3–20.

CHLUPÁČ, I. and HAVLÍČEK, V. 1965. *Kodymirus* n. g., a new aglaspid merostome of the Cambrian of Bohemia. *Sborník Geologickych Věd. Paleontologie*, **6**, 7–20.

CONG, P., MA, X., HOU, X., EDGECOMBE, G. D. and STRAUSFELD, N. J. 2014. Brain structure resolves the segmental affinity of anomalocaridid appendages. *Nature*, **513**, 538–542.

DUNLOP, J. A. 2002. Arthropods from the Lower Devonian Severnaya Zemlya Formation of October Revolution Island (Russia). *Geodiversitas*, **24**, 349–379.

—— and LAMSDELL, J. C. 2017. Segmentation and tagmosis in Chelicerata. *Arthropod Structure & Development*, **46**, 395–418.

EDGECOMBE, G. D. and RAMSKÖLD, L. 1999. Relationships of Cambrian Arachnata and the systematic position of Trilobita. *Journal of Paleontology*, **73**, 263–287.

—— STRULLU-DERRIEN, C., GÓRAL, T., HETHERINGTON, A. J., THOMPSON, C. and KOCH, M. 2020. Aquatic stem group myriapods close a gap between molecular divergence dates and the terrestrial fossil record. *Proceedings of the National Academy of Sciences*, **117**, 8966–8972.

ETTER, W. 2002. Solnhofen: plattenkalk preservation with *Archaeopteryx*. 327–352. *In* BOTTJER, D. J., ETTER, W., HAGADORN, J. W. and TANG, C. M. (eds). *Exceptional fossil preservation: A unique view on the evolution of marine life*. Columbia University Press, 403 pp.

—— and TANG, C. M. 2002. Posidonia Shale: Germany's Jurassic marine park. 265–291. *In* BOTTJER, D. J., ETTER, W., HAGADORN, J. W. and TANG, C. M. (eds). *Exceptional fossil preservation: A unique view on the evolution of marine life*. Columbia University Press, 403 pp.

FU, D.-J., ZHANG, X.-L. and SHU, D.-G. 2011. Soft anatomy of the Early Cambrian arthropod *Isoxys curvirostratus* from the Chengjiang biota of South China with a discussion on the origination of great appendages. *Acta Palaeontologica Polonica*, **56**, 843–852.

GAINES, R. R. 2014. Burgess Shale-type preservation and its distribution in space and time. 123–146. *In* LAFLAMME,

M., SCHIFFBAUER, J. D. and DARROCH, S. A. F. (eds). *Reading and writing of the fossil record: Preservational pathways to exceptional fossilization*. The Paleontological Society Papers, **20**, 314 pp.

GARCÍA-BELLIDO, D. C. and COLLINS, D. H. 2006. A new study of *Marella splendens* (Arthropoda, Marrellomorpha) from the Middle Cambrian Burgess Shale, British Columbia, Canada. *Canadian Journal of Earth Sciences*, **43**, 721–742.

—— —— 2007. Reassessment of the genus *Leanchoilia* (Arthropoda, Arachnomorpha) from the Middle Cambrian Burgess Shale, British Columbia, Canada. *Palaeontology*, **50**, 693–709.

GÖPEL, T. and WIRKNER, C. S. 2015. An "ancient" complexity? Evolutionary morphology of the circulatory system in Xiphosura. *Zoology*, **118**, 221–238.

GULLAN, P. J. and CRANSTON, P. S. 2010. *The insects: An outline of entomology*. 4th edn. Wiley-Blackwell, 568 pp.

GÜRICH, G. 1931. *Mimaster hexagonalis*, ein neuer Kruster aus dem unterdevonischen Bundenbacher Dachschiefer. *Paläontologische Zeitschrift*, **13**, 204–238.

HAUG, J. T., MAAS, A. and WALOSZEK, D. 2010. (for 2009). †*Henningsmoenicaris scutula*, †*Sandtorpia vestrogothiensis* gen. et sp. nov. and heterochronic events in early crustacean evolution. *Earth & Environmental Science Transactions of the Royal Society of Edinburgh*, **100**, 311–350.

—— WALOSZEK, D., MAAS, A., LIU, Y. and HAUG, C. 2012*a*. Functional morphology, ontogeny and evolution of mantis shrimp-like predators in the Cambrian. *Palaeontology*, **55**, 369–399.

—— BRIGGS, D. E. G. and HAUG, C. 2012*b*. Morphology and function in the Cambrian Burgess Shale megacheiran arthropod *Leanchoilia superlata* and the application of a descriptive matrix. *BMC Evolutionary Biology*, **12**, 162.

HAUG, C., BRIGGS, D. E., MIKULIC, D. G., KLUESSENDORF, J. and HAUG, J. T. 2014. The implications of a Silurian and other thylacocephalan crustaceans for the functional morphology and systematic affinities of the group. *BMC Evolutionary Biology*, **14**, 159.

HENDRICKS, J. R. and LIEBERMAN, B. S. 2008. New phylogenetic insights into the Cambrian radiation of arachnomorph arthropods. *Journal of Paleontology*, **82**, 585–594.

HESSELBO, S. P. 1992. Aglaspidida (Arthropoda) from the Upper Cambrian of Wisconsin. *Journal of Paleontology*, **66**, 885–923.

HIRST, S. and MAULIK, S. 1926. On some arthropod remains from the Rhynie Chert (Old Red Sandstone). *Geological Magazine*, **63**, 69–71.

HOU, X.-G. 1987. Three new large arthropods from Lower Cambrian, Chengjiang, eastern Yunnan. *Acta Palaeontologica Sinica*, **26**, 272–285. [in Chinese, English summary]

—— 1999. New rare bivalved arthropods from the Lower Cambrian Chengjiang fauna, Yunnan, China. *Journal of Paleontology*, **73**, 102–116.

—— and BERGSTRÖM, J. 1997. Arthropods of the Lower Cambrian Chengjiang fauna, southwest China. *Fossils & Strata*, **45**, 1–116.

—— ALDRIDGE, R. J., BERGSTRÖM, J., SIVETER, D. J., SIVETER, D. J. and XIANG-HONG, F. 2004. *The Cambrian fossils of Chengjiang, China: The flowering of early animal life*. Blackwell Science, 244 pp.

ISTVÁN, D. 2018. digiCamControl v. 2.1.1.0. http://www.digicamcontrol.com/

JELL, P. A. 1997. Introduction to suborder Eodiscina. 384–386. *In* KAESLER, R. L. (ed.) *Treatise on invertebrate paleontology. Part O. Arthropoda 1 (Revised)*. The Geological Society of America & University of Kansas. 536 pp.

JONES, W. T., FELDMANN, R. M. and SCHWEITZER, C. E. 2015. *Ceratiocaris* from the Silurian Waukesha Biota, Wisconsin. *Journal of Paleontology*, **89**, 1007–1021.

KJELLESVIG-WAERING, E. N. 1986. A restudy of the fossil Scorpionida of the world. *Palaeontographica Americana*, **55**, 1–287.

KLUESSENDORF, J. 1990. Depositional and taphonomic aspects of a Silurian (Brandon Bridge, Llandovery-Wenlock) fossil Konservat Lagerstätte from Waukesha, Wisconsin (U.S.A.), predictability of North American Silurian fossil Konservat Lagerstätten, and some insights into ichnofacies. Unpublished PhD thesis, University of Illinois at Urbana-Champaign, 115 pp.

—— 1994. Predictability of Silurian *Fossil-Konservat-Lagerstätten* in North America. *Lethaia*, **27**, 337–344.

KÜHL, G., BRIGGS, D. E. G. and RUST, J. 2009. A great-appendage arthropod with a radial mouth from the Lower Devonian Hunsrück Slate, Germany. *Science*, **323**, 771–773.

LAMSDELL, J. C. 2013. Revised systematics of Palaeozoic 'horseshoe crabs' and the myth of monophyletic Xiphosura. *Zoological Journal of the Linnean Society*, **167**, 1–27.

—— STEIN, M. and SELDEN, P. A. 2013. *Kodymirus* and the case for convergence of raptorial appendages in Cambrian arthropods. *Naturwissenschaften*, **100**, 811–825.

—— BRIGGS, D. E. G., LIU, H. P., WITZKE, B. J. and McKAY, R. M. 2015*a*. A new Ordovician arthropod from the Winneshiek Lagerstätte of Iowa (USA) reveals the ground plan of eurypterids and chasmataspidids. *Science of Nature*, **106**, 8.

—— —— —— —— —— 2015*b*. The oldest described eurypterid: a giant Middle Ordovician (Darriwilian) megalograptid from the Winneshiek Lagerstätte of Iowa. *BMC Evolutionary Biology* **15**, 169.

—— LODUCA, S. T., GUNDERSON, G. O., MEYER, R. C. and BRIGGS, D. E. G. 2017. A new Lagerstätte from the Late Ordovician Big Hill Formation, Upper Peninsula, Michigan. *Journal of the Geological Society*, **174**, 18–22.

—— GUNDERSON, G. O. and MEYER, R. C. 2019. A common arthropod from the Late Ordovician Big Hill Lagerstätte (Michigan) reveals an unexpected ecological diversity within Chasmataspidida. *BMC Evolutionary Biology*, **19**, 8.

LAURIE, M. 1900. On a Silurian scorpion and some additional eurypterid remains from the Pentland Hills. *Transactions of the Royal Society of Edinburgh*, **39**, 575–590.

LEGG, D. A., SUTTON, M. D. and EDGECOMBE, G. D. 2013. Arthropod fossil data increase congruence of morphological and molecular phylogenies. *Nature Communications*, **4**, 2485.

LEHMANN, W. M. 1955. *Vachonia rogeri* n.g.n.sp. ein Branchiopod aus dem unterdevonischen Hunsrückschiefer. *Paläontologische Zeitschrift*, **29**, 126–130.

LEROSEY-AUBRIL, R., XHU, X. and ORTEGA-HERNÁNDEZ, J. 2017. The Vicissicaudata revisited–insights from a new aglaspidid arthropod with caudal appendages from the Furongian of China. *Scientific Reports*, **7**, 11117.

LIEBERMAN, B. S., KURKEWICZ, R., SHINOGLE, H., KIMMIG, J. and MACGABHANN, B. A. 2017. Disc-shaped fossils resembling porpitids or eldonids from the early Cambrian (Series 2: Stage 4) of western USA. *PeerJ*, **5**, e3312.

LIU, Y., HOU, X.-G. and BERGSTRÖM, J. 2007. Chengjiang arthropod *Leanchoilia illecebrosa* (Hou, 1987) reconsidered. *GFF*, **129**, 263–272.

—— MELZER, R. R., HAUG, J. T., HAUG, C., BRIGGS, D. E. G., HÖRNIG, M. K., HE, Y.-Y. and HOU, X.-G. 2016. Three-dimensionally preserved minute larva of a great-appendage arthropod from the early Cambrian Chengjiang biota. *Proceedings of the National Academy of Sciences*, **113**, 5542–5546.

LIU, J., STEINER, M., DUNLOP, J. A. and SHU, D. 2018. Microbial decay analysis challenges interpretation of putative organ systems in Cambrian fuxianhuiids. *Proceedings of the Royal Society B*, **285**, 20180051.

LIU, Y., ORTEGA-HERNÁNDEZ, J., ZHAI, D. and HOU, X. 2020. A reduced labrum in a Cambrian great-appendage euarthropod. *Current Biology*, **30**, 3057–3061.

LODUCA, S. T. and TETREAULT, D. K. 2017. Ontogeny and reproductive functional morphology of the macroalga *Wiartonella nodifera* n. gen. n sp. (Dasycladales, Chlorophyta) from the Silurian Eramosa Lagerstätte of Ontario, Canada. *Journal of Paleontology*, **91**, 1–11.

—— KLUESSENDORF, J. and MIKULIC, D. G. 2003. A new noncalcified dasycladalean alga from the Silurian of Wisconsin. *Journal of Paleontology*, **77**, 1152–1158.

MA, X., HOU, X., EDGECOMBE, G. D. and STRAUSFELD, N. J. 2012. Complex brain and optic lobes in an early Cambrian arthropod. *Nature*, **490**, 258–261.

MANNING, P. L. and DUNLOP, J. A. 1995. The respiratory organs of eurypterids. *Palaeontology*, **38**, 287–297.

MAYERS, B., ARIA, C. and CARON, J.-B. 2019. Three new naraoiid species from the Burgess Shale, with a morphometric and phylogenetic reinvestigation of Naraoiidae. *Palaeontology*, **62**, 19–50.

McLAUGHLIN, P. A. 1982. Comparative morphology of crustacean appendages. 197–256. *In* ABELE, L. G. (ed.) *The biology of Crustacea: Embryology, morphology, and genetics*. Academic Press, 442 pp.

MIKULIC, D. G. and KLUESSENDORF, J. 1999. Stasis and extinction of Silurian (Llandovery-Wenlock) trilobite associations related to oceanic cyclicity. *Journal of Paleontology*, **73**, 320–325.

—— BRIGGS, D. E. G. and KLUESSENDORF, J. 1985*a*. A Silurian soft-bodied biota. *Science*, **228**, 715–717.

—— —— —— 1985*b*. A new exceptionally preserved biota from the Lower Silurian of Wisconsin U.S.A. *Philosophical Transactions of the Royal Society B*, **311**, 75–85.

MOORE, R. A., BRIGGS, D. E. G., BRADDY, S. J., ANDERSON, L. I., MIKULIC, D. G. and KLUESSENDORF, J. 2005. A new synziphosurine (Chelicerata: Xiphosura) from the Late Llandovery (Silurian) Waukesha Lagerstätte, Wisconsin, USA. *Journal of Paleontology*, **79**, 242–250.

MÜLLER, K. J. 1983. Crustacea with preserved soft parts from the Upper Cambrian of Sweden. *Lethaia*, **16**, 93–109.

—— and WALOSSEK, D. 1987. Morphology, ontogeny and life-habit of *Agnostus pisiformis* from the Upper Cambrian of Sweden. *Fossils & Strata*, **19**, 1–124.

MUSCENTE, A. D., SCHIFFBAUER, J. D., BROCE, J., LAFLAMME, M., O'DONNELL, K., BOAG, T. H., MEYER, M., HAWKINS, A. D., HUNTLEY, J. W., McNAMARA, M., MACKENZIE, L. A., STANLEY Jr, G. D., HINMAN, N. W., HOFMANN, M. H. and XIAO, S. 2017. Exceptionally preserved fossil assemblages through geologic time and space. *Gondwana Research*, **48**, 164–188.

ORR, P. J., BRIGGS, D. E. G. and KEARNS, S. L. 1998. Cambrian Burgess Shale animals replicated in clay minerals. *Science*, **281**, 1173–1175.

—— SIVETER, D. J., BRIGGS, D. E. G., SIVETER, D. J. and SUTTON, M. D. 2000. A new arthropod from the Silurian Konservat-Lagerstätte of Herefordshire, UK. *Proceedings of the Royal Society B*, **267**, 1497–1504.

ORTEGA-HERNÁNDEZ, J. 2015. Homology of head sclerites in Burgess Shale euarthropods. *Current Biology*, **25**, 1625–1631.

RAK, Š., ORTEGA-HERNÁNDEZ, J. and LEGG, D. A. 2013. A revision of the Late Ordovician marrellomorph arthropod *Furca bohemica* from Czech Republic. *Acta Palaeontologica Polonica*, **58**, 615–628.

RAYMOND, P. E. 1935. Leanchoilia and other Mid-Cambrian Arthropoda. *Bulletin of the Museum of Comparative Zoology*, **76**, 205–230.

RUDKIN, D. M., YOUNG, G. A. and NOWLAN, G. S. 2008. The oldest horseshoe crab: a new xiphosurid from Late Ordovician konservat-lagerstätten deposits, Manitoba, Canada. *Palaeontology*, **51**, 1–9.

—— CUGGY, M. B., YOUNG, G. A. and THOMPSON, D. P. 2013. An Ordovician pycnogonid (sea spider) with serially subdivided 'head' region. *Journal of Paleontology*, **87**, 395–405.

SCHIFFBAUER, J. D., WALLACE, A. F., BROCE, J. and XIAO, S. 2014*a*. Exceptional fossil conservation through phosphatization. 59–82. *In* LAFLAMME, M., SCHIFFBAUER, J. D. and DARROCH, S. A. F. (eds). *Reading and writing of the fossil record: Preservational pathways to exceptional fossilization*. The Paleontological Society Papers, **20**, 314 pp.

—— XIAO, S., CAI, Y., WALLACE, A. F., HUA, H., HUNTER, J., XU, H., PENG, Y. and KAUFMAN, A. J. 2014*b*. A unifying model for Neoproterozoic-Paleozoic exceptional fossil preservation through pyritization and carbonaceous compression. *Nature Communications*, **5**, 1–12.

SCHNEIDER, C. A., RASBAND, W. S. and ELICEIRI, K. W. 2012. NIH Image to ImageJ: 25 years of image analysis. *Nature Methods*, **9**, 671–675.

SCHOLTZ, G. and EDGECOMBE, G. D. 2005. Heads, hox and the phylogenetic position of trilobites. 139–165. *In* KOENEMANN, S. and JENNER, R. A. (eds). *Crustacea*

and arthropod relationships. Crustacean Issues, **16**, CRC Press, 430 pp.

—— —— 2006. The evolution of arthropod heads: reconciling morphological, developmental and palaeontological evidence. *Development Genes & Evolution*, **216**, 395–415.

SEILACHER, A., REIF, W.-E. and WESTPHAL, F. 1985. Sedimentological, ecological and temporal patterns of fossil Lagerstätten. *Philosophical Transactions of the Royal Society B*, **311**, 5–23.

SIVETER, D. J., FORTEY, R. A., SUTTON, M. D., BRIGGS, D. E. G. and SIVETER, D. J. 2007. A Silurian 'marrellomorph' arthropod. *Proceedings of the Royal Society B*, **274**, 2223–2229.

—— BRIGGS, D. E. G., SIVETER, D. J., SUTTON, M. D., LEGG, D. and JOOMUN, S. 2014. A Silurian short-great-appendage arthropod. *Proceedings of the Royal Society B*, **281**, 20132986.

—— —— —— —— —— 2017. A new crustacean from the Herefordshire (Silurian) Lagerstätte UK, and its significance in malacostracan evolution. *Proceedings of the Royal Society B*, **284**, 20170279.

STEIN, M. 2013. Cephalic and appendage morphology of the Cambrian arthropod *Sidneyia inexpectans* Walcott, 1911. *Zoologischer Anzeiger*, **253**, 164–178.

—— WALOSZEK, D. and MAAS, A. 2005. *Oelandocaris oelandica* and the stem lineage of Crustacea. 55–71. *In* KOENEMANN, S. and JENNER, R. A. (eds). *Crustacea and arthropod relationships*. Crustacean Issues, **16**, CRC Press, 430 pp.

—— —— —— HAUG, J. T. and MÜLLER, K. J. 2008. The stem crustacean *Oelandocaris oelandica* re-visited. *Acta Palaeontologica Polonica*, **53**, 461–484.

—— PEEL, J. S., SIVETER, D. J. and WILLIAMS, M. 2010. *Isoxys* (Arthropoda) with preserved soft anatomy from the Sirius Passet Lagerstätte, lower Cambrian of North Greenland. *Lethaia*, **43**, 258–265.

STRAUSFELD, N. J. 2012. *Arthropod brains: Evolution, functional elegance, and historical significance*. Belknap Press, 830 pp.

STÜRMER, W. and BERGSTRÖM, J. 1976. The arthropods *Mimetaster* and *Vachonisia* from the Devonian Hunsrück Shale. *Paläontologische Zeitschrift*, **50**, 78–111.

—— —— 1978. The arthropod *Cheloniellon* from the Devonian Hunsrück Shale. *Paläontologische Zeitschrift*, **52**, 57–81.

SUTTON, M. D., BRIGGS, D. E. G., SIVETER, D. J., SIVETER, D. J. and ORR, P. J. 2002. The arthropod *Offacolus kingi* (Chelicerata) from the Silurian of Herefordshire, England: computer based morphological reconstructions and phylogenetic affinities. *Proceedings of the Royal Society B*, **269**, 1195–1203.

SUZUKI, Y. and BERGSTRÖM, J. 2008. Respiration in trilobites: a reevaluation. *GFF*, **130**, 211–229.

SWOFFORD, D. L. 2002. PAUP*. Phylogenetic analysis using parsimony (*and other methods). v. 4.0a167. Sinauer Associates.

TANAKA, G., HOU, X., MA, X., EDGECOMBE, G. D. and STRAUSFELD, N. J. 2013. Chelicerate neural ground pattern in a Cambrian great appendage arthropod. *Nature*, **502**, 364–367.

VACCARI, N. E., EDGECOMBE, G. D. and ESCUDERO, C. 2004. Cambrian origins and affinities of an enigmatic fossil group of arthropods. *Nature*, **430**, 554–557.

VAN ROY, P. 2006. (for 2005). An aglaspidid arthropod from the Upper Ordovician of Morocco with remarks on the affinities and limitations of Aglaspidida. *Transactions of the Royal Society of Edinburgh: Earth Sciences*, **96**, 327–350.

VANNIER, J., GARCÍA-BELLIDO, D. C., HU, S.-X. and CHEN, A.-L. 2009. Arthropod visual predators in the early pelagic ecosystem: evidence from the Burgess Shale and Chengjiang biotas. *Proceedings of the Royal Society B*, **276**, 2567–2574.

VON BITTER, P. H., PURNELL, M. A., TETREAULT, D. K. and STOTT, C. A. 2007. Eramosa Lagerstätte—exceptionally preserved soft-bodied biotas with shallow-marine shelly and bioturbating organisms (Silurian, Ontario, Canada). *Geology*, **35**, 879–882.

VON SIEBOLD, C. T. 1848. Lehrbuch der vergleichenden Anatomie der Wirbellosen Thiere. 1–679. *In* VON SIEBOLD, C. T. and STANNIUS, H. (eds). *Lehrbuch der vergleichenden Anatomie*. Verlag von Veit & Co., 1845–1848, Berlin, 679 pp.

VRAZO, M. B., BRETT, C. E. and CIURCA, S. J. Jr 2017. Paleoecological and stratigraphic controls on eurypterid Lagerstätten: a model for preservation in the mid-Paleozoic. *Paleobiology*, **43**, 383–406.

WAHLENBERG, G. 1818. Petrificata Telluris Svecanae. *Nova Acta Regiae Societatis Scientiarum Upsaliensis*, **8** (1–116), 1–4.

WALCOTT, C. D. 1911. Middle Cambrian Merostomata. Cambrian geology and paleontology II. *Smithsonian Miscellaneous Collections*, **57**, 17–40.

—— 1912. Middle Cambrian Branchiopoda, Malacostraca, Trilobita and Merostomata. Cambrian geology and paleontology II. *Smithsonian Miscellaneous Collections*, **57**, 145–228.

WALOSSEK, D. and MÜLLER, K. J. 1990. Upper Cambrian stem-lineage crustaceans and their bearing upon the monophyletic origin of Crustacea and the position of *Agnostus*. *Lethaia*, **23**, 409–427.

WALOSZEK, D. and DUNLOP, J. A. 2002. A larval sea spider (Arthropoda: Pycnogonida) from the Upper Cambrian 'Orsten' of Sweden, and the phylogenetic position of pycnogonids. *Palaeontology*, **45**, 421–446.

WENDRUFF, A. J. 2016. Paleobiology and taphonomy of exceptionally preserved organisms from the Brandon Bridge Formation (Silurian), Wisconsin, USA. Unpublished PhD thesis, Ohio State University, 240 pp.

—— BABCOCK, L. E., MIKULIC, D. G. and KLUESSENDORF, J. 2018. New cheloniellid arthropod with large raptorial appendages from the Silurian of Wisconsin, USA. *bioRχiv*. https://doi.org/10.1101/407379

—— —— WIRKNER, C. S., KLUESSENDORF, J. and MIKULIC, D. G. 2020*a*. A Silurian ancestral scorpion with fossilised internal anatomy illustrating a pathway to arachnid terrestrialisation. *Scientific Reports*, **10**, 14.

—— —— KULESSENDORF, J. and MIKULIC, D. G. 2020*b*. Paleobiology and taphonomy of exceptionally preserved organisms from the Waukesha Biota (Silurian), Wisconsin, USA. *Palaeogeography, Palaeoclimatology, Palaeoecology*, **546**, 109631.

WHITTINGTON, H. B. 1997. The trilobite body. 87–135. *In* KAESLER, R. L. (ed.) *Treatise on invertebrate paleontology.*

Part O. Arthropoda 1 (Revised). The Geological Society of America & University of Kansas. 536 pp.

XIAO, S. and SCHIFFBAUER, J. D. 2009. Microfossil phosphatization and its astrobiological implications. 89–117. *In* SECKBACH, J. and WALSH, M. (eds). *From fossils to astrobiology: Records of life on Earth and the search for extraterrestrial biosignatures*. Cellular Origin, Life in Extreme Habitats & Astrobiology, **12**, Springer, 546 pp.

YANG, J., ORTEGA-HERNÁNDEZ, J., BUTTERFIELD, N. J. and ZHANG, X.-G. 2013. Specialized appendages in fuxianhuiids and the head organization of early euarthropods. *Nature*, **494**, 468–471.

—— —— —— LIU, Y., BOYAN, G. S., HOU, J.-B., LAN, T. and ZHANG, X.-G. 2016. Fuxianhuiid ventral nerve cord and early nervous system evolution in Panarthropoda. *Proceedings of the National Academy of Sciences*, **113**, 2988–2993.

ZHANG, X.-G., SIVETER, D. J., WALOSZEK, D. and MAAS, A. 2007. An epipodite-bearing crown-group crustacean from the Lower Cambrian. *Nature*, **449**, 595–598.